A Novel Biosensor for the Long-Term Optical Integration of Neuronal Activity

Dissertation zur Erlangung des Doktorgrades der Naturwissenschaften

an der Fakultät für Biologie

der Ludwig-Maximilians-Universität München

vorgelegt von

Jonathan A.G. Mackinnon

München, den 26.04.2012

Betreuer: Dr. Oliver Griesbeck

Erstgutachter: Dr. Oliver Griesbeck

Zweitgutachter: Prof. Dr. Elisabeth Weiss

Tag der mündlichen Prüfung: 16.07.2012

Table of Contents

Table of Figures

Abbreviations

2DG	2-deoxy-D-[^{14}C] glucose
2DG-6P	2-deoxyglucose-6-phosphate
$^{\circ}$C	Degrees Celsius
Å	Angstrom
APS	Ammonium Persulfate
BAPTA	1,2-bis(o-Aminophenoxy)ethane-N,N,N',N'-tetraacetic acid
bp	Base pair
BD	Electrical Field Stimulation Burst Duration
Ca^{2+}	Calcium
CaM	Calmodulin
CBP	Calmodulin-binding Peptide
CCD	Charge-Coupled Device
CFP	Cyan Fluorescent Protein
Ch	mCherry Fluorescent Protein
CIsS	Calpain Insensitive Substrate FRET pair
Citrine	Yellow Fluorescent Protein variant
CMV	Cytomegalovirus
cp	Circularly permuted
CSS	Calpain Sensitive Substrate FRET pair
ΔF/F	Change in Fluorescence/Starting Fluorescence
ΔR/R	Change in Ratio/Starting Ratio
ΔSp	Spectrin peptide Mutant
DIV	Days in vitro
DMEM	Dulbecco's Modified Eagle Medium
DMSO	Dimethyl sulfoxide
DNA	Deoxyribonucleic acid
E18	Embryonic day 18
EC$_{50}$	Half maximal effective concentration
ECFP	Enhanced Cyan Fluorescent Protein
EDTA	ethylenediamine tetraacetic acid
EGTA	ethylene glycol-bis[β-amino-ethyl ether] N,N,N',N'-tetraacetic acid
FACS	Fluorescence-Activated Cells Sorting
FKBP	FK506 binding protein
FP	Fluorescent Protein
FRB	FKBP-rapamycin binding domain
FRET	Fluorescence Resonance Energy Transfer

FS	Electrical Field Stimulation Field Strength
GECI	Genetically Encoded Calcium Indicator
GFP	Green Fluorescent Protein
HBSS	Hanks' balanced salt solution
HEK	Human Embryonic Kidney cells
HEPES	N-(2-hydroxyethyl)piperazine-N'-(2-ethanesulfonic acid)
HS	Hippocampal CA1 neuron Stimulation
IPTG	Isopropyl-β-D-thiogalactopyranoside
IRES	Internal Ribosomal Entry Site
ITI	Electrical Field Stimulation Inter Train Interval
K_d	Dissociation Constant
LB	Lysogeny Broth
M	Molar
M13	Calmodulin Binding Peptide (also known as skMLCK)
MCS	Multiple Cloning Site
Mg^{2+}	Magnesium
MOPS	3-(N-morpholino)propanesulfonic acid
PAGE	Polyacrylamide Gel Electrophoresis
PAS	Primary Afferent neuron Stimulation
PBS	Phosphate Buffered Saline
PCR	Polymerase Chain Reaction
PMSF	Phenylmethylsulfonylfluoride
PW	Electrical Field Stimulation Pulse Width
ΔR/R	Change in Ratio/Ratio
RT	Room temperature
SAS	Spontaneous Activity Stimulation
SDS	Sodium Dodecyl Sulfate
SF	Electrical Field Stimulation Frequency
SFV	Semliki Forest Virus
Sp	Spectrin Calmodulin Binding Peptide
TAE	Tris-EDTA buffer
TBS	Theta Burst Stimulation
TEV	Tobacco Etch Virus
TnC	Troponin C
TS-FRET	TEV Sensitive FRET pair
TTX	Tetrodotoxin
wt	Wild-type
YFP	Yellow Fluorescent Protein

1 Abstract

The identification of the functional neuronal circuitry involved in a given process still remains a crucial scientific challenge in anatomical Neuroscience. The development of the 2-Deoxyglucose technique (2DG) provided the first, and only, non-invasive strategy for identification of metabolically active neurons. However, the inability to distinguish metabolised 2DG in stimulus-responsive neurons from unmetabolised 2DG has made the desire for novel tools to elucidate neuronal circuit organisation unfulfilled.

Here we present a genetically encoded calcium "Integrator" that labels active neuron ensembles with an irreversible change in fluorescence. This calcium integrator represents the first genetically encoded neuroanatomical biosensor for the identification of functional anatomical circuits.

In order to generate the calcium Integrator three architectural approaches were undertaken; i) a calcium-dependent protease FRET integrator, ii) an artificial calcium-dependent protease FRET integrator and iii) a "Bimolecular Fluorescence Complementation"-based Integrator. Of these three approaches the complementation Integrator has been engineered to yield the first biosensor, with an EC_{50} of 420 nM, which is responsive to endogenous cellular calcium transients. Furthermore, the application of a virus-induced Integrator in cell culture yield a maximal 1580 % increase in fluorescence, after 4 hour stimulation using simulated physiological firing patterns, and has successfully been shown to differentiate between different neuronal firing patterns. In addition the criteria needed for split-protein biosensor development has been highlighted with an additional demonstration that complementation can be applied for the development of alternative split-protein based strategies.

2 Introduction

Since the foundation of anatomical neuroscience was laid by Golgi and Ramón y Cajal, significant efforts have been made to improve our understanding of neuroanatomical architecture and neuronal circuits. In recent years, the popularity of genetically encoded methodologies utilising Fluorescent Proteins (FPs) has provided researchers with an unprecedented ability to study large populations of neurons simultaneously. Despite the generation of many genetically encoded biosensors directed towards monitoring cellular processes such as dynamic signalling processes, biochemical events, and protein-protein interactions, there is a growing desire to apply non-invasive genetically encoded methodologies to unravel neuroanatomical architecture and circuits. Notable methodologies such as "Brainbow" (Livet et al., 2007) and "Transynaptic Tracers" (Wickersham et al., 2007) that utilise FPs to resolve neuronal architectures with high spatial resolution, have opened a window into this research field. However, the tools available for investigating functional neuroanatomical circuits are insufficient with the only tool available being that of the non-genetically encoded 2-Deoxyglucose method (Sokoloff et al., 1977). This method has enabled the labelling of large populations of metabolically active neurons; albeit with poor spatial resolution. Thus, the application of genetically encoded methodologies for the identification of functional neuroanatomical circuits would undoubtedly achieve an improvement in resolution and grant significant insight into the structure of functional neuronal circuits. Furthermore, it would provide a valuable method for the study of circuitry with a single cell resolution.

2.1 2-deoxyglucose (2DG)

To date, the 2-deoxyglucose (2DG) histochemical technique is the only method that labels large populations of neurons with an irreversible signal output (Sokoloff et al., 1977). By administration of radiolabelled 2DG (2-deoxy-D-[^{14}C] glucose) to conscious animals active neuron ensemble can be labelled due to the exchange of glucose between the cerebral ventricles and the surrounding tissue. Once integrated into metabolically active cells the 2DG is phosphorylated by hexokinase to 2-deoxyglucose-6-phosphate (2DG-6P) whereby it is unable to undergo further metabolism and therefore confined in the cell until autoradiographic detection. Since its initial development 2DG has enjoyed significant application as the only technique for neuronal network determination to presented stimuli. For example, the 2DG technique has been eloquently demonstrated in the fly optic lobe (**Figure 1A**) where it has provided whole brain structural resolution comparable to silver stain techniques (**Figure 1 B,C**) (Fischbach and Dittrich, 1989; Bausenwein and Fischbach, 1992).

However, with a poor spatial resolution of 100 µm this technique prevents individual neuron identification (Kai Kai and Pentreath, 1981). Optimisation of the 2DG method primarily focused on improving the spatial resolution through the replacement of the ^{14}C label with ^{3}H (**Figure 1D**) (Des Rosiers and Descarries, 1978). In addition Durham and colleagues further improved the resolution via the combination of ^{3}H-2DG with paraffin histology and emulsion autoradiography, successfully eliminating film autoradiography and necessity for unfixed tissue samples (Durham et al., 1981). These improvements significantly enhancing the resolution that enabled 2DG use with: conventional and electron microscopy (EM) (Kai Kai and Pentreath, 1981), double-labelling immunohistochemistry (McCasland, 1996), and whole brain reconstructions using autoradiographic sections (Kim et al., 1995).
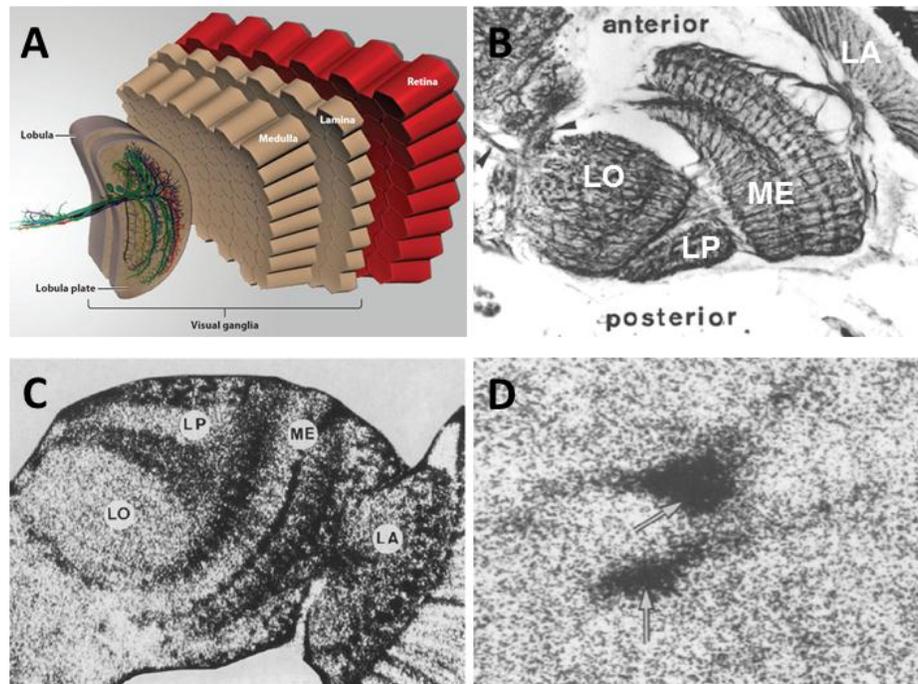
Figure 1: 2-Deoxyglucose (2DG) autoradiography
A) Schematic of the *Drosophila melanogaster* optic lobe (Borst et al., 2010). **B)** Holmes-Blest silver stained horizontal section of the fly optic lobe (LO: Lobula, LP: Lobula Plate, ME: Medulla, LA Lamina (Adapted from (Fischbach and Dittrich, 1989)). **C)** [^{14}C] 2-DG labeling of the fly optic lobe (Bausenwein and Fischbach, 1992). **D)** Dry-mount autoradiogram from the mouse ventrolateral medulla after injection of [^{3}H] 2-DG showing single cell labeling (Duncan et al., 1990).

Despite the success of this method, a discrepancy remains between signal output and neuronal activity. Fundamentally this problem arises due to the inability to distinguish between phosphorylated and unphosphorylated 2DG, and the variation in processed label intensity. The lack of distinction between the metabolised 2DG-6P product and the unmetabolised 2DG within the cell constitutes a major issue in neuronal activity determination. Transport of glucose/2DG into cells had been shown to occur at a much higher rate than phosphorylation; thus without an adequate method for distinguishing phosphorylated from unphosphorylated 2DG the degree of neuronal activity cannot be reliably determined (Lund-Andersen, 1979). In addition, the level of signal attained can display high degrees of variability depending on handling and fixation methodology. For example, comparison by Kai *et al.* of glutaraldehyde fixed tissue from three different research groups found that the amount of label retained by the tissue varied from

10% to 90% (Kai Kai and Pentreath, 1981) . This not only highlights the signal variability when using 2DG but also the unsuitability for comparing 2DG results from different sources. Finally, even with technical improvements, the discovery that 2DG could be used to reduce epilepsy progression by acting as a glycolytic inhibitor (Garriga-Canut et al., 2006) brings into serious doubt the physiological validity of applying 2DG to study neuronal network function. It is most likely the case that 2DG application has a significant impact on neuronal function and communication. Despite this, 2DG is still widely used for metabolic activity imaging with several fluorodeoxyglucose analogs (^{18}F-FDG) available that are, for example, used in combination with Computed tomography (CT) for the identification of tumours in mice (Kovar et al., 2009) or the identification of epileptic foci (Tsytsarev et al., 2012).

2.2 Genetically encoded biosensor mechanisms

Since the initial discovery of the Green Fluorescent Protein (GFP) from *Aequorea Victoria* (Shimomura et al., 1962), and the subsequent sequence identification and expression in *E.coli* and *C.elegans* (Prasher et al., 1992; Chalfie et al., 1994), GFP has revolutionised the Life Sciences. Comprising of a S65-Y66-G67 chromophore surrounded by an 11-stranded β-barrel structure (Ormö et al., 1996; Yang et al., 1996), GFP has been the subject of almost two decades of structural improvement and spectral diversification (Chudakov et al., 2010 provides a recent comprehensive review) that has resulted in a multitude of FP variants leading to a range of genetically encoded biosensors.

Genetically encoded biosensors based on GFP have been generated to monitor many cellular events with the objective of converting a molecular event into a designated signal output detectable via fluorescence microscopy. Genetically encoded biosensors confer many advantages over other probes designed for monitoring cellular events (such as Ca^{2+} dyes) including the diversity of application, the capacity for targeted biosensor expression (for example targeting to subcellular targets, or cell-specific expression) and the ability to undertake chronic imaging. Furthermore, as genetically encoded biosensors are genetically expressed

external application is not required unlike synthetic probes that require either application via injection of individual cells or administration to a localised area whereby the dye is incorporated into the cells via diffusion (Tsien, 1981). This limits not only the number of cells visualized but also imposes a time limit for which the investigation can proceed. Genetically encoded biosensors on the other hand can be expressed stably (either by transient transfection, viral infection or transgenic expression) and can be studied for weeks without notable loss of signal. The mechanisms by which genetically encoded biosensors yield a detectable signal can be divided into single fluorophore biosensors, Fluorescence Resonance Energy Transfer (FRET) biosensors, and split-protein biosensors (**Figure 2**). In principle, genetically encoded biosensors belong to two categories defined by the type of signal generated. The first category, the reversible biosensors, consists of the majority of single fluorescence biosensors and FRET biosensors; whereas the second category, the irreversible biosensors, primarily consists of split-protein strategies and a selection of biosensors using cleavable FRET substrates. The advantages and disadvantages of each method will be discussed in detail in the following subsections.
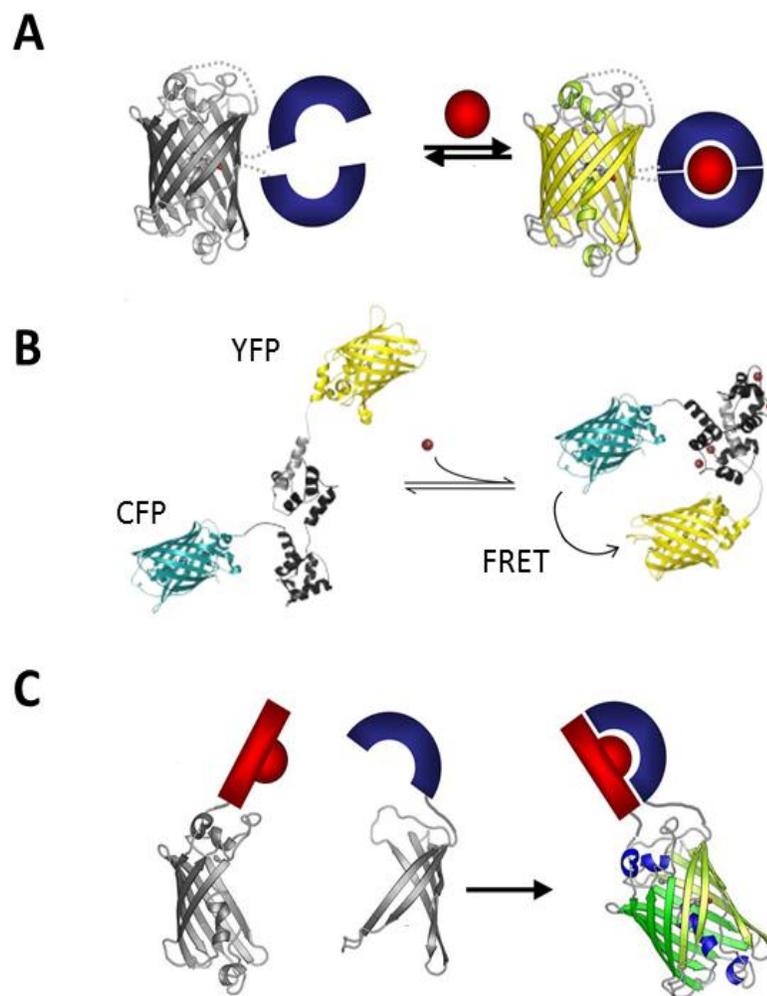
Figure 2: Genetically encoded biosensor mechanisms
A) Schematic of single-fluorophore biosensor mechanism. The fluorophore remains non-fluorescent when the two binding elements (blue semicircles) are in the open form and on binding of the analyte (red) the two elements undergo a conformational change which renders the FP fluorescent (Adapted from Ibraheem and Campbell, 2010)). **B)** Schematic of FRET-based biosensor mechanism. In the unbound state the fluorophores are further apart resulting in lower FRET and, once the binding element undergoes conformational changes (upon binding of the analyte), the fluorophores are brought closer together resulting in higher FRET (Adapted from McCombs and Palmer, 2008)). **C)** Schematic representation of the split protein mechanism "Bimolecular Fluorescence Complementation" where the interactions of two proteins (red and blue) bring together the two non-fluorescent protein fragments that refold and become fluorescent (Adapted from Ibraheem and Campbell, 2010).

2.2.1 Reversible Biosensors

2.2.1.1 *Single-Fluorophore biosensors*

Biosensors that employ a single fluorophore take advantage of either the fluorophores photophysical qualities or utilise circular-permuted fluorescent proteins (cpFPs) that typically results in an increase in fluorescence upon sensor activation. Biosensors that take advantage of photophysical qualities employ FPs that are either natively susceptible or artificially developed for detection of a variety of molecular events, such as halide ions (Jayaraman, 2000), voltage (Guerrero et al., 2002), or changes in pH (Kneen et al., 1998).

Due to the limited ability to exploit the integral photophysical qualities of FPs, the majority of single-fluorophore biosensors are developed utilising circularly-permuted FPs (cpFPs); involving the combination of proteins responsive to the desired molecular event and a redesigned fluorophore possessing alternate N- and C- termini. This results in a distorted secondary structure that correlates biosensor conformational change with changes in fluorescence intensity (**Figure 2A**). The advantage of this mechanism over FRET-based biosensors is the unrivalled dynamic range due to the low fluorescence intensity achieved in the absence of the analyte of interest. Furthermore, single-fluorophore biosensors have been developed for a significantly wider range of applications than those employing endogenous FP characteristics and include maltose (Marvin et al., 2011), Ins(1,3,4,5)P$_4$ (Sakaguchi et al., 2009), cGMP (Nausch et al., 2008) and ATP (Berg et al., 2009) biosensors. One biosensor group belonging to this class, the single-fluorophore Genetically Encoded Ca^{2+} Indicators (GECIs), have been one of the most intensely researched and improved group of single-fluorophore biosensors. The developmental strategies undertaken for single-fluorophore GECIs will be elaborated on in Section 2.3.

2.2.1.2   Fluorescence Resonance Energy Transfer Biosensors

In addition to single-fluorophore biosensors a number of sensors exploit FRET as a method for measuring an analyte of interest. Typically this type of biosensor employs two FPs flanking an analyte binding domain that undergoes conformational changes (upon analyte binding) which result in either an increase or decrease in FRET (**Figure 2B**). The two FPs act as a "donor" and an "acceptor" FP whereby an excited state fluorophore, the donor, transfers its energy to an acceptor FP via non-radiative energy transmission that in turn reaches an excited state (Forster, 1946). In essence, when applying donor excitation the recording of emission from both the donor and acceptor one can document the FRET ratio changes that correspond to the analyte binding.

The ratiometric nature of FRET-based biosensors confers several advantages over single-fluorophore biosensors. For example, when developing FRET-based biosensors the FRET-efficiency parameters can be taken into account to assist further rational design approaches. The first parameter, the "Spectral Overlap Integral", describes the overlap between donor emission and acceptor absorption, an essential consideration when selecting a FRET-pair. However, it is worth noting that despite many efforts to develop further red shifted FRET-pairs most FRET biosensors still utilise cyan (CFP) and yellow (YFP) fluorescent protein variants (**Figure 3A**) (Piston and Kremers, 2007). The second parameter, "Förster Radius", dictates that energy transfer can only occur under conditions of close proximity (10-60 Å), a fact that must be taken into account when considering selection of the analyte binding domain. The final parameter, the "Orientation Factor", describes the orientation of the dipole moments of the donor and acceptor fluorophore. Whilst this orientation factor is largely irrelevant when considering small synthetic dyes, such as the "Alexa" dyes (Roy et al., 2008), it becomes highly relevant when considering biosensors with a FRET-based mechanism that contains 40 Å FPs. Whilst this is not a directly quantifiable factor for biosensor design (without the crystal structure of the proposed biosensor) it provides knowledge to improve biosensor performance through understanding the biophysical principles of FRET , for example, by the introduction of amino acids that rigidly shift the orientation or by the incorporation of cpFP donor or acceptor variants. An additional highly advantageous feature of FRET biosensors became apparent with

the application of FRET-biosensors *in vivo*. When using FRET-based biosensors the dual-channel ratiometric readout is less prone to misrepresentative recordings that can occur with single readout sensors due to motion artefacts, inconsistent labelling concentrations and variations in illumination or recording signals.

FRET-based biosensors can utilise a number of mechanisms such as conformational-dependent FRET change (**Figure 3B**) and protein-protein interaction dependent FRET that have been used to generate a host of FRET-based biosensors for the detection of many events including voltage (Akemann et al., 2010), cGMP (Niino et al., 2010), and ICAP (Friedrich et al., 2010). Similar to the single-fluorophore biosensors one of the most engineered biosensor groups in the FRET-based class belongs to the GECI category, and will be discussed in detail in Section 2.3.
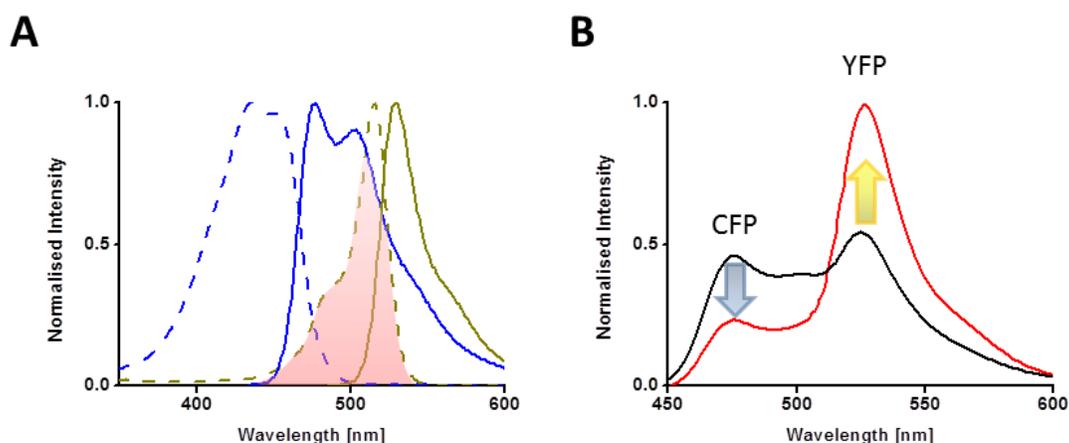
Figure 3: Spectral overlap of FRET-pair CFP/YFP and an example of FRET
A) Excitation (dashed) and emission (solid) spectra of the most common FP FRET pair; CFP (blue) and YFP (yellow). The area shaded in red illustrates the spectral overlap between CFP emission and YFP excitation. **B)** Emission spectra of the Genetically Encoded Ca^{2+} Indicator "TN-XXL" using CFP excitation in a Ca^{2+}-free solution (black) and after 1mM $CaCl_2$ (red) is added.

2.2.2 Irreversible Biosensors

2.2.2.1 Split Protein Interactions

Split protein strategies are a diverse group of genetically encoded tools that are based on the fusion of two binding partners to rationally designed protein fragments that regain function once the two binding partners interact to form heterodimers. Whilst the field of split proteins is orientated towards the understanding of protein interactions, the biosensor applications are not to be dismissed and indeed several significant attempts have been undertaken. The ability to regain protein function upon recombination of two complementary protein fragments was first demonstrated with bovine pancreatic ribonuclease (RNase) by splitting the protein into the N-terminal peptide and the rest of the molecule. These two fragments were shown to subsequently regain enzymatic activity upon mixing the two solutions (Richards, 1958). However, the ground-breaking step for the split protein field came when it was discovered that ubiquitin could be split and reconstituted in living cells (*S.cerevisiae*) by the association of two naturally dimerising proteins (Johnsson and Varshavsky, 1994). In the proceeding decades there have been several other proteins identified that can form functional complexes (**Figure 4**). In principle split protein methods can be divided into two categories; split proteases such as β-galactosidase (Rossi et al., 1997), dihydrofolate reductase (Pelletier et al., 1998), and Tobacco Etch Virus (TEV) protease (Wehr et al., 2006) or proteins that result in increased bioluminescence or fluorescence; such as firefly luciferase (Paulmurugan et al., 2002), *renilla* luciferase (Paulmurugan and Gambhir, 2003), and GFP (Ghosh et al., 2000).
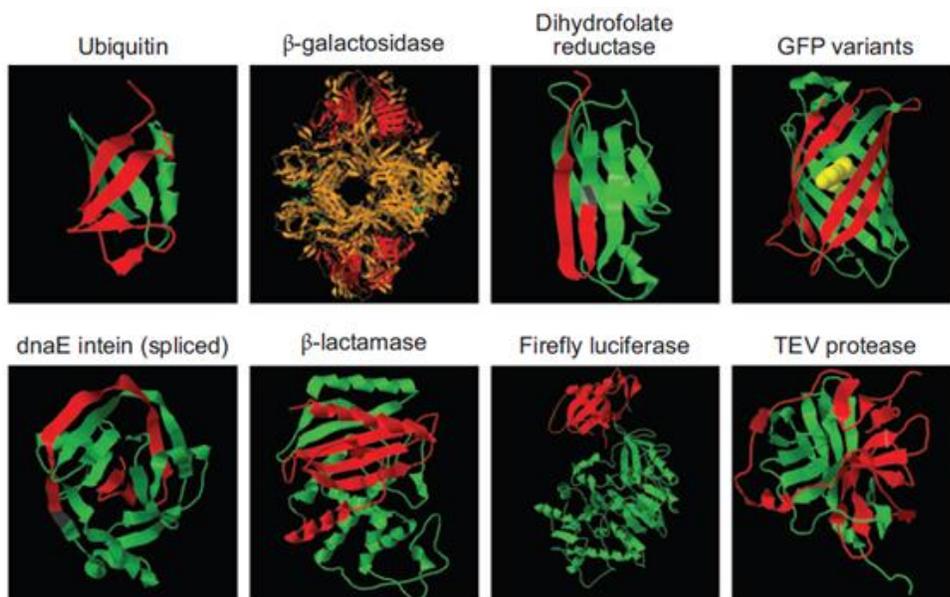
Figure 4: Split proteins used for protein-protein interaction studies
Structures of proteins used for the investigation of protein-protein interactions. The separate fragments are indicated in red and green. The overlap between fragments is indicated in orange (Kerppola, 2008).

2.2.2.2   Bimolecular Fluorescence Complementation

Despite several split-protein strategies being developed Bimolecular Fluorescence Complementation has emerged as the most frequently used strategy to date. The formation of fluorescent FPs is achieved via the recombination of non-fluorescent FP fragments that are brought into close proximity via protein pairs that form heterodimers (**Figure 2C**). Since its initial demonstration, the extensive research by Tom Kerppola has served to secure FPs as the leading split-protein method available. Two studies published in quick succession demonstrated that the complementation system can not only be used to study the subcellular co-localisation of interacting proteins (Hu et al., 2002) but also that different FPs can be split at different locations (at amino acid 155 and 173 positions) and recombined together or in combination resulting in FP chimeras (Hu and Kerppola, 2003). A pallet of blue to yellow FP combinations were developed using the dimerising proteins bJun and bFos (Patel et al., 1994) which has been used in a variety of organisms to study protein interactions. This selection has been further expanded to include red FPs such as: mRFP (Jach et al., 2006), mCherry (Fan et al., 2008), TagRFP (Qin et al., 2009) and mKate (Chu et al., 2009). Methodological adaptations of FP

complementation have further been used in structural biology (Song and Wilmanns, 2008), signalling networks (Rose et al., 2010) and high throuput screening (Gehl et al., 2009).

In recent years, several complementation-based biosensors have emerged that respond to extracellular application of agonists when expressed in cells. The first of these, based on a split-EGFP architecture, used EF-hands I and II of calbindin D9k that dimerised with extracellular Ca^{2+} application (Chen et al., 2009). The poor performance of the sensor yield a maximal increase of 30%, however, the half-life of complementation ($t_{1/2}$) was reached within minutes contradicting the previously held belief that $t_{1/2}$ was approximately one hour (Kerppola, 2008). A more detailed study by Robida and Kerppola used the rapamycin-induced dimerisation of the FK506 binding protein (FKBP) and the FKBP-rapamycin binding domain (FRB) (Chiu et al., 1994) in combination with fragments of the yellow FPs "YFP" and "Venus" (and the cyan FP "CFP" as a transfection marker). Using Fluorescence-Activated Cell Sorting (FACS) they identified four key points regarding the use of complementation. These results demonstrated that fluorescence complementation was detectable in 10 min after rapamycin addition (longer than reported by Chen et al. 2009) and possessed a $t_{1/2}$ of four hours that was significantly longer than previously thought. In combination these two observations indicated that any kinetic study aimed at the determination of the rate of complementation can only determine the rate for a particular set of dimerising proteins and cannot be generalised to the whole methodology. Furthermore, it was confirmed that the N-terminal fragment has a greater effect on complementation fluorescence intensity and in doing so identified two complementation pairs that can be used for different applications. Use of YN and YC (YN: YFP 1-155, YC: 156-238) was recommended when minimal spontaneous background fluorescence was desired, and VyN (Venus 1-155) when background fluorescence is not a factor of concern and maximal fluorescence intensity is desired. Finally also it was also observed that facilitation of protein refolding at 30 ^{o}C is enhanced in comparison to physiological temperatures (37 ^{o}C) but unexpectedly the ratio of induced versus non-induced complementation is higher at 37 ^{o}C due to the reduced spontaneous association of FP fragments.

The most recent complementation biosensor by McLachlan and colleagues was generated to detect Estrogenic Compounds, with the potential use for high-throughput screening (McLachlan et al., 2011). Using complementary fragments of Venus (VN154, VN155) six biosensors were generated with varying length of the oestrogen receptor alpha (ERα). The importance of this work lies in the unique architecture of the biosensor; rather than using two separate proteins that dimerise spontaneously or under induction they use the ERα domain flanked by the complementary Venus fragments that rely on conformational changes for complementation to occur. The biosensors featured here demonstrated not only the variability of responses elicited using Bimolecular Fluorescence Complementation in designs containing similar architectures but also counter intuitively demonstrated that despite the close proximity of the fragments spontaneous complementation can be avoided by certain orientations of the intervening protein.

2.2.2.3   Cleavable FRET substrates

Despite the majority of FRET-based biosensors being reversible there are several biosensors that consist of cleavable FRET substrates for monitoring endogenous protease behaviour. Typically these are not directly responsive to changes in intracellular environments but rather are responsive as the secondary effect to protease activation. As the substrate site has to be identified for the protease under investigation this category does not consist of a significant number of members. Despite this, members include biosensors directed towards Type 1 Matrix Metalloproteinase (MT1-MMP) (Ouyang et al., 2008), Caspase-3 (Xu et al., 1998), and Calpain 1 (Vanderklish et al., 2000). The elegant characteristic of this FRET application lies in the concept that biosensors can be developed to simultaneously respond to more than one desired element. This feature began with the generation of a dual-Caspase FRET biosensor (Wu et al., 2006). Developed using three FPs that form two FRET-pairs Wu *et al.* were able to generate a biosensor that responded to not only Caspase-3 but also Caspase-6 via the insertion of a cleavage motif for Caspase-3 between CFP and YFP and a cleavage motif for Caspase-6 between the YFP and mRFP to yield a CFP-*c3*-YFP-*c6*-mRFP biosensor. An alternative dual-

protease strategy was developed for investigating two proteases crucial in the role of cancer invasion and metastasis. Incorporating four FPs, tethered via a transmembrane domain, the biosensor employed one FRET-pair that could be cleaved by the Metalloproteinase MT1-MMP and another for cleavage by the proto-oncogene tyrosine-protein kinase *Src* (Ouyang et al., 2010). The first FRET pair, located on the outer surface of the plasma membrane, used a mOrange2 and mCherry pair to flank the cleavage site of MT1-MMP, whereas on the inner membrane an ECFP/Citrine combination were used for detection of Src.

2.3   Genetically Encoded Ca²⁺ Indicators

The largest biosensor group, the "Genetically encoded Ca^{2+} Indicators" (GECIs), were designed to monitor neuronal Ca^{2+} transients and serve as the foremost example of rational design of genetically encoded biosensors. Principally all GECIs employ very similar elements, one or two FPs and a Ca^{2+}-binding element that either undergoes conformational changes or binds to target peptides. Of particular interest are the design and evolution strategies employed to generate improved GECI biosensors. Outlined below is the fundamental structural unit common to all GECIs, the EF-hand, and elaboration of the strategies undertaken for GECI engineering.

2.3.1   The canonical EF-hand and Ca²⁺ binding proteins

The EF-hand, first identified in parvalbumin, consists of a helix-loop-helix motif encoded by approximately 30 amino acids that are capable of coordinating a Calcium (Ca^{2+}) or Magnesium (Mg^{2+}) ion (Kretsinger and Nockolds, 1973). Typically EF-hands are found in pairs and as a result most EF-hand containing proteins possess multiples of two (typically 2, 4 or 6). Within the EF-hand the loop region gives rise to the ion coordination space via negatively charged amino acids and the most typical form, the canonical EF-hand, exhibits a central nine amino acid binding loop with 3 amino acids extending into the following helix. These chelating residues are identified by two methods based on; i) the linear position (**Figure 5B**) and ii) the

tertiary geometry imposed by their alignment on the axes of a pentagonal bipyramid (**Figure 5A**) (Gifford et al., 2007). The twelve amino acid sequence coordinates the metal ion via seven coordinating ligands relating to six amino acids. Of particular significance are the highly conserved N/D residues located at position 1, 3, and 5 that form the coordination positions +X, +Y, +Z respectively. Additionally, the most conserved amino acid, glutamic acid, at position 12 acts as the –Z coordination amino acid that provides two chelating groups as a bidentate side chain. Whilst chelating groups are formed directly from these amino acids the –Y and –X chelating groups (position 7 and 9 respectively) are formed from the amino acid carbonyl group (-Y) either directly or through a bridged water molecule (-X), and thus account for the lack of conserved amino acids between different EF-hands. Upon Ca^{2+} binding the EF-hands undergo a structural rearrangement from almost parallel helices of each EF-hand in the "apo" (unbound state) to perpendicular helices in the saturated (bound state) that exposes a methionine-rich hydrophobic surface which is the basis for target recognition (Gifford et al., 2007). As EF-hands usually occur in pairs the Ca^{2+}-binding is positively cooperative whereby Ca^{2+} binding to one EF-hand presents a positive structural effect on the paired hand, thus facilitating Ca^{2+} binding to this hand. This paired function of EF-hands does not extend to other pairs present in the protein and as a consequence EF-hand pairs often display independent binding properties and biological function (Jurado et al., 1999).

The ubiquitously expressed Calmodulin (CaM) and the skeletal/cardiac muscle restricted Troponin C (TnC) belong to a family of highly homologous EF-hand proteins with a 70% primary sequence homology (da Silva et al., 2002). Both proteins contain four EF-hands (I to IV) that comprise the N-lobe and C-lobe structures (**Figure 5C**) that are described as retaining a dumbbell structure due to the central flexible linker that separates the two binding pairs. During this transition from the apo to the saturated state the binding of Ca^{2+} occurs in a specific order based on the affinity of the EF-hands for Ca^{2+}. Due to the paired occurrence of EF-hands occur in pairs the order of Ca^{2+} binding exhibits a lobe-to-lobe order with the pattern of binding being EF-Hand III – IV – I – II. This corresponds to the Ca^{2+} binding first to the C-lobe and subsequently to the N-lobe (Gilli et al., 1998). Upon Ca^{2+} binding to the higher-affinity C-lobe the CaM or TnC interacts with the N-terminal of the target peptide (Calmodulin Binding

Peptides (CBPs) or Troponin I (TnI) respectively), after which the N-lobe of CaM or TnC binds to the C-terminal of this peptide (**Figure 5D**) (Tripet et al., 2003; Yamniuk and Vogel, 2004).

A) Pentagonal bipyramid Ca^{2+} coordination geometry of the canonical EF-hand.

B) EF-Hand Coordination

1	2	3	4	5	6	7	8	9	10	11	12
D	x	D/N	x	D/N	x	x	x	x	x	x	E
+X		+Y		+Z		-Y		-X			-Z
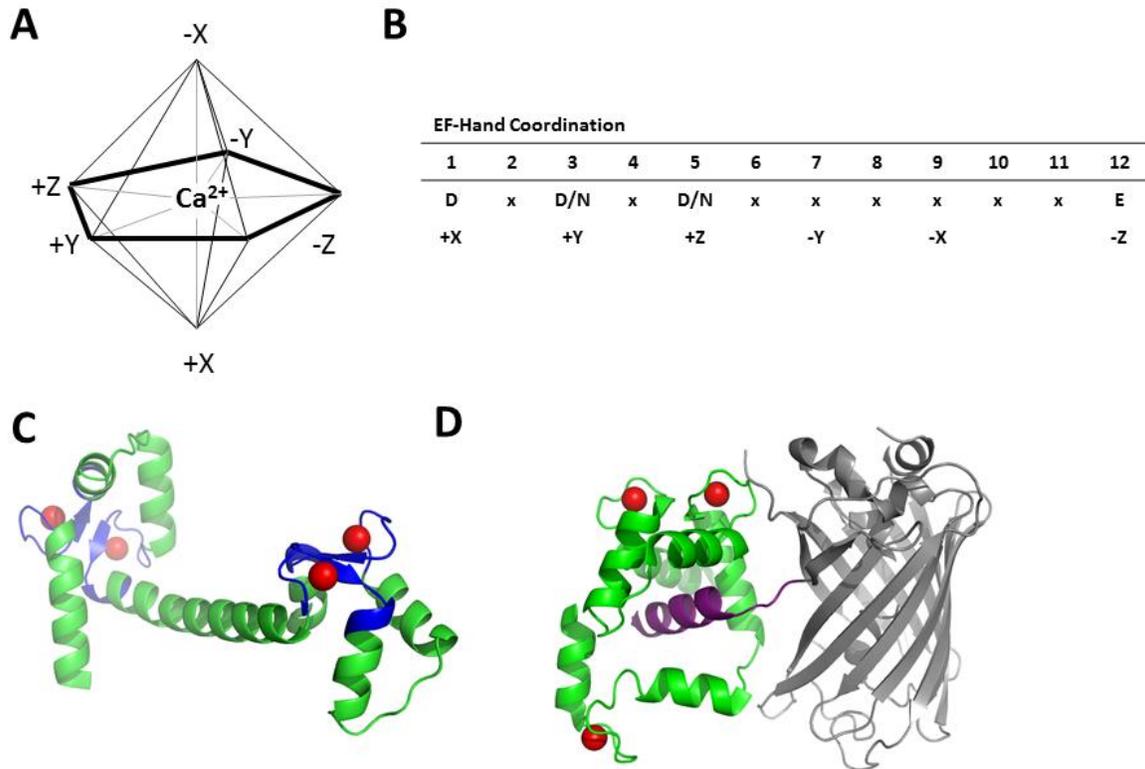
Figure 5: Ca^{2+} binding to the EF-hand and the structure of Calmodulin (CaM)
A) Pentagonal bipyramid Ca^{2+} coordination geometry of the canonical EF-hand. **B)** Consensus sequence for the canonical EF-hand (Adapted from Bertini et al., 2003). **C)** Crystal structure of CaM (green) with the EF-hands (blue) bound to Ca^{2+} (red).PDB: 3CLN. **D)** Crystal structure of GCaMP2, demonstrating how CaM (green) wraps around the CBP M13 (purple) in the Ca^{2+} bound state. (NB: only 3 Ca^{2+} ions (red) are represented in this PDB file; grey: EGFP). PDB: 3EK4.

2.3.2   Rational design of GECIs

2.3.2.1   Single-Fluorophore GECIs

The single-fluorophore GECIs (or circular-permuted FP GECIs; cpGECIs) can be largely divided into three groups: the Camgaroos, Pericams, and GCaMPs, based on their architectural design (**Figure 6A**). The original design demonstrated by Baird *et al*. proved that despite the rigidity of the FP structure a functional FP could be produced when the N- and C- termini were changed (Baird et al., 1999). Furthermore, it was demonstrated that the incorporation of *Xenopus* Calmodulin (XCaM) into a circular-permuted Yellow Fluorescent Protein (cpYFP) exhibited a Ca^{2+}-dependent fluorescence modulation via the conformational change of XCaM (upon Ca^{2+} binding) leading to a preferred deprotonated form of the chromophore. Despite the initial cpGECI (Camgaroo-1) being later improved by the replacement of YFP with the less environmentally-sensitive FP "Citrine" (Griesbeck et al., 2001), to yield Camgaroo-2, the dissociation constant (K_d) for Ca^{2+} did not improve significantly (from 7μM to 5.3 μM), consequently limiting the use of this GECI group.

A significant improvement in the Ca^{2+} affinity of the single-fluorophore GECIs was performed through the development of the Pericam group that exploited the same cp-Y145 variant of YFP as Camgaroo-1 but utilised the alternative architecture of sandwiching the cpYFP between the Calmodulin Binding Peptide (CBP) "M13" and the XCaM (E104Q). By eliciting Ca^{2+}-induced interactions of CaM and M13 it was demonstrated that the novel biosensor group possessed a K_d range between 0.2 μM -1.7 μM that enabled the detection of neuronal Ca^{2+} transients (Nagai et al., 2001).

In a parallel development GCaMP was generated utilising the same architecture as the Pericam with the substitution of YFP for GFP. Furthermore, the design of this GECI differed from that of Pericam due to the application of wild-type (wt) CaM (derived from rat) and the M13 peptide as flanking proteins surrounding a cpGFP that displayed an apparent K_d of 235 nM (Nakai et al., 2001). By the incorporation of several mutations within the GFP, namely V163A and S175G to improve temperature stability and A206K to prevent dimerisation, (and two further random mutations: V93I, D180Y) GCaMP2 was generated that demonstrated a K_d of 150

nM (Tallini, 2006). Structural analysis via the crystallisation of Ca^{2+}-bound and Ca^{2+}-unbound states (Wang et al., 2008) and subsequent biophysical analysis (Akerboom et al., 2009) revealed a solvent pocket that formed the basis for structure-guided mutagenesis (and semi-rational library screening) leading to the successful production of GCaMP3. Two GFP mutations (M153K and T203V) and one CaM mutation (N60D) in GCaMP2 yielded a 3 -fold increase in dynamic range and increased the affinity for Ca^{2+} by 1.3 -fold (Tian et al., 2009).
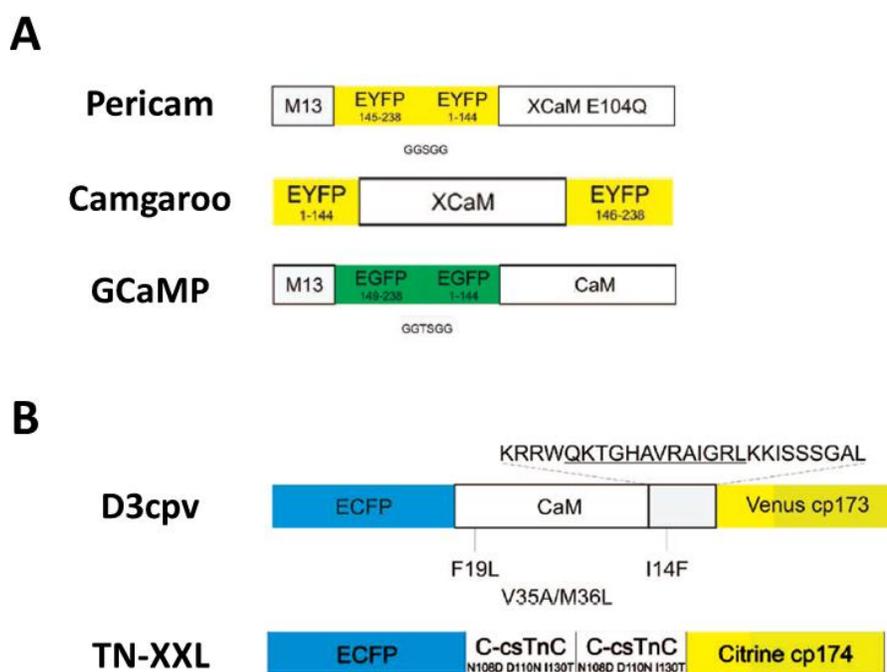
Figure 6: Summary of GECI architectures
Schematic representation of **A)** single-fluorophore GECI and **B)** FRET-based GECI architectures (Adapted from Mank and Griesbeck, 2008).

2.3.2.2   FRET-based GECIs

Comparable to the single-fluorophore GECIs the FRET-based GECIs have also been the subject of substantial genetic engineering to improve the functionality in order to resolve single action potentials *in vivo* (**Figure 6B**). This GECI architecture consists of two groups: i) the Cameleons and ii) the Troponin based group.

The Cameleons utilise the CaM/M13 interaction pair (similar to that of the GCaMPs) that are sandwiched between ECFP and EYFP (Miyawaki et al., 1997). Once CaM interacts with M13 a conformational change occurs that brings the two fluorophores into close proximity and results in increased FRET. Since the initial "Yellow Cameleon-2" several attempts to improve the sensor by mutating the CaM domain have been proven to be unsuccessful. However, significant improvements have been achieved by focusing on optimising the YFP component, in particular the substitution of EYFP with cpVenus (Nagai et al., 2002). The largest dynamic range has been demonstrated by YC3.6 that incorporates a cp173Venus acceptor FP (Nagai et al., 2004). Under this strategy this group boasted a range of Ca^{2+} affinities from 50-250 nM; yet cell transfection saw a substantial reduction in biosensor performance, most likely attributable to the interaction of CaM with the ubiquitously expressed cellular CaM and CBPs. Consequently, in order to reduce this "endogenous interference" one particular approach described in Palmer *et al.* used computational remodelling to develop a bump-and-lock redesigned M13/CaM interface and resulted in the D3cpv (Design 3 cpVenus). With an affinity of 600 nM this was not the most affine of the yellow cameleon series yet cellular performance demonstrated a 5 -fold increase in dynamic range (Palmer et al., 2006) that enabled the detection of single action potentials firing at a rate of under 1 Hz (Wallace et al., 2008). More recently, in contrast to the previously held belief that restriction of rotational freedom is beneficial to biosensor function, the addition of poly-glycine linkers improved the Ca^{2+} affinity of YC 2.6 to yield the Cameleon-Nano group with an affinity range of 15 – 140 nM (Horikawa et al., 2010).

Another strategy employed by Oliver Griesbeck utilised an alternative Ca^{2+}-binding motif, Troponin C (TnC), that possessed a very similar structure to Calmodulin, however, unlike Calmodulin it is not ubiquitously expressed in all cell types but restricted to skeletal and cardiac

muscle (Parmacek et al., 1990). Sandwiched between CFP and Citrine the activity of this biosensor relies on the conformational rearrangement of TnC that, when bound to Ca^{2+}, results in increased FRET. The first indicator denoted TN-L15 (owing to the truncation at L15) possessed a Ca^{2+} affinity K_d of 710nM (Heim and Griesbeck, 2004) that enabled the generation of the first transgenic mouse line expressing a GECI without inhibited biosensor performance (Heim et al., 2007). The disadvantage of TN-L15, the relatively high Mg^{2+} sensitivity, became the inspiration for further development that resulted in the generation of TN-XL that possessed several mutations aimed specifically at reducing the magnesium sensitivity (N109D, D111N, N145D, and D147N of the TnC C-lobe). Engineering this high speed sensor came at the sacrifice of Ca^{2+} affinity (K_d: 2200 nM) that prevented the observation of low Ca^{2+} concentration changes associated with single action potentials (Mank et al., 2006). To circumvent this low affinity the domain structure was modified; the N-lobe (EF-hands I and II) was removed and the C-lobe was doubled to give a structure of EF-hand III, IV, III, IV. With an additional reversal of the N145D and D147N mutations TN-XXL was generated with a K_d value of 800 nM (Mank et al., 2008).

2.4 Research Objective

In order to develop a functional genetically encoded Integrator several design strategies were considered and implementation of each will be discussed in detail in the following subsections. Whilst each design possessed theoretical merit the physical limitations generally encountered when developing new biosensors dictated the requirement for a multi-strategy approach. The approaches considered were the following; i) application of a Ca^{2+}-dependent protease that cleaves a FRET substrate, ii) the generation of an artificial Ca^{2+}-dependent protease that cleaves a FRET substrate, and iii) a Bimolecular Fluorescence Complementation split protein approach that involves the Ca^{2+}-induced formation of a fluorescent protein.

The first stage of Integrator development focused on the establishment of an *in vitro* platform. Subsequently, biosensor optimisation *in vitro* took place in order to maximise Integrator performance. In tandem, a stimulation method was established in cultured dissociated hippocampal neurons to reliably induce calcium transients over the course of several hours. Once completed, a combination of *in vitro* refinement and cell culture-based evaluation was undertaken until the Integrator exhibits significant performance in the cell based assay. Finally, a mechanism to induce Integrator expression was introduced and evaluated to enable temporal control over Integrator expression that is required for future *in vivo* use.

2.5 Integrator design approaches

2.5.1 Approach 1: Ca^{2+}-dependent protease FRET Integrator

Conceptually one of the simplest Integrator architectures involved a FRET-pair that flanks a protease substrate site cleaved by a Ca^{2+}-dependent protease (**Figure 7**). The Ca^{2+}-dependent protease selected for this approach, μ-Calpain, was chosen due to its high calcium affinity; with a dissociation constant (K$_d$) of 10-50 μM (Dutt et al., 2002). μ-Calpain is a heterodimeric Ca^{2+}-dependent cysteine protease ubiquitously expressed in mammalian tissue and is comprised of two subunits, the large CAPN1 (80 kDa) and the small CAPNS1 (30 kDa) subunit. Structurally, CAPN1 consists of four domains; I and II comprise the protease core with the active site residues, domain III consists of an unknown function, and domain IV contains 5 EF-hand motifs that are responsible for binding Ca^{2+}. For protease function CAPN1 requires heterodimerisation with the small subunit CAPNS1 that consists of two domains, of which domain VI possesses an additional 5 EF-hands (Saez et al., 2006). Although CAPN1 domain III and CAPNS1 domain V appear to have no clear structure, these domains have been proposed to be important in cell biology applications (Larsen et al., 2004). Upon Ca^{2+} binding to domains IV and VI the heterodimer undergoes conformational changes that increase the accessibility/reactivity of the active site leading to autolysis that results in two proteolytic subunits, a 76 -78 kDa subunit and an 18 kDa subunit (Lee et al., 2007).

Development of a μ-Calpain Reporter (ECFP/EYFP FRET-pair flanking the μ-Calpain substrate) from α-Spectrin by Vanderklish *et al* demonstrated a FRET reduction in cells when Ca^{2+} transients were elicited by glutamatergic agonists (Vanderklish et al., 2000). However, ensuing research brought these findings into doubt by the observation that the FRET Reporter was bound by μ-Calpain but resists cleavage (Takatsuka et al., 2005). Therefore the approach taken here was the *in vitro* development of a μ-Calpain variant that can become proteolytically active by lower Ca^{2+} concentrations (compared to the original) for the development of a FRET-based Integrator.
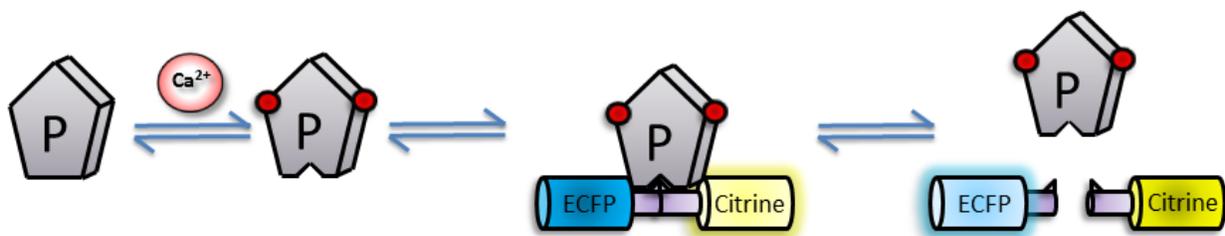
Figure 7: Schematic illustrating proposed mechanism for µ-Calpain Integrator
Upon Ca^{2+} binding to the µ-Calpain protease (P) autolysis occurs whereby the active site can bind to the substrate site (purple) located in-between enhanced CFP (ECFP) and the YFP variant "Citrine". Once cleaved the FRET pair exhibits a FRET reduction, i.e. reduced Citrine emission and increased ECFP emission upon ECFP excitation.

2.5.2 Approach 2: Artificial Ca^{2+}-dependent protease FRET Integrator

The second Integrator approach explored involved two strategies for the generation of an artificially Ca^{2+}-dependent protease that cleaves a FRET reporter. The first strategy employed the structural rearrangement of a Ca^{2+}-binding element (upon Ca^{2+} binding) in order to induce conformational changes of an inactive protease that yields a recovery of proteolytic function. The second strategy made use of a split protein architecture whereby two inactive fragments of a protease are brought together in a Ca^{2+}-dependent manner. These two fragments subsequently refold and become proteolytically active.

For both approaches the NIa protease from the Tobacco Etch Virus, the TEV protease, was selected for two primary reasons; namely the lack of TEV protease/substrate homologs in mammalian cells, and the previously demonstrated split protein application. With a structure similar to serine proteases (such as chymotrypsin and trypsin) the TEV protease is widely used in biotechnology for the endoproteolytic removal of affinity tags due to its substrate sequence specificity (Zhdanov et al., 2003).

2.5.2.1   Conformation-dependent Protease Integrator

For this strategy the Troponin C (TnC) EF-Hands III and IV (C-lobe) were chosen to be inserted into the TEV protease primarily due to the absence of endogenous TnC or TnC-interacting elements in nervous tissue. In addition, the C-lobe was chosen as this displays the largest conformational change to Ca^{2+} (Mank et al., 2008) whilst maintaining a relatively small size to maximise the likelihood of regaining proteolytic function upon Ca^{2+} binding. The proposed mechanism for this strategy employs a proteolytically-inactive TEV protease with an inserted TnC EF III+IV that undergoes conformational rearrangement upon Ca^{2+} binding to the TnC rendering a proteolytically active TEV protease. Once this occurs the TEV protease would cleave a TEV-substrate FRET Reporter (TS-FRET; ECFP- ENLYFQGS-Citrine), thus resulting in a reduction in the FRET ratio (**Figure 8**).
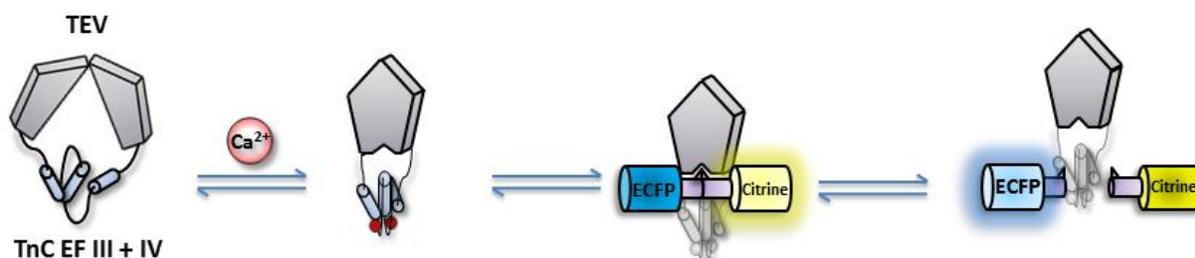
Figure 8: Schematic illustrating mechanism of conformation-induced protease activation
Upon Ca^{2+} binding the Troponin-C EF-Hands III and IV undergo a conformational change that renders the previously inactive TEV protease active whereby it binds to and cleaves a FRET Reporter that consists of CFP (ECFP) and Citrine flanking a TEV restriction site (TS-FRET).

2.5.2.2   Split TEV Integrator

The second strategy considered for the generation of an artificial Ca^{2+}-dependent protease is based on the fusion of split-TEV fragments to Ca^{2+}-dependent interacting proteins that could be used to restore protease activity in a Ca^{2+}-dependent manner (**Figure 9**). In order to apply a split-TEV strategy for the Integrator the CaM and M13 peptide were chosen from the D3cpv FRET GECI due to the computationally redesigned ΔCaM (F19L, V35A, M36L) and ΔM13 (K5Q, N7T, F8G, I9H, S12R, A14F, N15G, F17A). This redesigned interaction interface, the "bump-and-lock" interface, possesses minimal wild-type CaM (wtCaM) interference (Palmer et al., 2006).
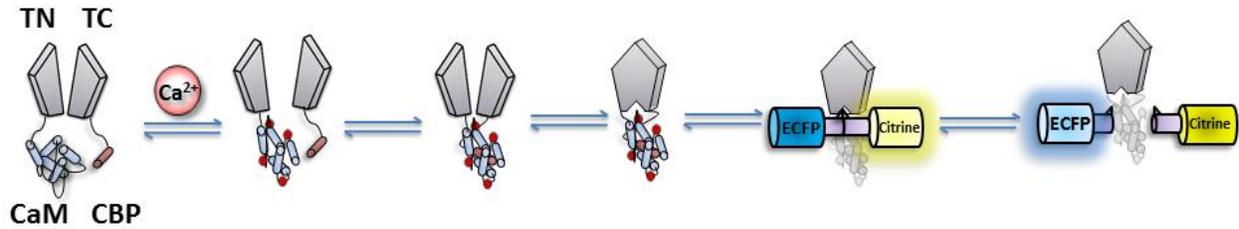
Figure 9: Schematic for split-TEV strategy.
CaM and M13 fused to N-TEV (TN; 1-118) and C-TEV (TC; 119-242) undergo a Ca^{2+} (red) dependent interaction that bring the two fragments of TEV into close proximity whereby they refold and form an active protease. Once active, the TEV protease can cleave the TS-FRET Reporter.

2.5.3 Approach 3: Bimolecular Fluorescence Complementation Integrator

In a similar approach to the split-TEV strategy, ΔCaM and ΔM13 can be fused to two fragments of a FP that would enable a Ca^{2+}-dependent recombination of two non-fluorescent fragments resulting in the recombination and recovery of FP fluorescence (**Figure 10**). Unlike the split-TEV approach this FP recombination concept has been established *in vitro* using the heterodimerising pair bJun and bFos (Hu et al., 2002). Application of the Bimolecular Fluorescence Complementation architecture confers one particular advantage over other split protein strategies, namely, due to the signal output (in this case the YFP variant "Citrine") being incorporated into the split-protein interaction the requirement for an additional FRET Reporter becomes redundant.
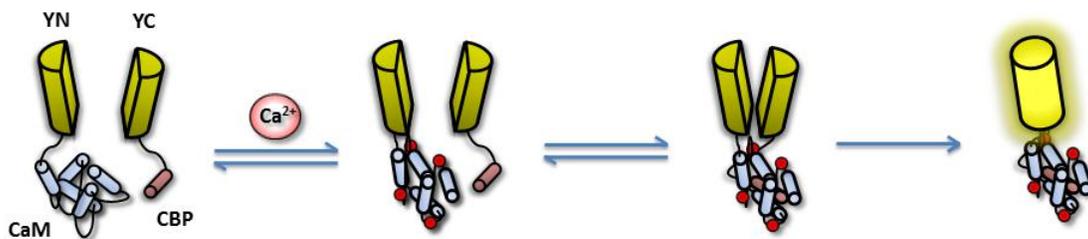
Figure 10: Schematic of Complementation Integrator.
Calmodulin (CaM) and the M13 Calmodulin-binding peptide (CBP) interact in a Ca^{2+}-dependent manner bringing two fragments of the YFP variant "Citrine", the N- (YN) and C- (YC) fragments, into close proximity where they refold and form a fluorescent protein.

3   Materials and Methods

3.1   Molecular Biology

3.1.1   Polymerase Chain Reaction

Developed in 1983 by Kary Mullis, Polymerase chain reaction (PCR) is a commonly used technique in molecular biology to amplify a distinct strand of DNA. This technique takes advantage of a thermally stable DNA polymerase with a bacterial or archeal origin. The most commonly used polymerase *Taq* (Thermus aquaticus) was the first thermostable polymerase used for PCR, however, since its discovery several other polymerases, for example *Vent* (Thermococcus litoralis) and *Pfu* (Pyrococcus furiosus), offer improved features such as increased thermostability and significantly decreased error rate of replication. Additional bioengineering strategies, for example Agilent's "Herculase II", further increase the affinity and subsequently reduced the PCR cycling times by fusing a *Pfu*-based DNA polymerase with a high affinity double-stranded DNA binding domain. Therefore, Herculase II was chosen for PCR reactions due to its enhanced reliability and high product yield (**Table 1**).

Table 1: PCR Reaction (<1.5kb)

Component	Volume (µl)
Forward Primer (100pM)	0.5 – 1
Reverse Primer (100pM)	0.5 – 1
Template DNA (100ng)	0.5 – 1
5xHerculase Buffer	10
DMSO (optional)	5
dNTPs (12.5mM)	1
Herculase II Polymerase	1
H_2O	30-37.5

All reaction components were added on ice and the PCR was initiated in a DYAD™ DNA Engine (MJ Research) at 95°C to reduce PCR primer dimerization and to increase specificity (**Table 2**). The addition of DMSO increases the yield of PCR product and was included when template DNA concentration was under 100 ng. However, in general DMSO was avoided due to the addition of DMSO resulting in an increased replication error rate.

Table 2: PCR Cycle

Cycle Temperature	<1kb	1-2kb	Step
1. 95°C	2min 20sec		
2. 95°C	20 sec		Denaturing
3. 55°C	20 sec		Annealing
4. 72°C	30 sec	1.0 min	Elongation
5. Repeat from 2.	29		
6. 72°C	3.0 min		
7. 15°C	Forever		
Total Time	1hr 18min	1hr 32min	

3.1.2   Site-directed mutagenesis

In addition to the use of PCR for the amplification of a desired fragment of DNA it can also be used for site-directed base substitutions. Mutations are introduced by substituting certain nucleotide bases in the primer sequence with the preferred sequence. To enable this, PCR primers are designed with the desired nucleotide substitutions flanked by at least 42 bases (14 codons) evenly divided between the N- and C- terminus.

Table 3: Site-Directed Mutagenesis Reaction

Component	Mutagenesis Reaction Volume (µl)	Control Reaction Volume (µl)
Forward Primer (10pM)	1	
Reverse Primer (10pM)	1	
Template DNA (100ng)	1	
5xHerculase Buffer	10	
dNTPs (12.5mM)	1	
Herculase II Polymerase	0.5	-
H$_2$O	35.5	36

Table 4: Site-Directed Mutagenesis Cycle

Cycle Temperature	Duration	Step
1. 95°C	30 sec	
2. 95°C	30 sec	Denaturing
3. 57°C	1.0 min	Annealing
4. 72°C	6.0 min	Elongation
5. Repeat from 2.	15	
7. 15°C	Forever	
Total Time	2hr 21min	

The site-directed mutagenesis protocol (**Table 3**) was performed for one or two mutation sites in parallel (one forward and one reverse primer for each mutation site). Upon site-directed mutagenesis PCR (**Table 4**) completion the template DNA was digested via addition of DpnI endonuclease (target sequence: Gm6ATC). As template DNA isolated from most *E.coli* strains is dam methylated it is susceptible to DpnI digestion which is specific for methylated and hemimethylated DNA (**Table 5**). Subsequent incubation of 1 hour was followed by transformation into XL-1 Blue competent cells, whereby 1 µl of the DpnI digested solution was used.

Table 5: DpnI Digest

Component	Mutagenesis Reaction (Herculase II PCR) Volume (µl)	Control Reaction (No Herculase II) Volume (µl)
PCR Product	20	
DpnI	1	
Incubation	4 Hours at 37°C	

3.1.3 Restriction of DNA

Restriction recognition sites are short palindromic sequences, typically 6 nucleotides in length that are recognised by restriction-site specific restriction endonucleases. These endonucleases cut the sequence between two nucleotides resulting in two overhanging "sticky ends" which are used to ligate pieces of DNA with complimentary overhangs. DNA for ligation was prepared using a "Preparative Digest" which employs restriction enzymes to digest 1-10 µg of vector (the vector backbone) or insert DNA (DNA fragment desired for insertion into the vector backbone) (**Table 6**). Additionally, DNA restrictions can also be used to determine whether the inserted DNA has successfully been integrated into the vector DNA, a process known as an "Analytical Digest".

Table 6: Restriction Digest Reaction

Component	Preparative Digest Volume (µl)	Analytical Digest Volume (µl)
DNA (100-1µg)	10	2
NEB (10x) Restriction Buffer	5	2
Bovine Serum Albumin, BSA (100x)	0.5	0.2
Restriction Enzyme #1	1	0.2
Restriction Enzyme #2	1	0.2
H$_2$O	32.5	15.4
Incubation at 37°C (hours)	16	1

3.1.4 Dephosphorylation of Vector DNA

Phosphatases catalyse the removal of 5' phosphate groups from the digested vector DNA preventing self-ligation and consequently improving the efficiency of "insert" DNA ligation into the vector. Antarctic Phosphatase was chosen for this step due to the requirement of heat-inactivation of the phosphatase (**Table 7**).

Table 7: Dephosphorylation of Vector

Component	Volume (µl)
Vector DNA (1-10µg)	30
NEB (10x) Antarctic Phosphatase Buffer	4
NEB Antarctic Phosphatase	1
H_2O	5
Incubation at $37^{o}C$ (hours)	1-2
Deactivation at $70^{o}C$ (min)	15

3.1.5 DNA ligation

DNA ligation can either be performed using a "blunt-end" ligation (ligates DNA without overhanging restriction sites) or "sticky-end" ligation (utilises digested DNA). Sticky-end ligation was performed due to the higher ligation yield generally obtained. In addition, DNA ligases are used to facilitate ligation as these catalyse the formation of phosphodiester bonds between juxtaposed 5' and 3' termini. The most commonly used ligase, isolated from bacteriophage T4, is the T4 DNA Ligase that exhibits optimal activity at $25\ ^{o}C$ (**Table 8**). The molar ratio of vector to insert DNA used in this reaction was that of 1:3 to 1:5. These concentrations were estimated by agarose gel electrophoresis.

Table 8: DNA Ligation

Component	Ligation Volume (µl)	Vector Control Volume (µl)
Vector DNA	1	1
Insert DNA	3	-
NEB Ligase Buffer (10x)	2	2
T4 DNA Ligase	1	1
H_2O	13	16
Incubate	3 hours at $25^{\circ}C$	

3.1.6 *Preparation of chemically-competent* E.coli

4 ml LB medium, inoculated with the desired *E.coli* strain, was incubated without antibiotics overnight at 37 $^{\circ}$C shaken at 250 rpm. 1 day cultures were added to 300 ml LB medium and grown to an OD_{600} of 0.5-0.6 before incubation for 20 min on ice. Cells were harvested by centrifugation at 2500 g for 20 min at 4 $^{\circ}$C. The supernatant was discarded and the cells were resuspended with 60-80 ml of cooled Inoue transformation buffer. Cell suspension was subsequently centrifuged at 2500 g for 15 min at 4 $^{\circ}$C and resuspended with 20ml cooled Inoue transformation buffer supplemented with 1.5 ml DMSO. The suspension was incubated on ice for 10min before being aliquoted (50 µl) and stored at -80 °C.

3.1.7 *Preparation of electro-competent* E.coli

20ml antibiotic-free LB medium, inoculated with the desired strain of *E.coli*, was grown overnight and added to 1 l pre-warmed LB medium (37 °C). Cells were subsequently grown to an OD_{600} of 0.4- 0.5 and the culture was incubated on ice for 10 min before harvest (centrifugation 2500 g for 10min at 4 °C). The supernatant was discarded and cells were resuspended in 150 ml of 10 % Glycerol and additionally incubated on ice for 1 hour. Centrifugation and resuspension steps were repeated three times, each time reducing the volume of 10 % glycerol, from 50 to 20 to finally 0.5 ml glycerol. Electro-competent *E.coli* were aliquoted in 50 µl aliquots and stored at -80 °C until required.

3.1.8 *Transformation of chemically-competent* E.coli

Chemically competent cells XL-1 Blue and BL21 were used for DNA replication and protein expression respectively. Cells were thawed on ice and transformed with 10 μl of the ligation mix and incubated on ice for 20min. Cells were subsequently heat-shocked for 1 min at 42 °C before 2 min incubation on ice. Transformations using ampicillin-resistant bacteria were plated out on ampicillin containing LB-agar plates. Bacteria with other antibiotic resistance were incubated with 200 μl antibiotic-free LB-media for 1 hour at 37 °C before plating on LB-agar plates containing the appropriate antibiotics.

3.1.9 *Transformation of electro-competent* E.coli

Electroporation of electrically-competent *E.coli* was performed when a high yield of transformed bacteria was desired. Cells were thawed on ice and added to a 2 ml pre-cooled electroporation cuvette (Peqlab) with 1-2 μl of DNA. An 1800 V electrical pulse (Equibio) was applied and 200 μl-1 ml SOC medium was immediately added (Invitrogen). Cells were incubated for 1 hour at 37 °C before subsequent plating on LB-agar plates supplemented with the appropriate antibiotic.

3.1.10 *Transposon Reaction and Screening*

Transposons are mobile prokaryotic or eukaryotic DNA sequences that can transpose themselves into new positions within the genome of individual cells. Since their first identification, over 60 years ago (McClintock, 1950), they are viewed as symbiotic as they contain antibiotic resistance genes that assist cell survival. In prokaryotic systems, the cell provides the cellular environment for element transposition (Wiegand and Reznikoff, 1992). The Tn class, a bacterial class of transposase, are used extensively in molecular biology as these single subunit transposases were subject to a triple mutation to yield hyperactive transposition (Hoffman and Jendrisak, 2002). These hyperactive transposases are ideal for in-vitro transcription studies. In this research, the EZ-Tn5[TM] in-frame Linker Insertion Kit (Epicentre)

(**Table 9**) was utilised. Hereby a random sequence was inserted that can be read in any of the three reading frames and encodes a NotI Kanamycin resistant gene flanked by 57 bp.

Table 9: Transposon Reaction

Component	Volume (µl)
Target DNA	2
EX-Tn5 Reaction Buffer (10X)	1
EZ-Tn5 <NotI/KAN-3> Transposon	0.8
H_2O	5.2
EZ-Tn5 Transposase	1
Incubate	2 hours at 37°C
EZ-Tn5 Stop solution (10X)	1
Incubate	10 minutes at 70°C

Upon completion of the transposon reaction, 1 µl of the reaction was added to XL-1 Blue electrocompetent cells and electroporated before transferral to agar plates with Kanamycin and Ampicillin antibiotics.

3.1.10.1 Transposon Screening

Due to the stop codon located at the end of the insertion fragment, bacterial colonies possessing the Transposon fragment could be selected for via selection of non-fluorescent bacterial colonies. The positive colonies were subsequently digested to remove the transposon before being re-streaked (**Figure 11**). Once colonies were selected via mCherry fluorescence (after transposon removal) the location of the insertion was determined from the original colony (with transposon inserted) via restriction digest and subsequent agarose gel electrophoresis. Chosen samples were subsequently purified either with the Transposon or with Troponin C EF-hands III + IV inserted.
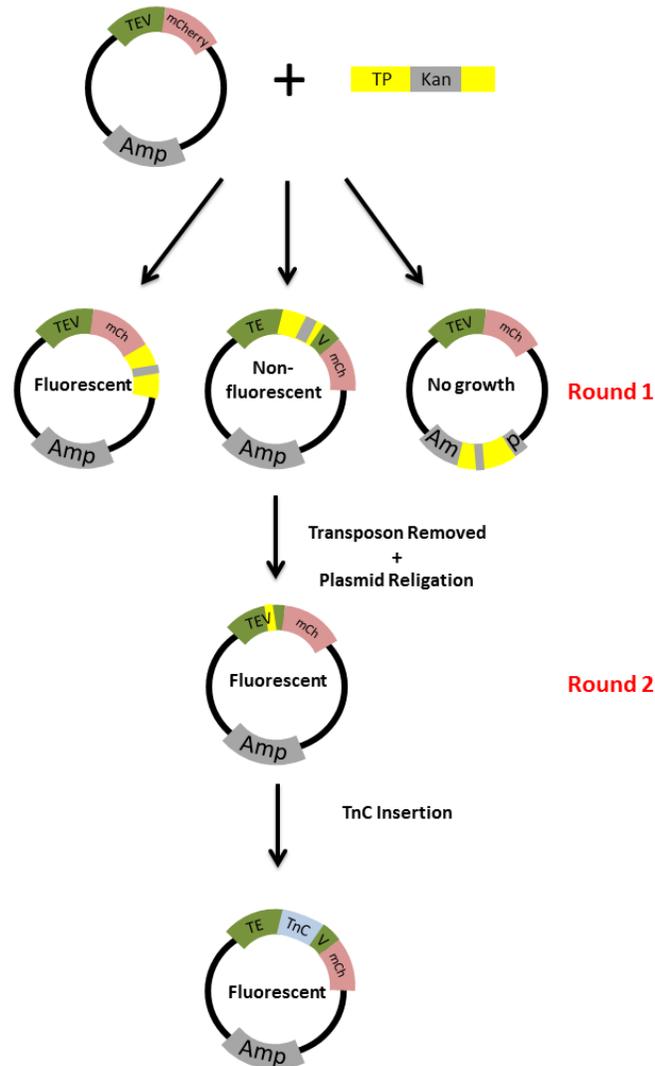
Figure 11: Transposon screening strategy
Schematic of screening strategy for ΔTEV-mCherry (mCh)-pRSETB. Random insertion of transposon fragment yields three outcomes for Round 1 of screening; i) fluorescent cells where the transposon is inserted downstream of mCherry, ii) non-fluorescent cells where the transposon is inserted before mCherry, or iii) no colony growth where the transposon interferes with the Ampicillin resistance. Round 2 of screening identified mCherry fluorescent colonies (with Transposon removed), after which a sample were selected for Troponin C (TnC) EF-hand III + IV insertion.

3.2 Protein Biochemistry

3.2.1 Protein Expression

For recombinant protein expression the cDNA of interest was cloned into the Multiple Cloning Site (MCS) of either pRSETB or pRSFDuet plasmid. Two features of these plasmids enable the successful expression and purification of the protein of interest; i) both plasmids carry a T7 RNA polymerase promoter that directs high-level expression in *E.coli* and ii) with the addition of a 6xHis-tag on either the N- or C- terminus the protein can be purified via affinity purification The plasmid, containing the cDNA of interest, was transformed into the *E.coli* strain BL21 before overnight incubation at 37 ^{o}C (200 rpm) in 5 ml of LB medium containing the corresponding antibiotic (50 mg/ml 1: 500). Pre-culture was used to inoculate 200 ml LB medium containing 1: 1000 antibiotic and incubated at 37 ^{o}C until an OD_{600} of 0.6 was reached. Protein expression was induced with 1mM Isopropyl-β-D-1-thiogalactopyranoside (IPTG) for 3-4 hours at 200 rpm at 25 ^{o}C. Bacterial cells containing the protein of interest were subsequently harvested by centrifugation (Sorvall) at 6000 g for 10 min at 4 ^{o}C and resuspended in 10 ml protein resuspension buffer supplemented with protease inhibitors (1 mM PMSF, 5 µg/ml Pepstatin and 1 µg/µl Leupeptin) In the purification of proteases the appropriate protease inhibitors were omitted. The resuspension was frozen at -80 ^{o}C to induce cell lysis and for storage.

3.2.2 Protein Purification

Cells were lysed using 1 mg of Lysozyme for 30 min on ice. Cell membranes were solubilized by the addition of 0.1 % Triton-X-100 detergent, 5 µg/ml DNAse and 5 µg/ml RNAse before the final lysis step by ultrasonification (Sonorex Ultrasonic Bath, Bandelin) for 30 min at 4 ^{o}C. Following centrifugation at 13,000 rpm the protein extract was loaded in to 400 µl Ni-NTA agarose beads (Quiagen) and incubated for 2 hours at 4 ^{o}C. Gravity flow purification was undertaken using a polypropylene column (Quiagen). Ni-NTA beads were washed with the resuspension buffer containing 10 mM imidazole in order to remove weakly bound protein.

Recombinant proteins are then eluted by the elution buffer containing a high concentration of 150 mM imidazole and 10 % glycerol. The protein was stored at -80 ^{o}C.

3.2.3 Western Blot

Dissociated hippocampal neurons were cultured in 12-well glass-bottom plates (MatTek). Cells were washed with 1x PBS before being lysed and boiled at 100 ^{o}C for 15 min. Protein concentration was determined using the Bradford Assay (Bio-Rad) and the absorbance at 595 nm was measured (TECAN plate reader, Tecan). 25 µg of protein was separated by SDS-PAGE using 10% Separation Gels. Gels were transferred to a nitrocellulose membrane via semi-dry blotting. Membrane was blocked for 1 hour in a non-fat milk buffer (5 % milk in 1x TBS-T) and subsequently incubated overnight at 4 ^{o}C in an anti-GFP primary antibody (1: 1000; Research Diagnostics Inc.). After six 5 min washing steps in 1x TBS-T the membrane was incubated with the anti-rabbit secondary antibody (1: 1000; Invitrogen) before an additional 30 min washing period. Membrane was immersed in an ECL solution (Santa Cruz) for 1 min and developed using Amersham Hyperfilm (GE-Healthcare). The membrane was additionally washed for 30 min before incubation for 1 hour with the anti-tubulin loading control antibody (1: 5000; Abcam). The membrane was subsequently incubated with the anti-mouse secondary antibody (1: 1000; Invitrogen) and developed using the technique described above.

3.3 Spectroscopy

3.3.1 *Fluorescent spectra of purified proteins*

Protein concentration was determined using a Nanodrop (Peqlab) and a 0.75 µM concentration per protein was used for each experiment unless otherwise stated. Fluorescence was measured using the fluorescence spectrophotometer (Varian). Proteins were diluted in 10 mM MOPS buffer containing 100 mM KCl and 25 µM EGTA in order to set the Ca^{2+} free ion concentration to zero. Additionally, 1 M $CaCl_2$ and $MgCl_2$ stock solutions were added (1: 1000) for experiments requiring 1 mM $CaCl_2$ and 1 mM $MgCl_2$. FRET fluorescence was measured at excitation and emission wavelength of 432 and 450-600 nm respectively (bandwidth 5 nm). For complementation the fluorescence measurement was carried out at an excitation and emission of 500 and 510-600 nm respectively (bandwidth 5 nm).

The following formula was used to calculate the ΔR/R for FRET changes:

$$\frac{\Delta R}{R} [\%] = \frac{R_{Max} - R_{Min}}{R_{Min}} * 100$$

Where:

Ratio (R) = Peak $\frac{Citrine}{CFP} = \frac{527nm}{475nm}$

R_{Max} = Ratio of Ca^{2+}-bound

R_{Min} = Beginning Ca^{2+} value at 0min

The same formula was applied for calculating the change in complementation fluorescence; however the ratio was replaced by a single wavelength fluorescence to generate ΔF/F. For experiments requiring a temperature of 37 °C a H_2O circulated cell holder (Varian) was used in conjunction with a water bath (Julabo). The peptide screen was performed using a 96-well plate and a 2 mM $CaCl_2$ concentration to induce detectable differences in spontaneous versus inducible complementation.

3.3.2   Spectroscopic determination of EC_{50}

Determination of the EC_{50} via Ca^{2+} titrations of biosensors required two proteins; the YN-CaM and the CBP-YC recombinant protein. Protein concentrations were determined using a Nanodrop (Peqlab) and 0.75 µM were combined in a total volume of 50 µl. These were subsequently frozen in liquid nitrogen and stored at -80 °C. For the determination of EC_{50} two Ca^{2+} solutions were prepared in accordance with previous literature (Tsien and Pozzan, 1989). The two solutions were combined in order to give a desired concentration of free Ca^{2+} ions determined by the Maxchelator program "Webmaxc" (**Table 10**). Upon addition of the protein solution to the series of Ca^{2+} solutions a 4 hour incubation time was undertaken either at room temperature or 37 °C.   Once fluorescence was recorded the ΔF/F (or ΔR/R) values were normalized to the highest value before plotting the log_{10} values of the free Ca^{2+} points using Origin 8.1. Determination of the EC_{50} values was achieved by sigmoidal fit.

Table 10: Ca^{2+} Titration Solution

Calcium Concentration at 37°C (µM)	Calcium Concentration at 25°C (µM)	10mM Ca₂EGTA Volume (µl)	10mM K₂EGTA Volume (µl)
0	0	-	950
0.083	0.1010	375	575
0.120	0.1394	450	500
0.228	0.2655	600	350
0.373	0.4337	700	250
0.711	0.826	800	150
1.1	1.3	850	100
2.3	2.7	900	50
4.0	4.6	920	30
6.0	6.9	930	20
11.3	12.9	940	10
20.9	23.4	946	4
27.2	29.8	948	2
36.0	38.7	950	-

3.4 Cell Culture

3.4.1 *Preparation of dissociated hippocampal neurons*

All of the following methodology was conducted in a laminar flow hood using sterilized equipment and standard aseptic techniques. Primary hippocampal neurons derived from rat embryos were removed and cultured as previously described (Audesirk et al., 2001) . Pregnant female E18 Wistar rats were sacrificed using CO_2 before opening of the abdomen and removal of the embryos. Using micro-dissection forceps and dissecting scissors the embryos were removed from the uterus and placed into a PBS-filled petri dish before decapitation and transferral of the heads to an additional PBS-filled dish. Using forceps the head was anchored to allow the opening of the longitudinal fissure. Once extracted, the brain was separated into the two hemispheres and the meninges were removed before final separation of the hippocampi from the adjacent tissue using a dissection microscope (Leitz). The hippocampi were then transferred to a 2 ml Trypsin solution (7 µM Hepes) pre-warmed to 37 °C. After five minutes incubation at 37 °C the hippocampi were dissociated by trituration. The triturated solution was then centrifuged at 2000 rcf for 2 min before the Trypsin solution was aspirated and the hippocampi were resuspended in 1 ml PBS with 1 % Pen/Strep. The neurons were centrifuged at 2000 rcf for 2 min before resuspension in 2 ml DMEM enriched with 10 % FCS and 1 % Pen/Strep and pre-warmed to 37 °C.

Glass-bottom culture dishes (35mm, MatTek) or µ-Dishes (Ibidi) were incubated overnight with Poly-L-Lysine before being washed with 1x PBS and the addition of 2 ml DMEM enriched with10% FCS and 1% Pen/Strep and subsequent incubation at 37°C, 5% CO_2 (Heracell, Thermo Scientific). Neurons were counted using a haemocytometer and plated at a density of 200,000 cells per dish. The medium was replaced after 12 hours by Neurobasal media supplemented with B27 and 60 mM NaCl and were retained for up to 1 week.

3.4.2   Passaging immortal cell lines

Upon reaching 80 % confluency the HEK293T cell line was washed with 1x PBS before addition of 2ml Trypsin and incubated for 5min at 37°C. Once cells detached 8 ml DMEM solution (DMEM enriched with 10% FCS and 1% Pen/Strep was added and the cells were triturated before seeding. For either 3.5 cm or 10 cm culture dished the seeding ration was 1:10 triturated solution to DMEM solution.

3.4.3   Transient transfection of mammalian cells

Delivering DNA to mammalian cells can be achieved by several methods, with some relying on physical manipulation (e.g. electroporation), the use of chemicals (e.g. Ca^{2+} phosphate), or lipofection. Lipofection utilises liposomes carrying genetic material to merge to the phospholipid bilayer of the cell membrane. This method is advantageous for several reasons; not only does it deliver a high transfection efficiency but also exhibits low toxicity, cell type versatility and a high level of reproducibility. The lipofection reagent Lipofectamine 2000 (Invitrogen) was used for transfection of both dissociated hippocampal neurons and immortal cell lines with the DNA of interest in the MCS of pCDNA3. For 35 mm glass-bottom culture dishes 7 µl of lipofectamine were incubated for 5 min with 250 µl of Opti-MEM in order to allow lipid vesicle formation. After vesicle formation 250 µl of Opti-MEM (with 1-3 µg DNA) were incubated at 25 ^{o}C for 20 min for DNA incorporation into lipid vesicles. During this time the cell culture dishes were prepared for transfection. For dissociated neurons this required the removal and storage of 500 µl conditioned media and for immortal cell lines this required a complete replacement of media containing antibiotics with antibiotic-free media. 500 µl of transfection mix was added to the plates and incubated at 37 ^{o}C with 5 % CO_2 for 3 hours prior to the replacement of the media/transfection mix with DMEM solution or Neurobasal (60 mM NaCl).

3.5 Generation of Semliki Forest Virus

The Semliki Forest Virus (SFV), a member of the alphavirus genus, is a positive-stranded RNA virus with an icosahedral capsid enveloped by a lipid bilayer that originated from the host cell. This dual plasmid infection system requires a helper plasmid (pSCA-Helper) that encodes the SFV structural proteins and the pSCA-1 plasmid yielding the coding sequence for the cDNA of interest and the packaging signal for the SFV.

10 cm dishes of HEK293T cells were incubated at 37 $^{\circ}$C with 5 % CO_2 until 70 % confluent before transient transfection of the two plasmids. In preparation for transient transfection the DMEM solution was removed from the HEK293T cells before washing with 1x PBS and the subsequent addition of 5 ml antibiotic-free DMEM solution. 40 µg total DNA at a ratio of 3:2 (pSCA-DNA: pSCAHelper) was added to a solution containing 50 µl Lipofectamine 2000. After a 30 min incubation period this solution was added to 10 cm dishes and allowed to incubate at 37°C with 5% CO_2 overnight (NuAire Incubator). The next morning, after verification of transfection by fluorescence microscopy (Olympus), the medium was changed and cells were incubated for an additional 2 days. The supernatant was subsequently and cellular debris was removed via 10 min centrifugation at 2500 g and 4 $^{\circ}$C. The viral particles were rescued by ultracentrifugation at 20,000 rpm for 90 min at 4 $^{\circ}$C (Beckman Coulter) and the supernatant was completely removed (95 % by aspiration, 5 % by 10 min ultracentrifuge tube inversion). The virus particles were resuspended in 200µl TBS and incubated overnight at 4 $^{\circ}$C. Specifically designed mutations within the glycoprotein render the virus inactive until the virus is proteolytically treated. This was achieved by incubation with α-chymotrypsin (1: 20 dilution) for 45 min at room temperature before protease inactivation with aprotinin (1: 15 dilution) for 10 min. Activated virus was aliquoted and stored at -80°C.

3.6   Dissociated Hippocampal neuron assays

Neurons possess several types of voltage-gated ion channels that function in response to a change in the electrical potential across the neuron. In order for neurons to exhibit such variety in firing response (i.e. burst firing, slow wave firing) several types of voltage-gated ion channels exist, each with its own response profile. One type of voltage-gated ion channel is the voltage-dependent Ca^{2+} channels, a group of gated channels that are activated upon membrane depolarization causing a Ca^{2+} influx that can induce dendritic neurotransmitter release amongst other roles. These channels are classified according to their response to current type, and are categorised as L-Type, N-Type, P/Q-Type, or R-Type. Ca^{2+} influx via the opening of voltage-gated Ca^{2+} channels result in increased intracellular Ca^{2+} concentrations.

3.6.1   12-well plate Electrical Field Stimulation

Using a 12-well plate one can apply Electrical Field Stimulation for varied time durations and record the cumulative output from many neurons. Neurons were therefore cultured for 3-6 days in 12-well culture plates (MatTek or Becton Dickinson) in Neurobasal (B27, 60mM NaCl). Transient transfection of cDNA or infection of SFV was subsequently carried out followed by media replacement. The lid was exchanged for a custom-built lid with 12 parallel pairs of platinum electrodes with 1 cm separation. This was connected to a custom built stimulator device and the culture plate was placed back in the 37 ^{o}C incubator. The stimulation protocol was initiated and wells were activated in a series of one hour steps (**Figure 12**) for 4 hours. The neurons were imaged with the iMIC Microscope (Till Photonics). For separate CYP and YFP imaging CFP and Citrine were imaged with an excitation wavelength of 432 nm and 505 nm respectively using a Dualband CFP/YFP filter; Exc1: BP 430/24, Exc2: BP 490/20. The emission was separated into CFP and YFP images using a Dualband CFP/YFP filter and a dichrotome dual-emission extension inbuilt into the iMIC. For FRET imaging both YFP and CFP were imaged using the CFP excitation wavelength. Image recording was performed using the dual-emission extension followed by image analysis using ImageJ software (NIH). Statistical analysis was performed using a one sample t-test.
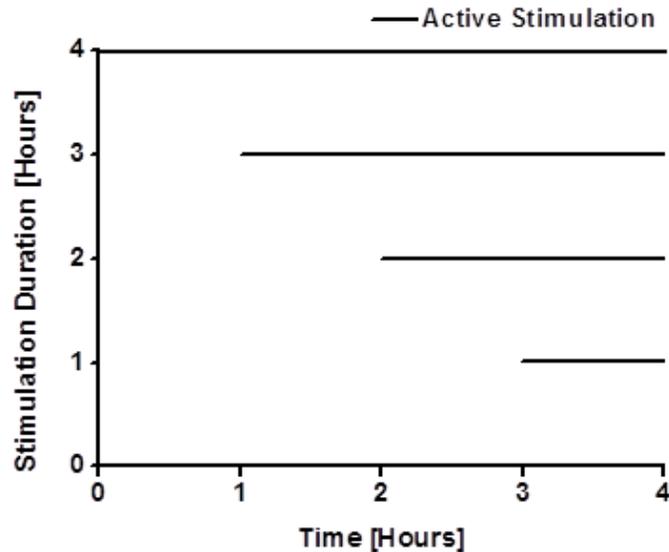
Figure 12: Electrical Field Stimulation of 12-well plates
Stimulation of dissociated hippocampal neurons with 4 hour stimulation was initiated at the beginning of the experiment and 3, 2, 1 hour stimulations were subsequently initiated to ensure the same experimental end point.

3.6.2   Electrical Field Stimulation for live-cell fluorescence microscopy

Neurons were cultured on 35 mm culture dishes for 3-4 days before experiment initiation. Glass-bottom μ-dishes (Ibidi) were used for imaging at 37 °C with the addition of a heating chamber (Ibidi). Culture dish media was exchanged for a HEPES buffered solution and allowed to equilibrate to 37 °C for 5 min. Upon being placed on the imaging stage two parallel platinum electrodes 1 cm apart were placed in the solution and connected to a triple output DC power supply (Agilent) via a custom built amplifier. Stimulus protocols were modified via LabView connected to a waveform generator (Agilent) and upon protocol execution the stimulation bursts were monitored by a 30 MHz Oscilloscope (Grundig). Cells were imaged at 5 min intervals using an iMIC as detailed in the section above and images were analysed using ImageJ software.

3.6.3   Fluo-4 AM Ca²⁺ dye imaging

In order to detect neuronal activity directly once can use the visualisation of Ca^{2+} transients using synthetic Ca^{2+} dyes such as Fluo-4 AM (Invitrogen). For use in 35 mm glass bottom culture dishes (MatTek) the 50 µg Fluo-4 AM aliquots were resuspended in 50 µl DMSO and a final Fluo-4 concentration of 5 µM was applied for 30 min. Media replacement and a 30 min incubation ensured de-esterification. Culture dishes were mounted on a 135 TV Axiovert Microscope possessing a 515 nm LED excitation wavelength. Field stimulation was applied as previously described and images were taken using an iXonEM+ Camera System (Andor Tech). Analysis was performed using ImageJ software.

3.6.4   LIVE/DEAD Viability/Cytotoxicity Assay

When performing cell stimulation experiments one vital consideration is whether the experimental paradigm can cause unwanted cellular toxicity leading to premature apoptosis. Viability assays can be used to determine the ratio of healthy to apoptotic cells via probes engineered to detect each condition. The LIVE/DEAD assay utilized two probes; Calcein AM and Ethidium Homodimer-1 (EthD-1). Live cell esterase activity converts the cell-permeant Calcein AM non-fluorescent probe to the fluorescent Calcein (excitation 495nm, emission 515nm). Contrastingly, EthD-1 cannot permeate intact membranes; however, once the membrane is damaged the probe can enter the nucleus where it undergoes a 40-fold enhancement in fluorescence (excitation 495nm, emission 635nm). The feature of fluorescence enhancement upon cellular interaction yields this dual-probe particularly beneficial as there is no background fluorescence. Upon completion of the 12-well Electrical Field Stimulation the cells were incubated with 1 µM Calcein and 6 µM EthD-1 in 1x PBS for 30 min before imaging Calcein (excitation 495nm ±15nm, emission CFP/YFP) and EthD-1 (excitation 495nm ±15nm, emission ET630/75nm). Cell counting was achieved using ImageJ and the percentage of cell survival was calculated using the following equation:

$$Cell\ Survival\ [\%] = \frac{Healthy\ Cell\ Population\ (Calcein)}{Total\ Cell\ Population\ (Calcein + EthD - 1)} * 100$$

3.7 Materials

3.7.1 Instruments

Instrument Name	Supplier
1103 Polychrome control Unit	Till Photonics (Germany)
135 TV Axiovert Microscope	Carl Zeiss (Germany)
30 MHz Oscilloscope	Grundig (Germany)
Arbitrary Waveform Generator (20mHz)	Agilent (USA)
Autoflow CO2 Water-Jacketed Incubator	NuAire, Plymouth (USA)
Cary 100 Scan UV-Visible Spectrophotometer	Varian (Australia)
Cary Eclipse Fluorescence Spectrophotometer	Varian (Australia)
Cary H_2O Circulated Cell Holder (Cary Eclipse)	Varian (Australia
CKX414 Inverted Microscope	Olympus (Japan)
Dissecting Microscope	Leitz (Germany)
DYAD^{TM} DNA Engine	MJ Research Inc. (USA)
EasyjecT Prima	Equibio (Germany)
GelDoc 2000 Videosystem	BioRad (USA)
Heracell 240 CO_2 Incubator	Thermo Scientific (USA)
HT200 Heating Chamber	Ibidi (Germany)
ImageJ Image Processing Program	National Institutes of Health (USA)
iMIC Digital Microscope	Till Photonics (Germany)
iXonEM+ Camera System	Andor Tech (USA)
M205 FA Fluorescence Microscope	Leica (Germany)
MB-5 Heating Circulator	Julabo (Germany)
Nanodrop 1000 Spectrophotometer	Peqlab (Germany)
Optima LE-80K Ultracentrifuge	Beckman Coulter (USA)
Origin 8.1 Software	OriginLab Corporation (USA)
PCO- Imaging Sensicam	Till Photonics (Germany)
Polychrome V	Till Photonics (Germany)
RC-5B Refrigerated super speed centrifuge	Sorvall (USA)
Sonorex Digital Ultrasonic Bath	Bandelin (Germany)
TECAN Plate Reader (GENios^{TM})	Tecan (USA)
Triple Output DC Power Supply	Agilent (USA)

3.7.2 Consumables

Consumable Name	Supplier
µ-Dish 35mm High	Ibidi (Germany)
2mm Electroporation Cuvettes	Peqlab (Germany)
Amersham Hyperfilm ECL	GE-Healthcare (USA)
Anti-GFP primary antibody	Research Diagnostics (USA)
Anti-Mouse secondary antibody	Invitrogen (USA)
Anti-Rabbit secondary antibody	Invitrogen (USA)
Anti-Tubulin primary antibody	Abcam (USA)
BCA Protein Assay kit	Pierce (Germany)
Bovine Serum Albumin (BSA)	Sigma (USA)
Dulbecco's modified Eagle's medium (DMEM) w/o Sodium Pyruvate; w/ 4500 mg/ml Glucose; w/ Pyridoxine-HCl	Invitrogen (USA)
Dulbecco's modified Eagle's medium /F12	Invitrogen (USA)
Falcon Tissue Culture Plate, 12 Well	Becton Dickinson (USA)
Fetal Bovine Serum	Gibco (USA)
Fluo-4 AM Calcium Dye	Invitrogen (USA)
Glass Bottom 12-Well Culture Plates Nr. P12G-0-14-F	MatTek Corp. (USA)
Glass Bottom Culture Dishes 35mm, Nr. P35G-0-14-C	MatTek Corp. (USA)
Herculase II Fusion DNA Polymerase	Stratagene (USA)
His Mag Sepharose Ni	GE Healthcare (UK)
Lipofectamine 2000	Invitrogen (USA)
LIVE/DEAD Viability/Cytotoxicity Kit	Molecular Probes (USA)
µ-Calpain (Porcine Erythrocytes)	Merck (Germany)
NeuroBasal medium	Gibco (USA)
Ni-NTA Agarose	Qiagen (Germany)
Opti-MEM I	Invitrogen (USA)

Polypropylene Columns	Qiagen (Germany)
Pure Yield Plasmid Midiprep System	Promega (USA)
QIAquick Gel Extraction Kit	Qiagen (Germany)
QIAquick Miniprep Kit	Qiagen (Germany)
QIAquick PCR Purification Kit	Qiagen (Germany)
Restriction Enzymes	New England Biolabs (USA)
SOC medium	Invitrogen (USA)
T4-Ligase	New England Biolabs (USA)
Western Blot Luminol	Santa Cruz Biotechnology (USA)

3.7.3   Buffers and Solutions

Name	Supplier
Ca_2EGTA Solution for Ca^{2+} Titrations	10 mM $K_2CaEGTA$ 1 mM $MgCl_2$ MOPS Buffer pH7.2 (up to 50ml)
DMEM/10 % FCS	500 ml DMEM 50 ml FCS, heat-inactivated
DNA Gel Loading Buffer (10 x)	100 mM Tris/HCl, pH 7.5 10 mM EDTA 50 % Glycerol 1 % Orange G
Electrical Field Stimulation Solution	135 mM NaCl 5 mM KCl 1.5 mM $CaCl_2$ 1.5 mM $MgCl_2$ 20 mM HEPES 10 mM Glucose pH: 7.4
HBSS	25 mM HEPES pH 7.4 140 mM NaCl 5 mM KCl 1 mM $CaCl_2$

	1 mM $MgCl_2$
	1 mM Glucose
	0.25% BSA
Inoue Transformation Buffer for competent cells	10 mM PIPES, pH 6.7
	250 mM KCl
	15 mM $CaCl_2$
	55 mM $MnCl_2$
K_2EGTA Solution for Ca^{2+} Titrations	10 mM K_2EGTA
	1.5549 mM $MgCl_2$
	MOPS Buffer pH7.2 (up to 50ml)
LB (Luria-Bertani) medium	20 g/l LB broth base pH 7,0
	in $ddH_2$0
LB Agar	LB Medium
	15 g Agar
	in 1 l ddH_2O
Lysis Buffer	250 mM Tris pH 7.5
	5 mM $MgCl_2$
	130 mM NaCl
	10 mM KCl
	1% Triton-X
	5% Glycerin
MOPS Buffer for fluorescence spectroscopy	10 mM MOPS, pH 7.5
	100 mM KCl
MOPS Buffer for Ca^{2+} Titrations	10 mM MOPS, pH 7.2
	100 mM KCl
Neurobasal/B27	500 ml Neurobasal medium
	10 ml B27 supplement
Neurobasal/B27 for Electrical Field Stimulation	500 ml Neurobasal medium
	10 ml B27 supplement
	60 mM NaCl
PBS (10 x)	100 mM Na_2HPO_4, pH 7.4
	20 mM KH_2PO_4
	1.37 M NaCl
	27 mM KCl
Poly-L-Lysine	0.01 % (w/v) Poly-L-Lysine Hydrobromide in H_2O
Protein Resuspension Buffer	20 mM $NaPO_4$, pH 7.8

	300 mM NaCl
10% SDS-PAGE Separation Gel	1.25ml 40% Acrylamide Mix
	1.25ml 1.5 M Tris (pH 8.8)
	50 µl 10% SDS (pH 7.2)
	50 µl 10% APS
	2 µl TEMED
	2.4 ml H_2O
5% SDS-PAGE Stacking Gel	250 µl 40% Acrylamide Mix
	250 µl 1.5 M Tris (pH 6.8)
	20 µl 10% SDS (pH 7.2)
	20 µl 10% APS
	2 µl TEMED
	1.44 ml H_2O
10x SDS-PAGE Running Buffer	250 mM Tris Base
	1.92 M Glycin
	1% SDS
	H_2O to 1 liter
TAE (10 x)	8.4 g Tris base
	11.4 ml glacial acetic acid
	20 ml of 0.5 M EDTA, pH 8.0
	H_2O to 1 liter
TAE (1 x)	40 mM Tris-acetate
	1 mM EDTA
10x TBS	200 mM Tris base
	1.37 M NaCl
	pH 7.6
	H_2O to 1 liter
1x TBS-T	100 ml 10x TBS
	900 ml H_2O
	1 ml Tween 20
10x Western Blot Transfer Buffer	250 mM Tris base
	1.92 M Glycerine
	H_2O to 1 litre

3.7.4 Chemicals

Chemical Name	Supplier
Agar	Sigma (USA)
Ampicillin, sodium salt	Roth (Germany)
Anhydrotetracycline hydrochloride	Sigma (USA)
BAPTA, tetrapotassium salt	Molecular Probes (USA)
Ca^{2+} Calibration Buffer Kit	Molecular Probes (USA)
Calcium Carbonate	Sigma (USA)
Calcium Chloride, dihydrate	Sigma (USA)
DMSO (Dimethylsulfoxide)	Roth (Germany)
Ethylene glycol tetraacetic acid (EGTA)	Sigma (USA)
Glucose (D-(+)-Glucose anhydrous, min 99%)	Sigma (USA)
Glycine	Merck (Germany)
HEPES free acid	Sigma (USA)
Imidazole	Merck (Germany)
Ionomycin, calcium salt	Sigma (USA)
Kanamycin, sulphate	Roth (Germany)
Leupeptin hydrochloride	Sigma (USA)
L-Glutamic acid	Roth (Germany)
Lysozyme	Sigma (USA)
Magnesium chloride hexahydrate	Merck (Germany)
MG-132 (Z-Leu-Leu-Leu-al)	Sigma (USA)
MOPS	Merck (Germany)
Nimodipine	Merck (Germany)
Penicillin-Streptomycin	Gibco (USA)
Pepstatin A	Sigma (USA)
Phenylmethylsulfonylfluoride (PMSF)	Sigma (USA)
PIPES	Sigma(USA)
Poly-L-lysine hydrobromide	Sigma (USA)

Potassium chloride	Merck (Germany)
Potassium Hydroxide	Merck (Germany)
Sodium bicarbonate	Sigma (USA)
Sodium chloride	Sigma (USA)
Sodium phosphate monobasic, anhydrous	Sigma (USA)
Tetrodotoxin (TTX)	Merck (Germany)
Triton-X-100	Sigma (USA)
Trizma Base	Sigma (USA)
Trypsin	Sigma (USA)
Trypsin-EDTA	Gibco (USA)
Yeast extract	Sigma (USA)

3.7.5 Plasmids, bacterial strains and cell-lines

Plasmid Name	Supplier
pRSETB	Invitrogen (USA)
pCDNA3	Invitrogen (USA)
pRSFDuet-1	Novagen (Germany)
pSCA-1	University of Toronto (Dr. Bremner)
pSCA-Helper	University of Toronto (Dr. Bremner)
Bacterial Strain	**Supplier**
BL21(DE3)	Invitrogen (USA)
TransforMax^{TM} EC100^{TM} Electrocompetent *E.coli*	EpiCentre (USA)
XL-1 Blue	Invitrogen (USA)
Mammalian Cell Line	**Supplier**
HEK 293T	ATCC (USA)
Hela	Invitrogen (USA)

4 Results

In order to develop this novel biosensor several progressive stages were undertaken (**Figure 13**). Once the Integrator concept design was determined an *in vitro* platform was required in order to demonstrate that an irreversible change in fluorescence can be elicited in response to Ca^{2+} and serve as a stage for further development. *In vitro* development and optimisation was further performed in order to tailor the fluorescent changes towards Ca^{2+} concentrations resembling neuronal Ca^{2+} transients (<1 mM) whilst retaining minimal spontaneous background activity. Upon completion, cell culture validation was required via exposing the Integrator to conditions of repeated neuronal depolarisation. Finally, an induction mechanism (or "on switch") was introduced and validated in order to provide temporal control over Integrator expression.
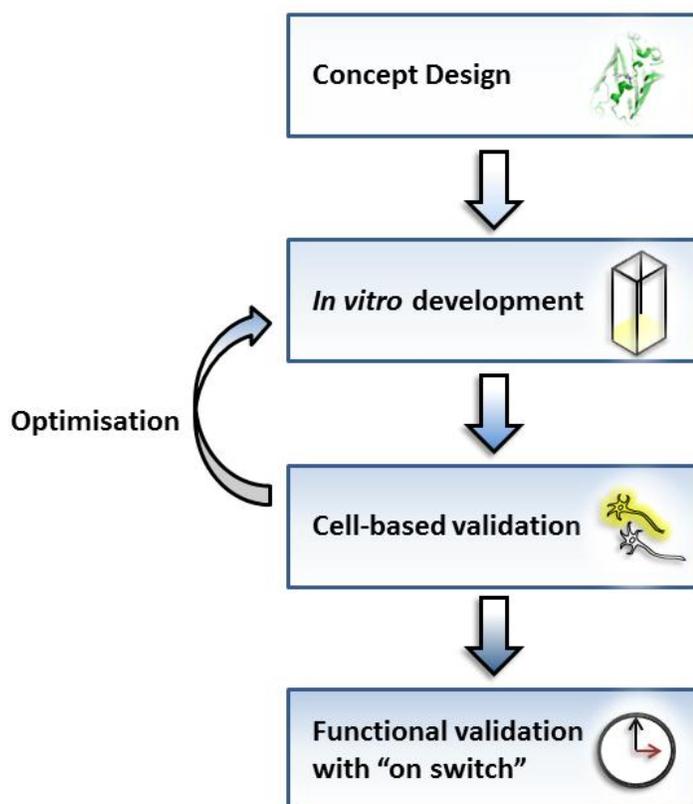

Figure 13: Approach for Integrator biosensor development

4.1 Approach 1: Ca²⁺-dependent protease FRET Integrator

4.1.1 Exploring the feasibility of a µ-Calpain Integrator

4.1.1.1 In vitro *determination of Reporter specificity*

Two FRET reporters were generated using a Calpain Sensitive Substrate (CSS) and the Calpain Insensitive Substrate (CIsS) (**Figure 14A**) (Vanderklish et al., 2000). Reporters were subsequently incubated with 20 µM commercial µ-Calpain (Merck; purified from Porcine Erythrocytes) in the presence or absence of 1 mM Ca^{2+} and the spectra were recorded for 3 hours (**Figure 14B-F**). CSS displayed a maximal 64 % FRET cleavage within the first hour with 1mM Ca^{2+} compared to 16 % cleavage displayed by CIsS. Both Reporters displayed a 4 % reduction without Ca^{2+} within the first hour (**Figure 14B**).
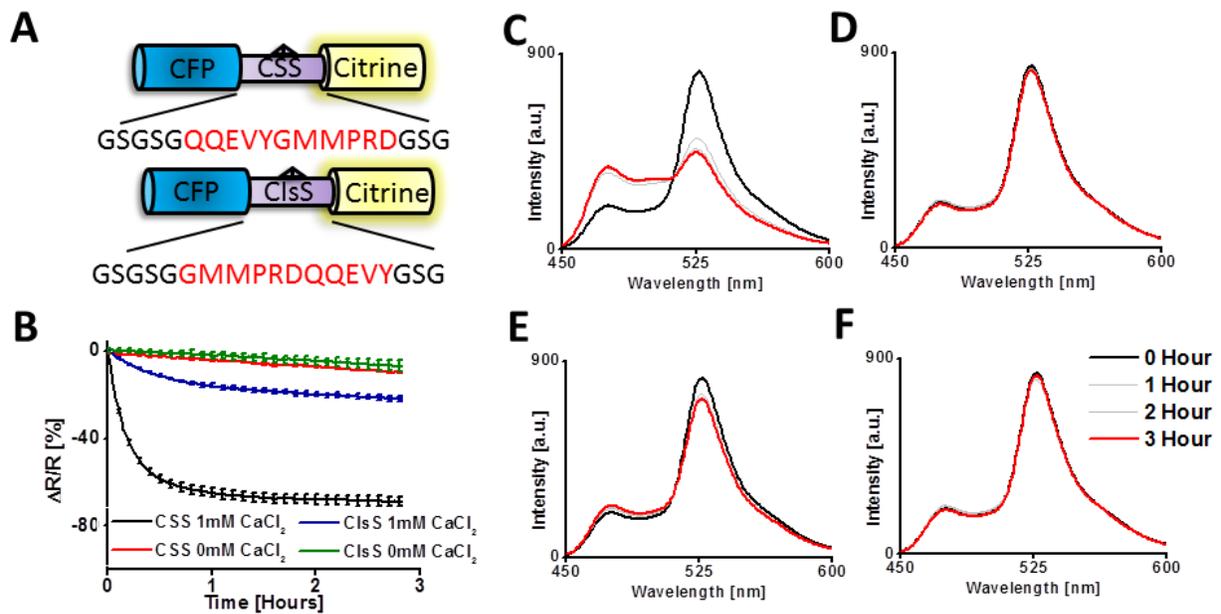

Figure 14: *In vitro* determination of Reporter activity
A) Schematic illustrating µ-Calpain cleavage sequences for the Calpain Sensitive Substrate (CSS; top) and the Calpain Insensitive Substrate (CIsS; bottom). **B)** FRET Ratio (YFP/CFP) kinetics of 20 µM µ-Calpain activity: CSS +1 mM Ca^{2+} (black), CSS + 0 mM Ca^{2+} (red), CIsS +1 mM Ca^{2+} (blue), and CIsS +0 mM Ca^{2+} (green). Error Bars ± SEM. **C-F)** Fluorescence emission spectra of Reporter at 0 hour (black), 1 and 2 hour (grey), and 3 hour (red) with 20 µM Calpain 1. **C)** CSS +1 mM Ca^{2+}. **D)** CSS + 0 mM Ca^{2+}. **E)** CIsS +1 mM Ca^{2+}. **F)** CIsS + 0 mM Ca^{2+}.

4.1.1.2   Evaluation of CSS FRET cleavage under physiological Ca^{2+}/Mg^{2+} conditions

In order to determine the *in vitro* physiological Ca^{2+} range for Reporter activation CSS was incubated with 20 µM commercial µ-Calpain in buffered solution containing 0, 0.01, 0.1 and 1 mM Ca^{2+} with 1 mM Mg^{2+} and the FRET ratio was recorded for 3 hours. Ca^{2+}-free and 0.01 mM Ca^{2+} displayed a higher rate of FRET reduction (15 % after 3 hours) compared to Mg^{2+}-free incubations (8 %) (**Figure 15A**). In comparison, 0.1 and 1 mM solutions found a similar almost maximal FRET reduction within the first hour, comparable with the kinetics observed in Mg^{2+}-free environments. Despite this a 28 % FRET cleavage in a 1 mM Ca^{2+}, 1 mM Mg^{2+} solution is significantly lower than the 64 % observed in a 1 mM Ca^{2+} solution (**Figure 15B**).
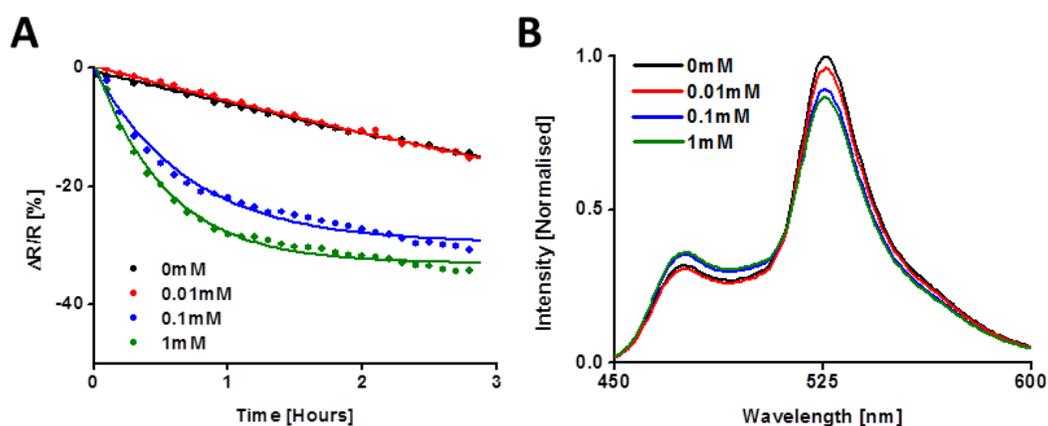

Figure 15: *In vitro* **assessment of CSS under physiological Ca^{2+}/ Mg^{2+} conditions**
A) Kinetics of FRET cleavage (YFP/CFP) of CSS incubated with 20µM µ-Calpain in the presence of 0mM (black), 0.01mM (red), 0.1mM (blue) and 1mM (green) Ca^{2+}. **B)** Fluorescence emission spectra after 3 hours of FRET cleavage with colour coding identical to **A**.

4.1.1.3   Generation of recombinant µ-Calpain constructs

In order to implement *in vitro* rational design modifications to µ-Calpain it was necessary to develop a recombinant DNA construct that would serve as the foundation for further modification. The large (CAPN1) and small (CAPNS1) subunit were initially combined with a mCherry tag (µ-C 1) and with the incubation of µ-C 1 with CSS no significant changes in FRET were observed after 1 hour with 1 mM Ca^{2+} (**Figure 16A**). Furthermore, increasing the Ca^{2+} concentration to 2 mM or 10 mM did not result in µ-Calpain function (**Figure 16B**). Alternate

strategies included separate expression of CAPN1 and CAPNS1-mCherry that would only be expressed in bacteria containing both plasmids due to the Ampicillin resistance of pRSETB and the Kanamycin resistance of pRSFDuet (**Figure 16D**; μ-C 2). Hereby, both subunits were expressed in pRSFDuet containing an Internal Ribosomal Entry Site (IRES) for separate expression of the two subunits, with and without a mCherry tag (μ-C 3 and μ-C 4 respectively). In no case did the expression of these recombinant proteins yield functional protease activity (**Figure 16C**).
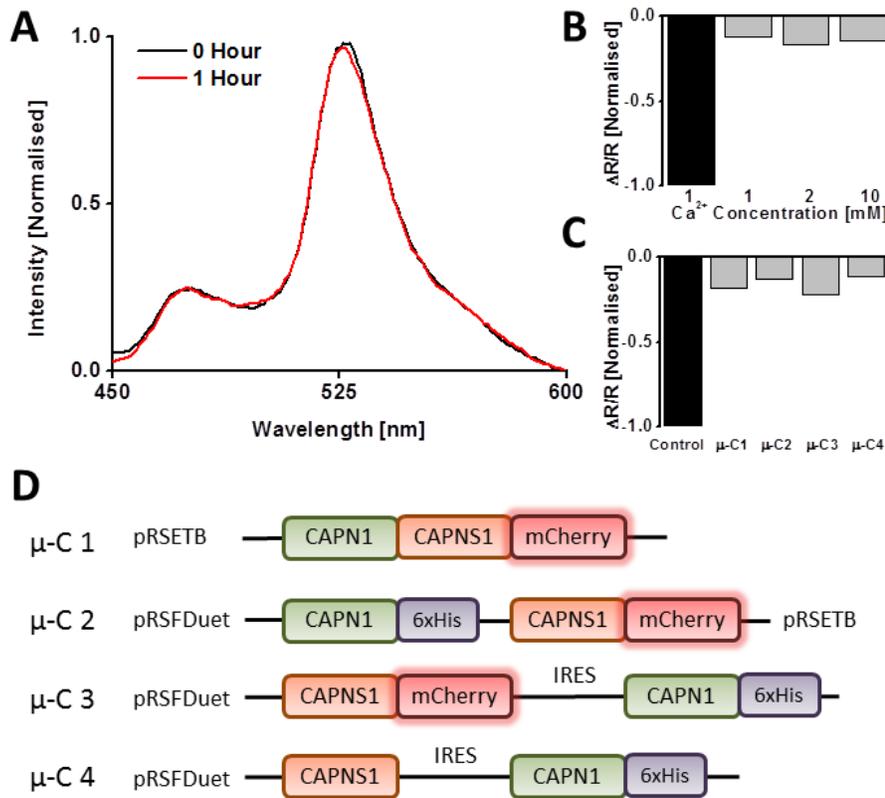

Figure 16: *In vitro* analysis of recombinant CAPN1 and CAPNS1
A) Fluorescence emission spectra of CSS with μ-C 1 before (black) and after (red) 1 hour incubation with 10 mM Ca^{2+}. **B)** Normalised FRET ratio changes of CSS after 1 hour with commercial μ-Calpain (black), or μ-Calpain (grey). The x-axis denotes concentration of Ca^{2+} used for incubation. **C)** 1 hour 10 mM Ca^{2+} incubations of CSS with μ-C constructs 1-4 (grey) and commercial μ-Calpain (black). **D)** Schematic indicating vectors and structure of recombinant subunits used in this approach.

4.2   Approach 2: Artificial Ca²⁺-dependent protease FRET Integrator

4.2.1   Approach 2a: Conformation-dependent Protease Integrator

4.2.1.1   Generating Truncated TEV with mCherry (ΔTEV-Ch)

In order to generate a screening strategy to determine insertion sites for Troponin C (TnC) it was first necessary to engineer a fluorescent tagged TEV. In this case mCherry was used, in order to identify bacterial colonies that acquired a Transposon insertion in the correct location (Section 3.1.10). Typically, when engineering novel protein function there is often a compromise between engineered and wild-type function; for example the split-TEV yield 50% proteolytic activity (Wehr et al., 2006). Thus, before the TnC domain was inserted an improvement to the TEV protease function was desired. Previous research indicated the presence of C-terminal auto-inhibition via 6 amino acids located at the C-terminus (Nunn et al., 2005). Thus, ΔTEV-Ch was generated via truncation at position 236 and insertion of a mCherry tag (Ch) for screening purposes (**Figure 17A**). Fluorescence spectra of TS-FRET were recorded in the presence of either wtTEV (**Figure 17B**) or ΔTEV-Ch (**Figure 17B, C**). Over 12 hours both proteases demonstrated a maximal 73 % reduction in FRET; however, they displayed significantly different kinetic FRET rates. WtTEV displayed a dissociation constant K_d value of 4.3 hours whereas the ΔTEV-Ch displayed a significantly increased rate of TS-FRET cleavage (K_d: 0.5h) (**Figure 17B**). Interestingly, upon maximal cleavage of TS-FRET, the fluorescence emission spectra displays only a 5 % dissimilarity compared to CFP alone (**Figure 17D**) indicating that this reduction in FRET corresponds to almost complete TS-FRET cleavage.
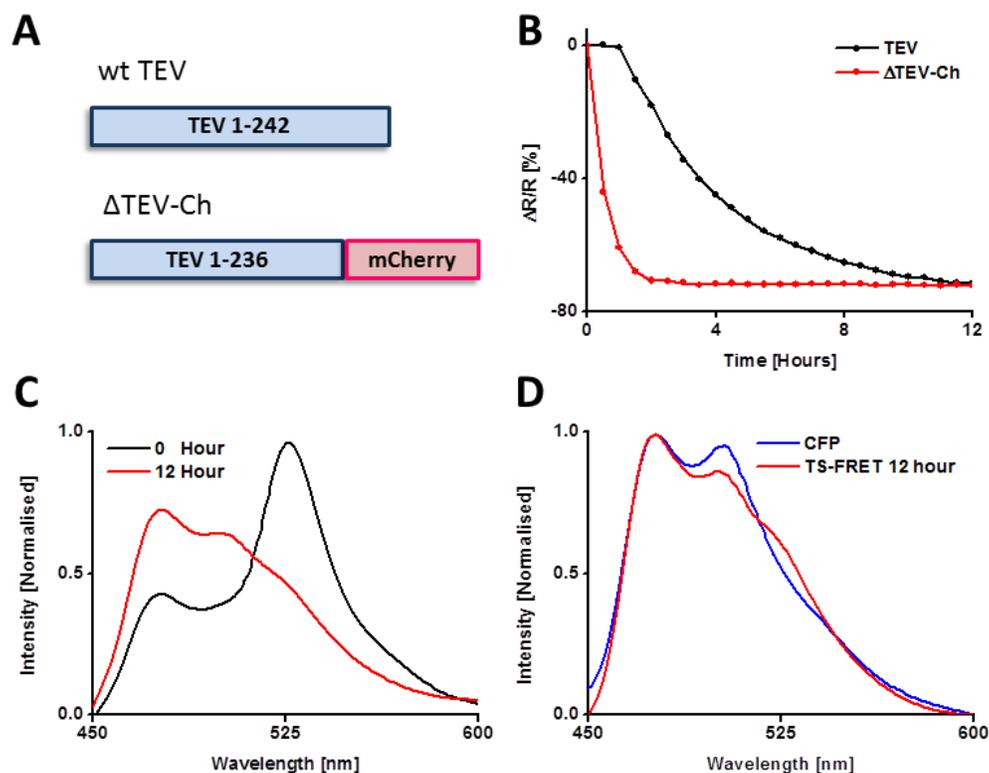
Figure 17: *In vitro* kinetics of wild type TEV and ΔTEV-Ch
A) Schematic representation of the two constructs. TEV consists of 242 amino acids that are reduced to 236 upon truncation of the autoinhibitory C-terminal domain (ΔTEV). **B)** Kinetics of TS-FRET cleavage by wt TEV (black) and ΔTEV-Ch (red). **C)** Fluorescence emission spectra of ΔTEV-Ch at 0 hour (black) and 12 hour (red). **D)** Fluorescence emission spectra of TS-FRET incubated for 12 hours with ΔTEV-Ch (red) and CFP alone (blue).

4.2.1.2   Transposon-based bacterial colony screening

Using the screening method outlined in Section 3.1.10 a screened population of approximately 200 colonies yield a insertion bias with a median quartile (Q2) of 185 amino acids (**Figure 18A**) with the upper (Q3) and lower quartile (Q1) being 210 and 170 respectively. From this a sample of 100 was selected and sequenced to ensure insertion in the correct reading frame. Once duplicate insertion sites were removed a sample size of 8 were chosen that span the Q1 – Q3 range (**Figure 18B**).
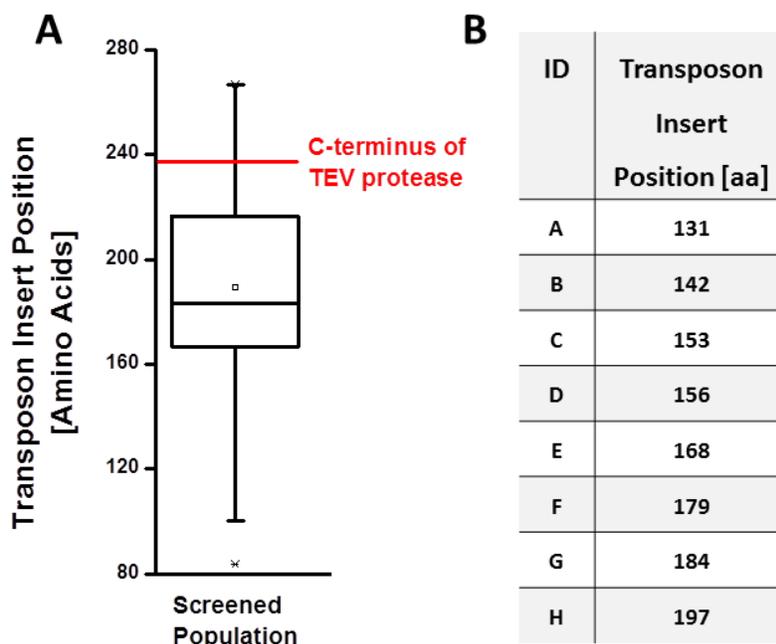
Figure 18: Sampling of insertion sites from screened bacterial colonies
A) Box-plot demonstrating position of transposon insertion site from the N-terminus of TEV. Red line indicates C-terminus of the ΔTEV protease. **B)** Transposon insertion positions (amino acids) of the 8 member sample used for further investigation.

4.2.1.3   Assessment of Ca^{2+}-dependent protease function

Assessment of protease function was determined by two steps. The first step involved determination of Transposon-inserted ΔTEV-Ch function (samples A-H) compared to insertion-free ΔTEV-Ch. Purified proteins were incubated for 1 hour with TS-FRET and ΔR/R ratio changes were quantified. The majority of Transposon-inserted constructs did not retain and significant protease function, however, insertion at position 131 and 197 yield proteases retaining 28 and 40 % activity respectively (**Figure 19A**). Regardless, all eight samples underwent the second assessment step via the evaluation of protease function upon TnC C-lobe insertion. In comparison with ΔTEV-Ch (**Figure 19B, C**) all constructs displayed an increase in FRET ΔR/R in a Ca^{2+} free environment (**Figure 17B, D**) indicative of protease interaction-induced FRET (an average increase of 20 %). With the addition of Ca^{2+} a similar FRET increase was observed indicating no Ca^{2+}-induced gain of proteolytic function.
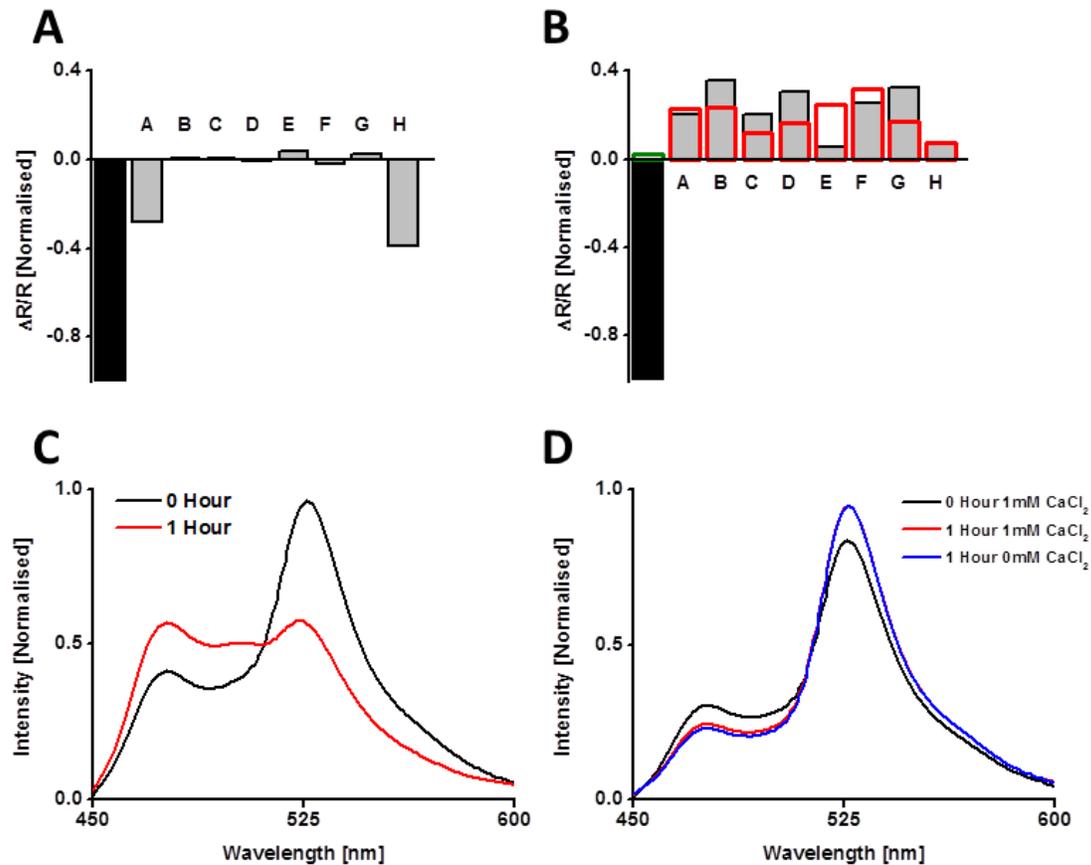
Figure 19: TnC C-lobe insertion and in vitro functional characterisation
A) Normalised ΔR/R of TS-FRET after 1 hour incubation with ΔTEV-Ch (black) or Transposon-inserted proteases (grey). **B)** Normalised ΔR/R of TS-FRET after 1 hour incubation alone (green), with ΔTEV-Ch (black), or TnC C-lobe inserted proteases in the absence (grey) or presence (red) of 1 mM Ca^{2+}. **C)** Fluorescence emission spectra of TS-FRET before (black) and after (red) 1 hour of ΔTEV-Ch incubation. **D)** Fluorescence emission spectra of TS-FRET incubated with "Sample C" before (black) or after 1 hour incubation with (red) and without (blue) $CaCl_2$.

4.2.2 Approach 2b: Split TEV Integrator

4.2.2.1 In vitro development of Ca²⁺-dependent split TEV protein

TEV fragments were fused to ΔCaM and ΔM13 in several configurations before each protein was purified and measured *in vitro* with TS-FRET and 1 mM Ca²⁺. The fluorescence emission spectra were recorded for 1 hour (**Figure 20A**) and compared to control TS-FRET and full TEV FRET measurements (**Figure 20A inset**). The configurations examined included; from the N- to C-terminal, TN-CaM/M13-TC, CaM-TN/M13-TC and TC-CaM/M13-TN. After 1 hour a maximal 18 % ΔR/R was recorded (**Figure 20B**), however, this was not due to a ratiometric change but rather an increase in ECFP fluorescence only. Additional purification and *in vitro* characterisation of FRB-TN and FKBP-TC (provided by Moritz Rossner) with the FRB/FKBP dimerising agent Rapamycin (1 mM) also failed to display any TS-FRET cleavage (data not shown). Thus, it was concluded that this *in vitro* platform was unsuitable for the evaluation of this split TEV architecture. Nevertheless, this Integrator strategy was assessed in dissociated hippocampal neurons using electrical field stimulation.
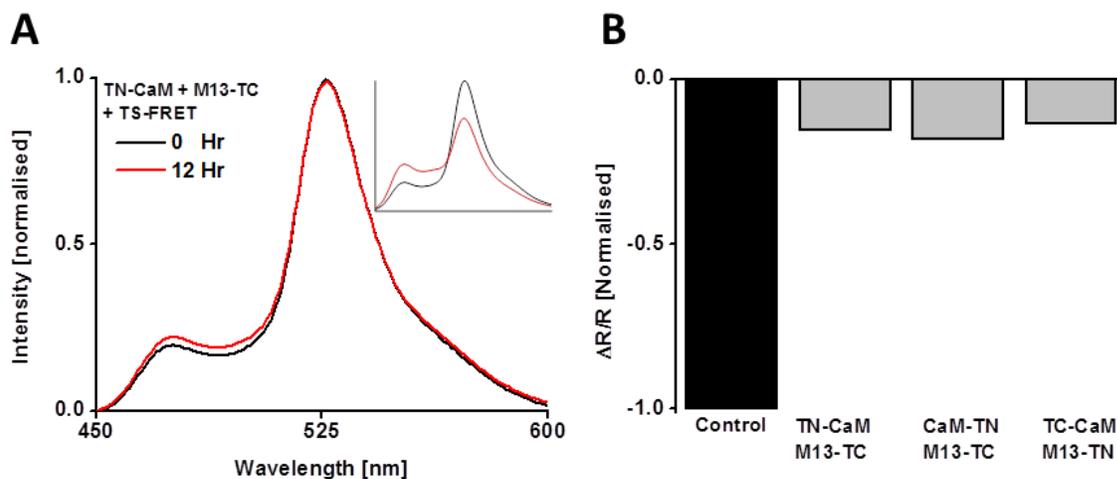
Figure 20: *In vitro* characterisation of split TEV fragments.
A) Normalised fluorescence emission spectrum of TS-FRET with TN-CaM and M13-TC before (black) and after 12 hours with 1 mM Ca²⁺ (red). Fluorescence emission spectrum of TS-FRET incubated with full TEV is also shown for comparison (inset; identical colour coding). **B)** Normalised ΔR/R of TS-FRET with full TEV control (black) and split TEV configurations (grey).

4.2.3 Calibration and application of Electrical Field Stimulation

In order to determine the functionality and operational parameters of Electrical Field Stimulation a series of stimulation experiments were conducted on dissociated hippocampal neurons using the Ca^{2+} dye Fluo-4-AM. The parameters (Burst Duration (BD), Stimulation Frequency (SF), pulse width (PW) and field strength (FS)) were each investigated in turn. In all cases a maximal ΔF/F of 60 % was reached (**Figure 21**). By this calibration it was determined that a 1 s pulse duration of 80 Hz frequency with a 1000 µs pulse width at 30 V would be appropriate stimulation parameters.
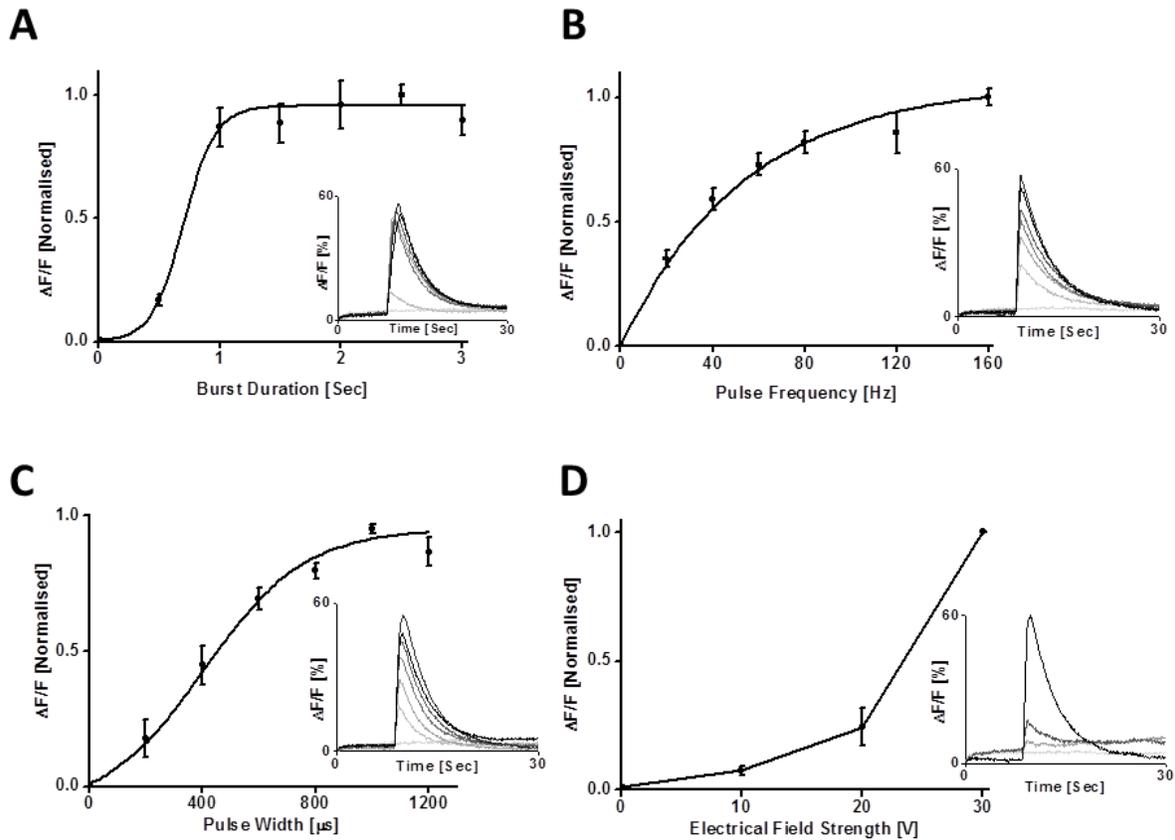
Figure 21: Configuration of Electrical Field Stimulation using Fluo-4-AM
A) Normalised ΔF/F responses of Fluo-4 to a series of burst durations (BD) ranging from 0.5 to 3 sec. **B)** Normalised ΔF/F responses to a pulse frequency (PF) range of 20-160 Hz. **C)** Normalised ΔF/F responses to a pulse width PW) range of 200-1200 µs. **D)** Normalised ΔF/F responses to applied field strengths (FS) of 10-30 V. **Insets:** 30 sec ΔF/F traces for each parameter value (monochrome gradient for lowest (light grey) to highest value (black) measured). Error bars ±SD.

Using the LIVE/DEAD cytotoxicity assay a burst (80 Hz PF, 1000 µs PW, 1 sec BD, at 30 V), with an intertrain interval (ITI) of 4 min, was shown to confer no significant effect on cell survival after 4 hours **(Figure 22A, B)** based on the ratio of live cells compared to all live and dead cells (**Figure 22C**). Based on structural studies determining the orientation of CaM-CBP interaction (Ishida and Vogel, 2006) the TN-CaM/M13-TC pair was chosen for dissociated hippocampal neuron studies. Ultimately a 2 hour stimulation timeframe was unable to induce significant cleavage of the TS-FRET pair compared to the stimulus-free condition (**Figure 22D**).
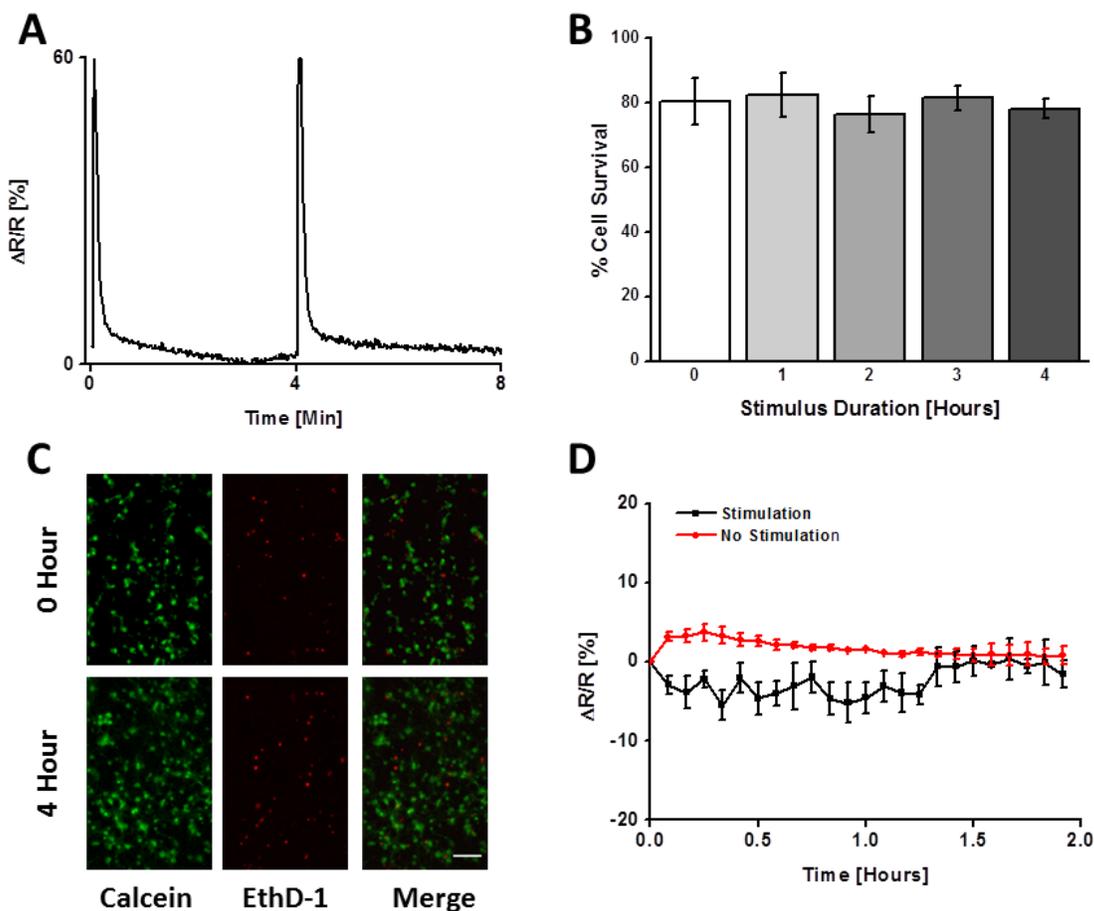
Figure 22: Cell stimulation frequency determination and application to split-TEV
A) Normalised fluorescence responses of Fluo-4 to an 80 Hz PF, 1000 µs PW, 1 sec BD, 30 V FS burst every 4 min. **B)** Quantification of cell survival using a 4 min pulse for up to 4 hours. **C)** Artificially coloured fluorescent microscopy images of the markers for cell survival (Calcein) and cell death (EthD-1), scale bar 50 µm. **D)** ΔR/R values for dissociated neurons stimulated for 2 hours with a burst every 4 min (black) or unstimulated (red). Error bars ±SD.

4.3 Approach 3: Bimolecular Fluorescence Complementation Integrator

4.3.1 In vitro *optimisation of Integrator*

4.3.1.1 Determination of appropriate location for splitting Citrine

Previous research identified two fragmentation sites where *Aequorea Victoria*-derived FPs can be split to yield the highest signal-to-background ratio (inducible complementation versus spontaneous association of fragments); the 155 and 173 amino acid positions (Hu and Kerppola, 2003). In order to determine the most suitable split site the two Citrine (denoted as "Y" for "YFP") combinations were integrated into a YN-ΔCaM and ΔM13-YC construction. Over 4 hours *in vitro* analysis of 154/155 protein recombination found a 470 % increase in Ca^{2+}-dependent complementation (signal) over spontaneous association (background) whereas using the 172/173 split a 65 % increase was observed (**Figure 23A, B**). Furthermore, the 172/173 split displayed a total complementation of 29 % compared to that of the 154/155 split leading to the selection of the 154/155 citrine fragments for further development.
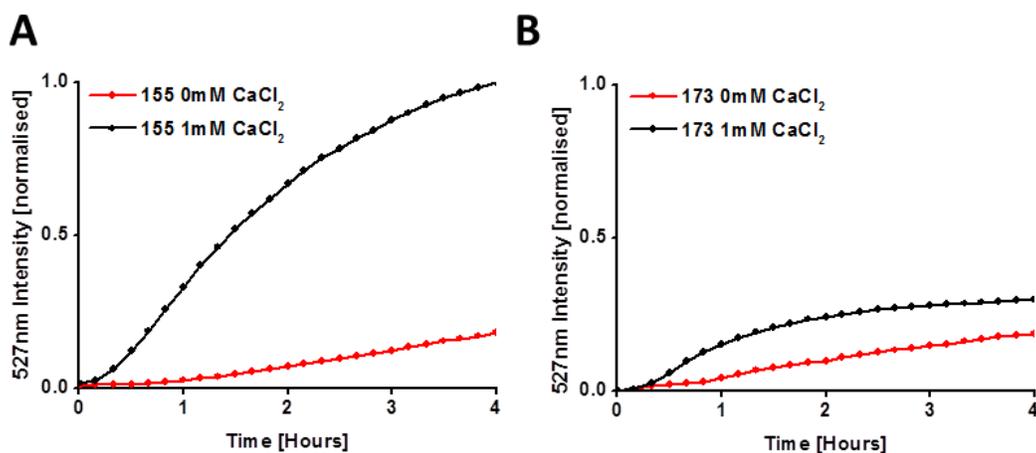

Figure 23: *In vitro* analysis of the 155 and 173 split Citrine.
A) Co-incubation of YN1-154-ΔCaM with ΔM13-YC155-238 in the presence (black) or absence (red) of 1 mM CaCl₂. **B)** Co-incubation of YN1-172-ΔCaM with ΔM13-YC173-238 in the presence (black) or absence (red) of 1 mM CaCl₂.

4.3.1.2 Determination of spontaneously interacting proteins

In order to yield maximal signal (Ca^{2+}-induced complementation) several steps were undertaken. The first step was to identify the source for the Ca^{2+}-free spontaneous background fluorescence observed in order to reduce the likelihood of high background Citrine fluorescence in cells. To determine whether the ΔCaM/ΔM13 or YN154/YC155 interactions were responsible for the Ca^{2+}-free complementation observed in **Figure 23A** the Citrine fragments were purified without ΔCaM or ΔM13. A 4 hour co-incubation of the YN or YC components (with the complementing component retaining the CaM or M13) yielded no significant change in fluorescence (**Figure 24A**). Thus, the ΔCaM/ΔM13 interaction was found to be responsible for the observed background complementation. Due to the ΔCaM and ΔM13 originating from a redesigned GECI architecture the determination of whether improvement in the signal or a reduction in background could be achieved using wtCaM or wtM13 was carried out. In comparison to the 470 % signal/background ratio observed with YN-ΔCaM and ΔM13-YC only a 250 % ratio was detected with wtCaM and wtM13 with a significant reduction in the overall signal (**Figure 24B**). In contrast the ΔCaM/wtM13 and wtCaM/ΔM13 combinations displayed a higher level of background complementation compared to the 1 mM Ca^{2+} environment. Hereby, the ΔCaM/ΔM13 combination is the most suitable combination for further development.
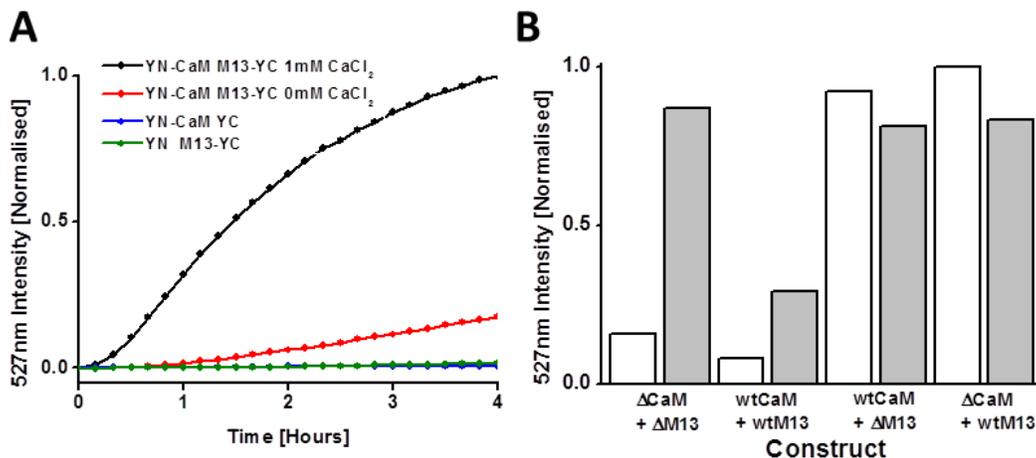
Figure 24: In vitro spectrophotometric analysis of spontaneous association
A) Co-incubation of YN1-154-ΔCaM with ΔM13-YC155-238 in the presence (black) or absence (red) of 1 mM $CaCl_2$. Co-incubation of YN/ΔM13-YC155 (green) or YN154-ΔCaM/YC (blue) in 1 mM $CaCl_2$. **B)** Citrine intensity after 4 hours of incubation of combinations of wtCaM, ΔCaM, wtM13, and ΔM13 with (white) and without (grey) 1 mM $CaCl_2$.

4.3.1.3 In vitro o*ptimisation of the ΔCaM/ΔM13 orientation*

During the design phase the orientation of ΔCaM and ΔM13 templates were defined based on the binding profile identified by the structural determination of GCaMP2 (Akerboom et al., 2009). Consequently, implementation of alternative orientations may yield improved signal/background ratios. To achieve this several components were generated; 4 for ΔCaM and 4 for ΔM13, each with N- or C- terminal YN or YC fragments. After 4 hours incubation two orientations yield the highest signal/background ratio, the original YN-ΔCaM/ΔM13-YC construction and a ΔCaM-YN/ΔM13-YC construction (**Figure 25**). *In vitro* kinetics displayed a reduced signal increase for ΔCaM-YN/ΔM13-YC compared to the original orientation with a further increased rate of background signal. Therefore, the original orientation was maintained for further development.
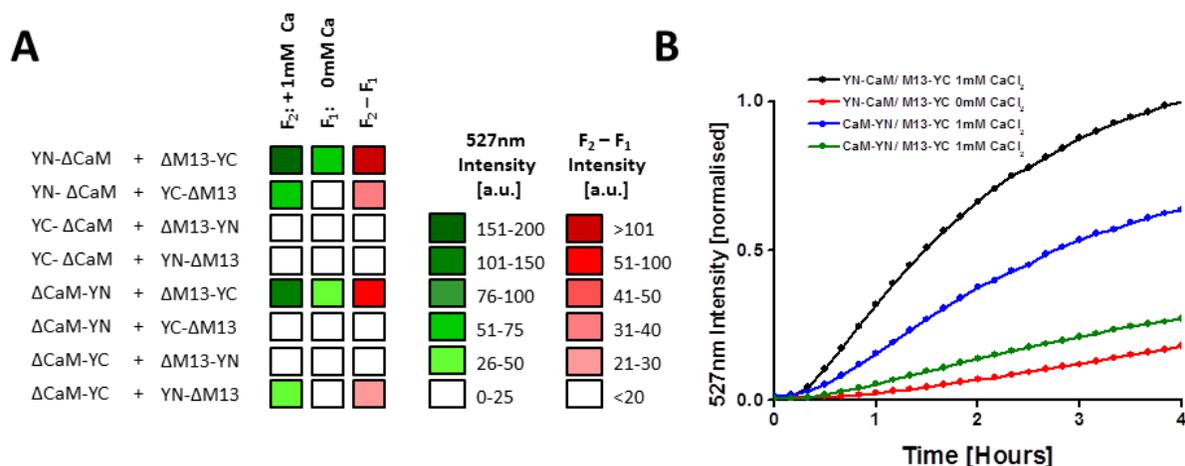
Figure 25: *In vitro* orientation specificity of complementation
A) 4 hour end-point Citrine intensity measurements for the 8 orientation combinations with (F_2) and without (F_1) 1 mM $CaCl_2$. **B)** Kinetics of Citrine refolding of YN-ΔCaM/ΔM13-YC with (black) and without (red) 1mM $CaCl_2$. ΔCaM-YN/ΔM13-YC with (blue) and without (green) 1 mM $CaCl_2$.

*4.3.1.4   In vitro a*ssessment of alternative FPs for fluorescence complementation

In order to further optimise the complementation Integrator, alternative FPs were considered which could potentially improve the signal/background ratio or generate a more red shifted Integrator. In order to achieve this several proteins were split either at the 155 amino acid position or in some cases the 159 position (corresponding to the end of the β-sheet), using the optimal CaM/M13 orientation described previously. In addition, the YN172/CC155 complementation pair was also investigated due to the previously reported *in vitro* success of this approach (Hu and Kerppola, 2003). After 4 hours the excitation and emission spectra were recorded (**Figure 26A**). In the majority of cases no complementation was observed, however, the YN172/CC155 combination yield a 238 % improvement over the YN/YC with a significantly broader excitation spectrum (**Figure 26B**). In addition the YN/CC possessed excitation maxima of 490 nm, a CFP/Citrine intermediate. Unfortunately, due to the 10-fold increase in background fluorescence this was not seen as an improved substitute for the YN/YC fragments (**Figure 26C**).
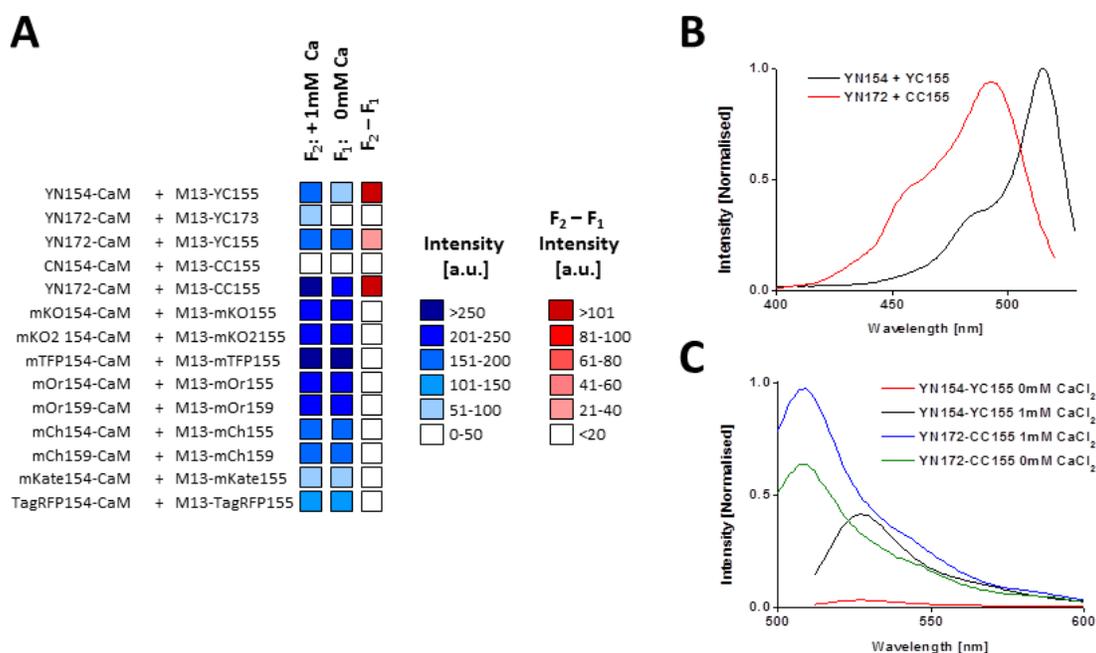
Figure 26: *In vitro* complementation of alternative FP candidates
A) 4 hour end point fluorescence of split FPs; Y-YFP, C-CFP, mKO-mKusabira Orange, mKO2, mTFP-Teal FP, mOr-mOrange, mCh-mCherry, mKate, TagRFP. **B)** Fluorescence excitation spectra of YN154-ΔCaM/ΔM13-YC155 (black) and YN172-ΔCaM/ΔM13-CC155 (red). **C)** Fluorescence emission spectra of YN154/YC155 with 1 mM $CaCl_2$ (black), 0 mM $CaCl_2$ (red) and YN172/CC155 with 1 mM $CaCl_2$ (blue), 0 mM $CaCl_2$ (green).

4.3.1.5 Cell-based validation of YN154-ΔCaM and ΔM13-YC155

With the *in vitro* verification of the most optimal Integrator architecture the assessment of biosensor characteristics in cells was performed. Transient transfection of HEK293T cells with YN-ΔCaM and ΔM13-YC revealed that 33 % of cells expressing CFP exhibited Citrine background fluorescence (**Figure 27A, C**). Furthermore, of these background-positive cells, the overall YFP fluorescence was 29 % as bright as CFP (**Figure 27A, B**). In order to confirm biosensor function, dissociated hippocampal neurons were transiently transfected with the two components before application of the stimulation protocol for 4 hours (80 Hz PF, 1000 μs PW, 1 sec BD, 30 V FS) whereby no significant increase in signal was observed (**Figure 27D**).
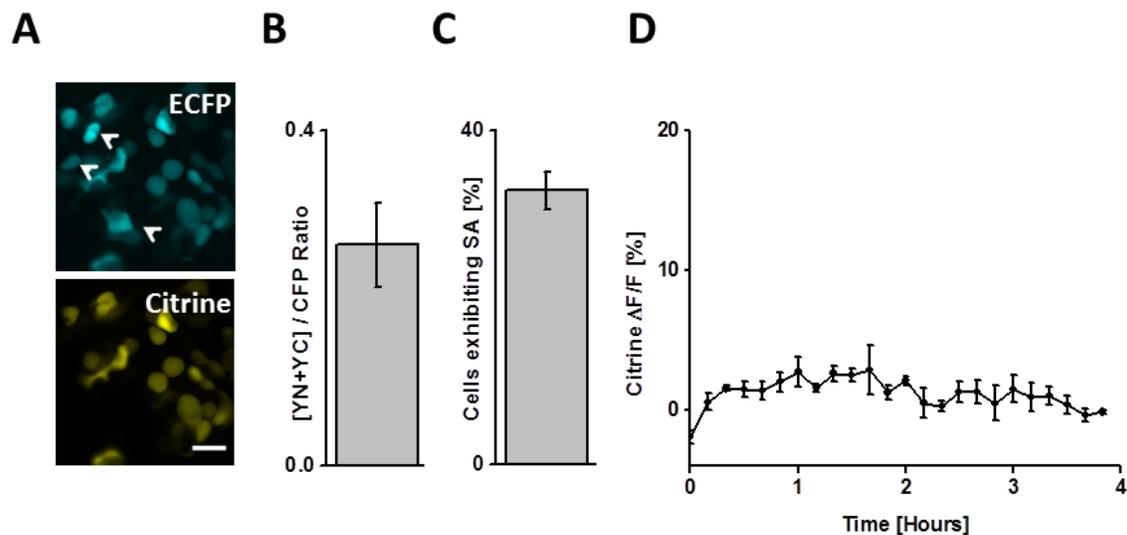
Figure 27: Cell culture characterisation of YN-ΔCaM and ΔM13-YC
A) Fluorescence microscopy images of HEK293T transiently transfected with YN-ΔCaM and ΔM13-YC (arrow heads denote cells expressing CFP but no YFP). **B)** Citrine/CFP ratio of HEK293T cells. **C)** Percentage of HEK293T cells exhibiting spontaneous association (background) yielding Citrine fluorescence. **D)** Citrine ΔF/F of hippocampal neurons stimulated with an 80 Hz PF, 1000 μs PW, 1 sec BD, 30 V FS pulse every 4 min for 4 hours. B+C error bars ±SD, D, error bars ±SEM.

4.3.1.6 In vitro *Peptide screen*

To reduce the background of YN154-ΔCaM/ΔM13-YC155 observed in HEK293T cells (**Figure 27B**) a peptide screen was undertaken in a 96-well plate using all currently known Ca^{2+}-dependent CaM binding peptides (Yamniuk and Vogel, 2004). A final concentration of 1.5 μM for each component was used and the proteins were incubated for 4 hours before measuring the Citrine emission (**Figure 28A**). This resulted in the identification of a novel peptide, the ΔSpectrin (lacking a Histidine at position 14 compared to the wt Spectrin sequence; KTASPWKSARLMV**H**TVATFNSIKE), that exhibited a higher signal/background ratio compared to the ΔM13 peptide. Kinetic studies found a 130 % increase in signal of ΔSpectrin (ΔSp) compared to ΔM13 with an additional 3-fold improvement in the signal/background ratio (**Figure 28B**). When transiently transfected in HEK293T cells (along with a CFP marker) ΔSp also displayed significantly lower background fluorescence that was 85 % lower compared to ΔM13 (**Figure**

28C, E). Additionally there was a significant 16 % reduction in the number of cells exhibiting background fluorescence when using ΔSp compared to ΔM13 (**Figure 28D, E**).
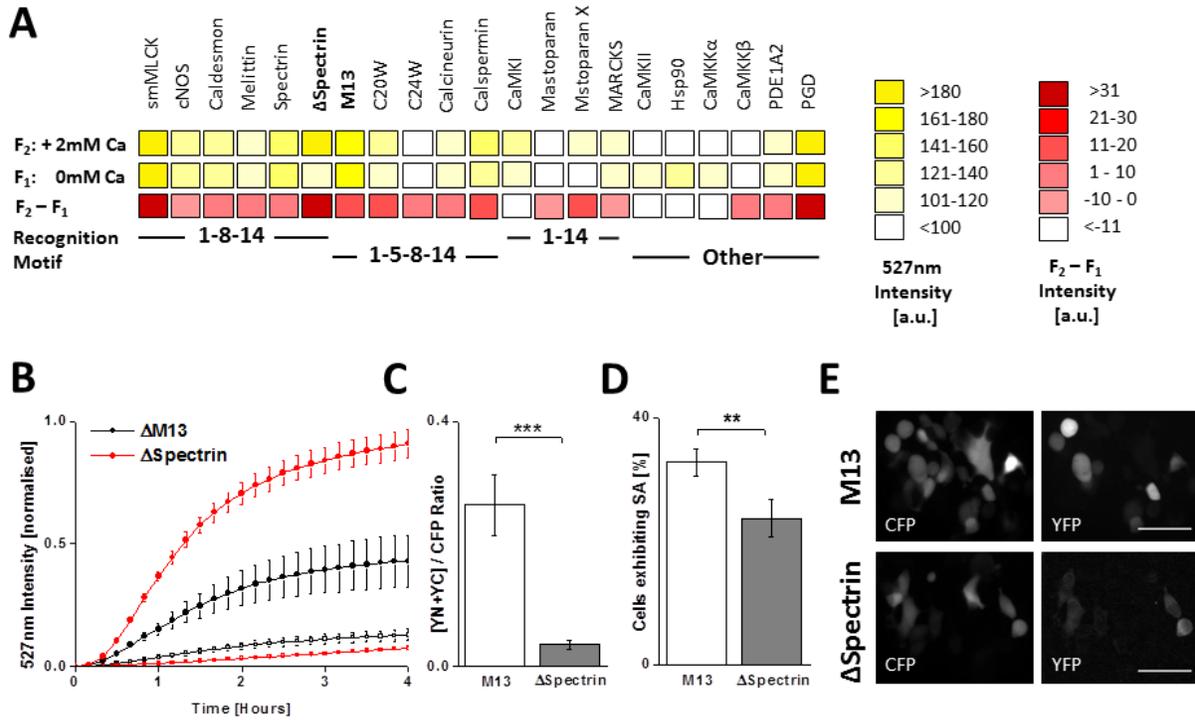
Figure 28: *In vitro* peptide screen and HEK293T ΔM13/ΔSpectrin comparison
A) 4 hour 96-well plate end point fluorescence of Ca^{2+}-dependent CBPs. **B)** Cuvette fluorescence emission kinetics of YN-CaM with ΔM13-YC (black) and ΔSpectrin (red) with 1 mM Ca^{2+} (filled circles) or 0 mM Ca^{2+} (open squares). **C)** Recombined Citrine/CFP ratio of ΔM13-YC (white) or ΔSpectrin-YC (grey) in HEK293T cells. **D)** Percentage of HEK293T cells containing spontaneous background complementation; ΔM13-YC: White, ΔSpectrin-YC: Grey. **E)** Fluorescence microscopy images of ΔM13 and ΔSpectrin, scale bar 50 μm. ***p<0.001, **p<0.02. B error bars ±SEM, D, error bars ±SD.

4.3.1.7 In vitro *assessment of a*lternative Citrine fragmentation sites

With a significantly improved signal/background ratio using ΔSp the remaining background fluorescence was hypothesised to be due to the optimal complementation of Citrine, and thus, by modification of the split location a further improvement in the signal/background ratio could be achieved. In order to investigate this several Citrine fragments were generated; YN154/ YC155 (original fragments), YN152, YN153, and YC154, that were fused to ΔCaM or ΔSp. Combinations were generated to result in a shift in split location into the β-sheet (YN153/ YC154) or to add or subtract an amino acid (YN154/ YC154 or YN152/ YC154 respectively) (**Figure 29A**). By shifting the split location to YN153/ YC154 a 27 % increase signal and a 22 % reduction in background were observed *in vitro* (**Figure 29B**). By comparison, the addition or subtraction of an amino acid yielded a reduction in the signal (23 % and 34 % respectively) with no decrease in background fluorescence. Thus the components YN153-ΔCaM and ΔSp-YC154 were selected for continuation.
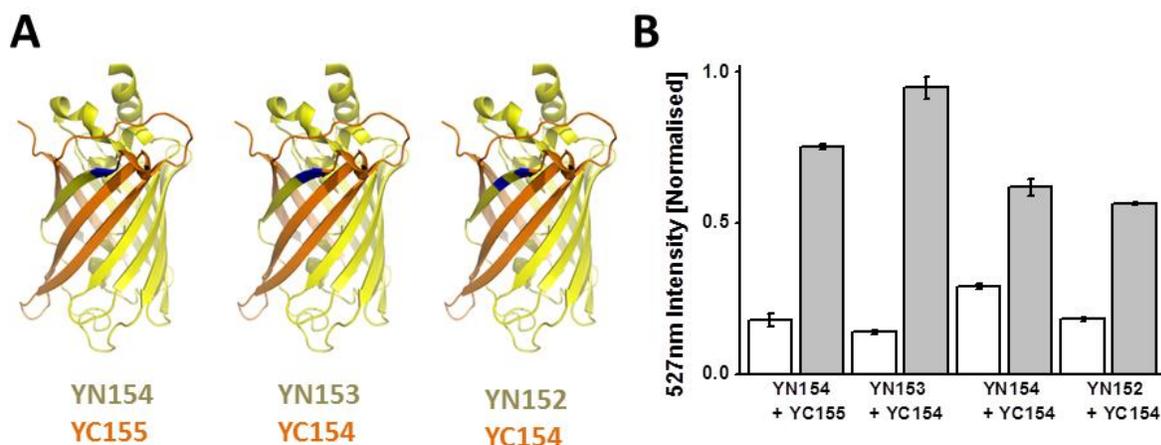

Figure 29: *In vitro* complementation of alternative fragmentation sites
A) Structural representation of alternative fragmentation sites. Yellow: N-fragment, orange: C-fragment, blue: fragment position. **B)** 4 hour end point *in vitro* fluorescence of alternative fragmentation sites co-incubated with 1 mM CaCl$_2$ (grey) or without (white). Error bars ± SEM.

4.3.1.8 Temperature dependency of fluorescence complementation

All *in vitro* experiments previously mentioned were performed at room temperature (RT), however, previous research has shown a strong temperature dependency of complementation (Robida and Kerppola, 2009). To determine the effect temperature played on Integrator function two questions were addressed; i) what effect does temperature have on complementation alone and ii) does temperature affect Integrator Ca^{2+} sensitivity? Firstly, to determine the temperature effect on complementation alone protein samples of YN-ΔCaM and ΔSp-YC were incubated for 4 hours at a temperature gradient ranging from RT to 37 ^{o}C in a 1 mM Ca^{2+} saturated environment. Interestingly no reduction in signal was observed at higher temperatures; however, a significant decrease in the background fluorescence was detected with increasing temperature (**Figure 30A**). Secondly, in order to determine temperature effects on both ΔCaM/Ca^{2+} binding and ΔCaM/ΔSp interaction, a Ca^{2+} titration series was generated to represent more physiological Ca^{2+} and Mg^{2+} ranges. YN-ΔCaM and ΔSp-YC were incubated for 4 hour with a Ca^{2+} range of 0 - 38.7 µM (for RT) or 0 – 36.0µM (37 ^{o}C). For evaluation of Ca^{2+} titrations two criteria were considered: the EC_{50} (the concentration of Ca^{2+} that elicits 50% total complementation), and the total Ca^{2+}-mediated complementation. In comparison to RT a 380 % reduction in total signal was observed at 37 ^{o}C and an additional decrease in Ca^{2+} sensitivity was observed by the increase in EC_{50} from 811 nM at RT to 2000 nM at 37 ^{o}C (**Figure 30B**).
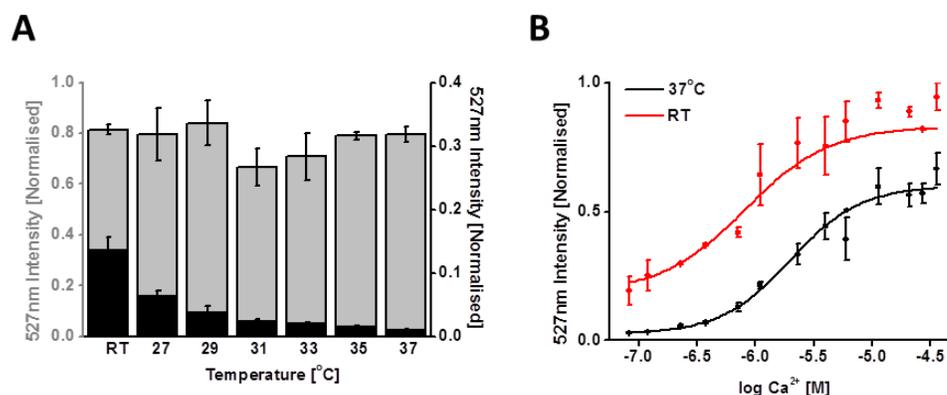

Figure 30: *In vitro* temperature dependency of fluorescence complementation
A) Citrine fluorescence of components YN-ΔCaM and ΔSp-YC measured after 4 hours with (grey) and without (black) 1 mM $CaCl_2$. **B)** Ca^{2+} titration at RT (red) or 37 ^{o}C (black). Error bars ± SEM.

4.3.1.9 Cell-based validation of YN153-ΔCaM and ΔSp154-YC

As the cell characterised ΔM13 peptide was replaced with the mutant ΔSp peptide it was necessary to first ascertain whether the ΔSp peptide formed complementation complexes with ΔCaM in a cellular environment. Exposure of transiently transfected HEK293T cells to high external Ca^{2+} concentrations via application of the ionophore "Ionomycin" resulted in a 214 % increase in the [YN+YC]/CFP ratio compared to control groups thus indicating a Ca^{2+}-dependent interaction ΔCaM/ΔSp (**Figure 31A**). Furthermore, to determine Integrator responses to endogenous Ca^{2+} transients Electrical Field Stimulation was applied to transiently transfected neurons with no significant change in the ΔF/F of Citrine detected (**Figure 31B, C**).
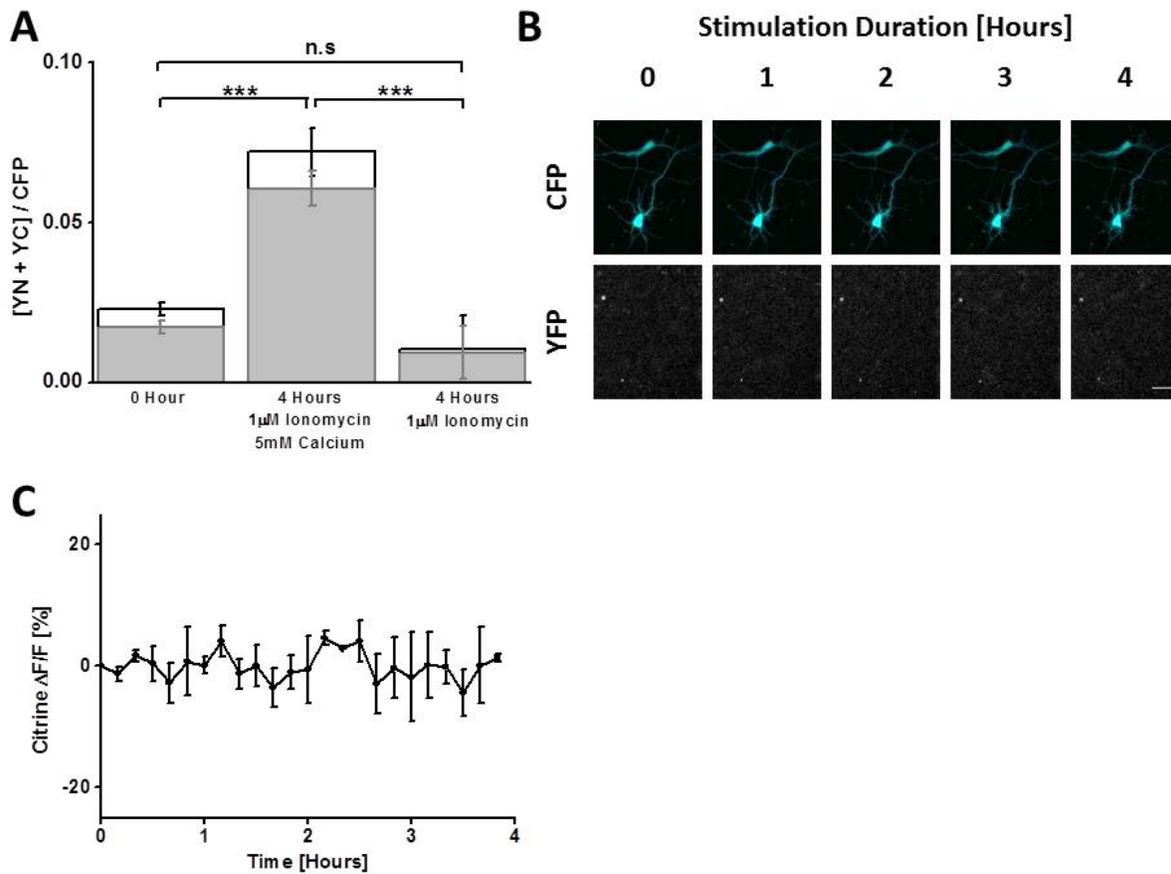
Figure 31: Cell culture characterisation of YN-ΔCaM and ΔSp-YC
A) HEK293T cells transfected with 3 µg (white) or 1.5 µg (grey) total DNA concentration. Cells were treated for 4 hours with 1 µM Ionomycin alone or with an additional 5 mM CaCl$_2$. **B)** Fluorescence microscope images of stimulated neurons, scale bar 50 µm. **C)** Live cell imaging ΔF/F values for transfected hippocampal neurons stimulated with 80 Hz, 1000 µs, 1 sec, 30 V burst every 4 minutes. ***p<0.001. A error bars ± SD. C, error bars ± SEM.

4.3.2   Integrator refinement for response to endogenous Ca²⁺ transients

With the success of developing a complementation-based Integrator responsive to exogenous Ca^{2+} application the next developmental step was to determine the Integrator's response to endogenous stimuli - a task that has not previously been achieved by the complementation field. Until now Integrator development has included not only optimisation of the fundamental architecture of the design (orientation, split location, and FP) but also the implementation of a new CaM binding peptide (ΔSp) specifically for the application of a CaM-peptide Integrator. The ensuing optimisation was directed towards improving the Ca^{2+} specificity of the CaM/ΔSp as well as improving the stability of the second component, ΔSp-YC154, and investigating whether by the addition of linkers the biosensor function could be improved.

4.3.2.1   Linker-based strategy for improving complementation

Recent research has highlighted the often understated impact that flexible linkers have on biosensor analyte affinity (Horikawa et al., 2010). The design architecture exploited by the complementation-based Integrator did not possess any linkers as it was logical that the addition of such linkers would increase the likelihood of background complementation. In order to investigate whether the signal could be improved by increasing the flexibility of ΔCaM or ΔSp three poly-glycine linkers were incorporated into both components with varying length (GGS, GGGS, and GGGGS). When the linkers were inserted between the YN153 and ΔCaM a respective 60, 30, 46 % reduction in the total complementation was observed (**Figure 32A**) with no improvement to Ca^{2+} affinity (EC_{50}: 2800, 3800, 2800 nM respectively). Similarly, when the GGS and GGGS were inserted in-between the ΔSp-YC154 a respective 19 and 52 % reduction in complementation was observed with no improvement to Ca^{2+}affinity (EC_{50}: 2800 and 3800 nM respectively) (**Figure 32B**). In contrast, addition of a GGGGS linker resulted in a 31 % increase in complementation independent of EC_{50} improvement.
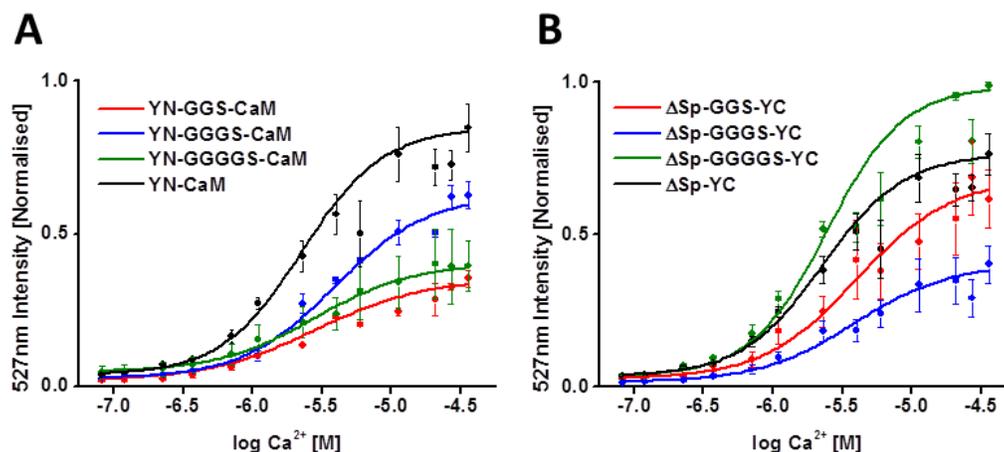
Figure 32: Ca^{2+} titrations of linker-modified components
A) Linkers integrated in-between YN153 and ΔCaM; Black: No linker, Red: GGS, Blue: GGGS, Green: GGGGS. Each sample was co-incubated with ΔSp- YC154. **B)** Linkers integrated in-between ΔSp and YC154; Black: No linker, Red: GGS, Blue: GGGS, Green: GGGGS. Each sample was co-incubated with YN153-ΔCaM. Error bars ± SEM.

4.3.2.2 Improving the Ca^{2+}-coordination of the ΔCaM component

In parallel, an alternative approach to increase the Ca^{2+} affinity of the Integrator was undertaken by the improvement of the coordination of Ca^{2+} in EF-hands II and III of CaM. Two positions were selected, N60 and N97 that were mutated to aspartate residues (N60D, N97D), one located in the low affinity N-lobe and the other in the high affinity C-lobe (**Figure 33A**). CaM mutants were generated individually or in tandem yielding varied outcomes (**Figure 33B**). Using the linker-free ΔSp-YC154 the N60D and N97D single mutations did not yield any increase in Ca^{2+} affinity (EC$_{50}$: 2900 nM, and 2800 nM respectively), however an 86 % increase in total complementation was observed with the N60D mutation. Additionally, the incorporation of both mutations resulted in a 115 % improvement in total complementation with an improved EC$_{50}$ of 1460 nM. However, in combination with ΔSp-GGGGS this improvement was not maintained as the Ca^{2+}-mediated complementation exhibited a 94 % reduction compared with the linker-free ΔSp-YC154 and an additional reduction in Ca^{2+} affinity was observed (1730nM) (**Figure 33C**). Thus, the linker was discarded and the CaM^{N60DN97D} mutations were retained for further Integrator development.
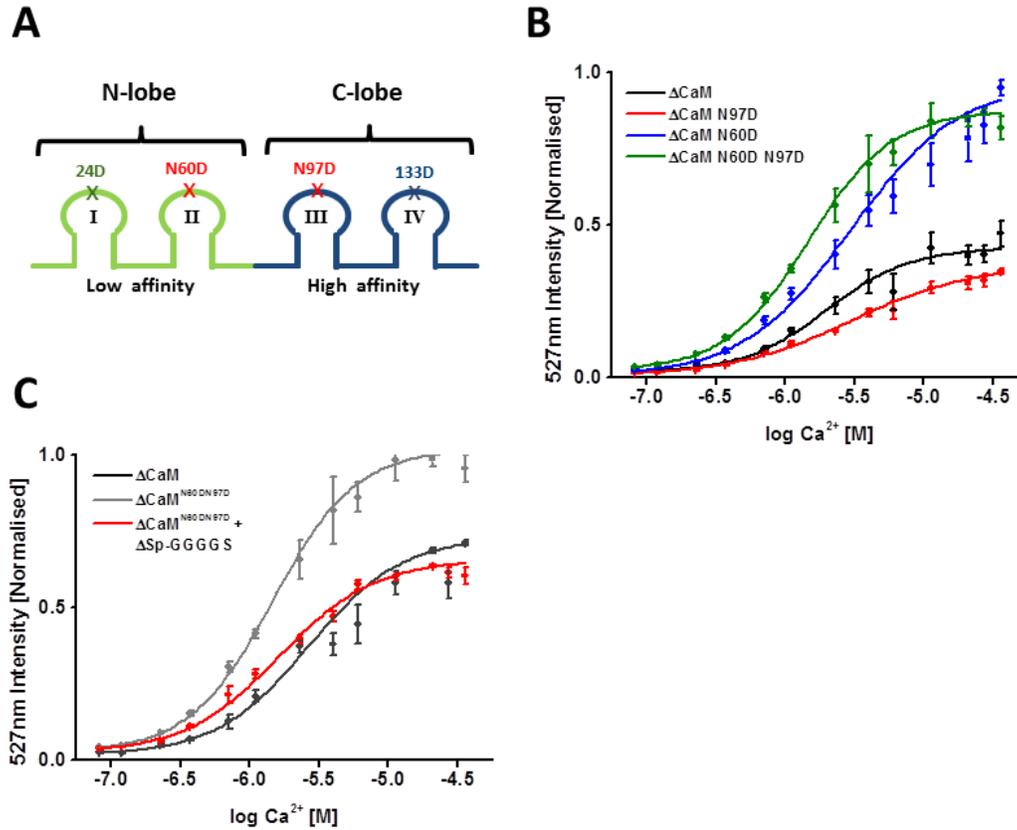
Figure 33: Ca^{2+} titrations of CaM mutations
A) Schematic illustrating the mutation points within the N- and C-lobe (Red: mutation sites). **B)** Ca^{2+} titrations of the original ΔCaM (black), N60D (blue), N97D (red) and N60DN97D (green) with the ΔSp-YC154. **C)** Ca^{2+} titrations of the original ΔCaM/ΔSp combination (black), CaM^{N60DN97D}/ ΔSp (grey), and the CaM^{N60DN97D}/ ΔSp-GGGGS (red). Error bars ± SEM.

4.3.2.3 Improving the stability of the ΔSp component

One central dogma of the ubiquitin system, the "N-end rule", stipulates that the N-terminal residue possesses the capacity to induce primary, secondary, or tertiary destabilisation (Varshavsky, 2008). The component ΔSp-YC possessed an N-terminal degradation residue (N-Degron) and without internal structure (due to the fusion of a short peptide to several β-sheets) it was postulated that stabilisation of this component via N- and C- terminal modification would enhance protein stability in a cellular environment. The first point of investigation was the addition of a C-terminal FP that would not only aid the stabilisation of the overall component but also provide a constitutive FP that would negate the requirement of an additional FP to be

transfected. Two FPs were considered, ECFP and ΔECFP (S30R Y39N A206K) with additional mutations for enhancing folding rate (**Figure 34A**). *In vitro* analysis of the ΔSp-YC-ECFP component exhibited 567 % reduced fluorescence in comparison to ΔSp-YC-ΔECFP (**Figure 34B**). Ca^{2+} titrations with YN-CaM^{N60DN97D} found that ΔSp-YC-ΔECFP enhanced the total complementation by 115 % with a negligible decrease in Ca^{2+} sensitivity (EC$_{50}$: 1510 nM). In contrast, by the addition of ECFP a 67 % decrease in signal and a significantly lower Ca^{2+} sensitivity of 2900 nM were observed (**Figure 34C**). Interestingly, as both ECFP variants displayed similar FRET ratio changes of 100 % neither variant conferred significant signal-to-noise improvements to rival that observed by complementation (**Figure 34D**).
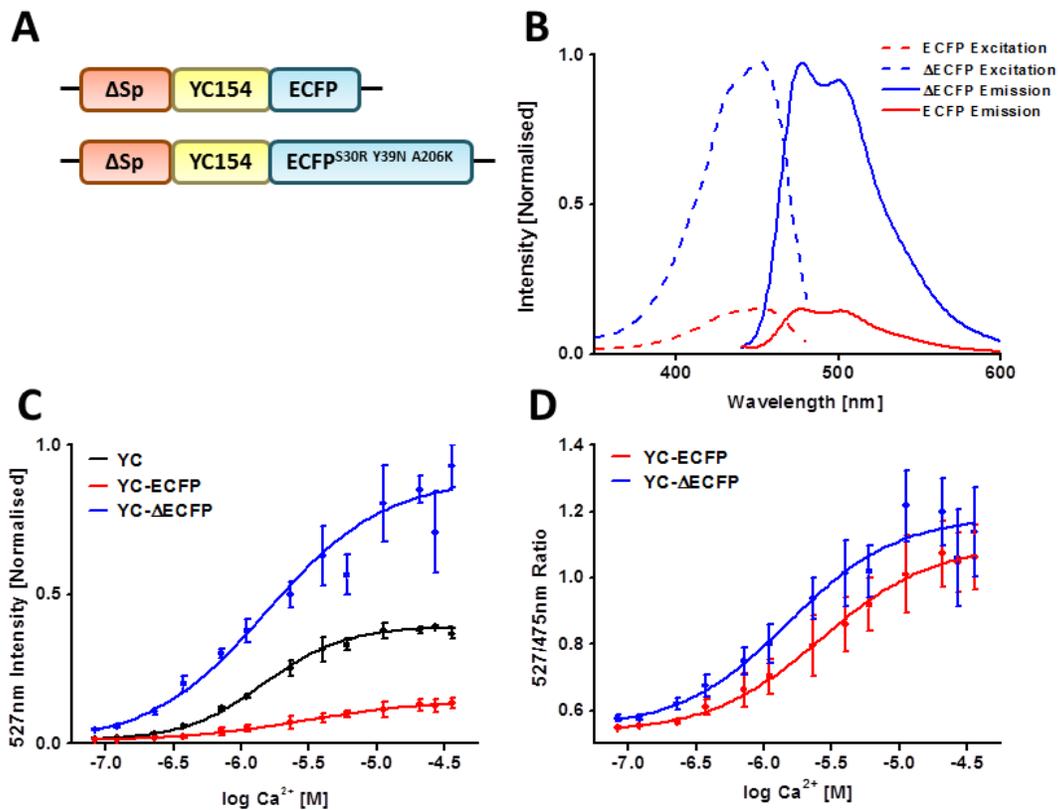
Figure 34: In vitro C-terminal incorporation of CFP variants
A) Schematic illustrating the architecture of the ΔSp component with the incorporation of ECFP or ΔECFP (S30R, Y39N, A206K). **B)** Fluorescence excitation and emission spectra of the two variants. Red: ECFP, Blue: ΔECFP. **C)** Complementation Ca^{2+} titrations of the original ΔSp (black), ΔSp-YC-ECFP (red), and ΔSp-YC- ΔECFP (blue) with YN-ΔCaM^{N60DN97D}. **C)** FRET ratio (527/475nm) Ca^{2+} titrations of the YN-ΔCaM^{N60DN97D} with either ΔSp-YC-ECFP (red), or ΔSp-YC ΔECFP (blue). Error bars ± SEM.

To prevent the primary and secondary destabilisation induced by the ΔSp N-Degron (Lys) several N-terminal sequence "caps" were generated with varying length; V, VA, VAA, and VAAA. *In vitro* analysis found that the majority of N-terminal modified components; V, VA, and VAAA induced a reduction in total complementation (10, 5 and 18 % respectively) and Ca^{2+} affinity (1700, 1690, and 1615 nM respectively) (**Figure 35A**). In contrast the VAA N-terminal cap induced a 17 % increase in complementation and a significant increase in Ca^{2+} affinity, 650 nM (**Figure 35B**).

For cellular stability analysis each of the N-terminal modified constructs were expressed in HEK293T cells with and without the addition of the proteasome inhibitor MG-132. In comparison to the transient transfection of ΔECFP alone, the original ΔSp sequence, beginning with the amino acids KT (Lys-Thr), exhibited 10.4 ± 0.8 % CFP fluorescence that increased to 36.5 ± 1.8 % CFP fluorescence in the presence of the proteasome inhibitor MG-132 (**Figure 35C**). In comparison to the original protein, all N-terminal modified sequences exhibited higher levels of CFP fluorescence of approximately 30 % of ΔECFP and increased to ~65 %. With the assumption that degradation-free CFP fluorescence (+10 µM MG-132) corresponds to maximal achievable fluorescence for this component it was found that, under cellular conditions, the original ΔSp peptide exhibited 28 ± 0.7 % fluorescence. However, by the stabilisation of the N-terminus a statistically significant higher fluorescence of ~50 % was recorded for all modified components (that did not display significant difference between themselves) indicating a 150 % reduction in proteasome-directed degradation (**Figure 35D**).
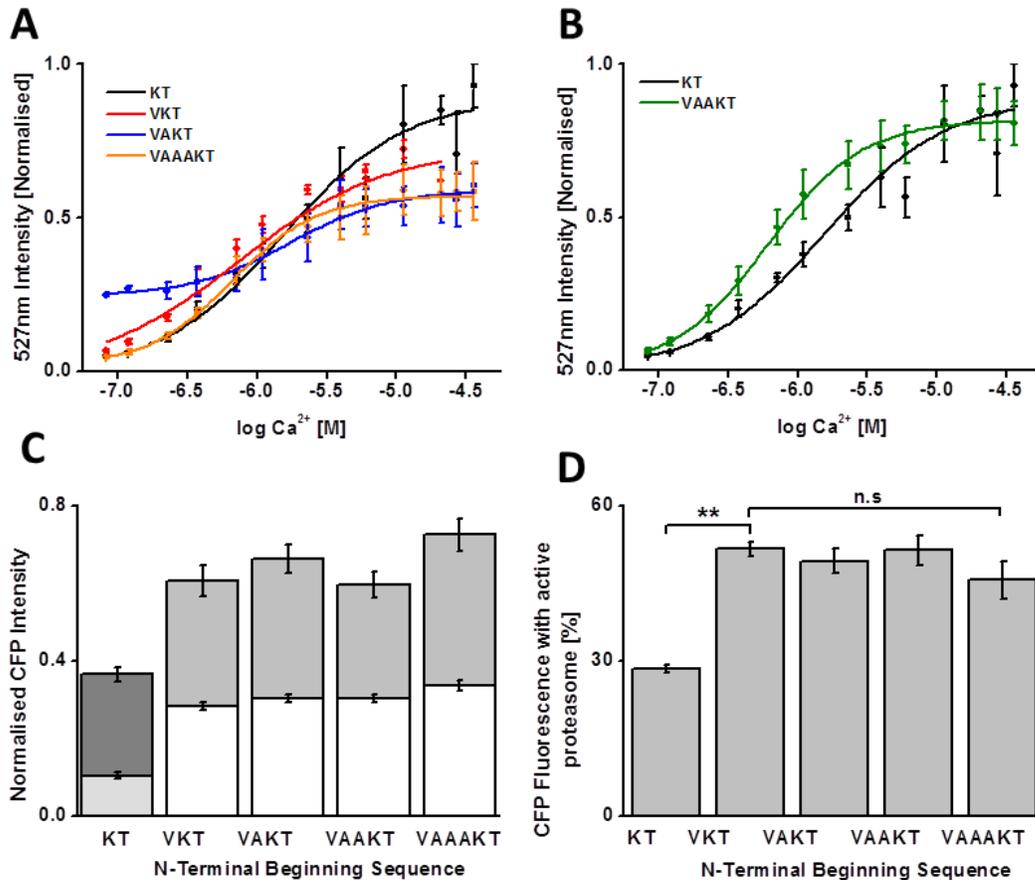
Figure 35: In vitro and cell culture characterisation of N-terminal modified components
A) Ca^{2+} titrations of YN-ΔCaM^{N60DN97D} with; black: ΔSp (YC- ΔECFP), red: VΔSp, blue: VAΔSp, orange: VAAAΔSp. **B)** Ca^{2+} titrations of YN-ΔCaM^{N60DN97D} with; black: ΔSp, green: VAAAΔSp. **C)** Normalised CFP fluorescence of HEK293T cells transfected with components possessing the N-terminal sequence KT (original), V, VA, VAA or VAAA (white/light grey). Cells co-incubated with 10 µM MG-132 are shown in grey/dark grey. **D)** Component CFP fluorescence under non-inhibited conditions as a percentage of maximal CFP fluorescence achieved using MG-132. **p<0.02. A+B error bars ± SEM, C+D error bars ± SD.

Finally, to ascertain whether the C-terminal incorporation of ΔECFP provided additional stability in cells, ΔECFP was replaced by ECFP. Hereby, ECFP a 67 % reduction (18.5 ± 1.6 %) of fluorescence in inhibitor-free conditions and a 42 % reduction (41.5 ± 1.3 %) in the presence of MG-132 when compared to ΔECFP (**Figure 36A**). Thus, the 51 ± 2.9 % of CFP fluorescence observed with VAAΔSp-YC-ΔECFP in the presence of active proteasome was reduced to 42.7 ± 1.9 % with the substitution of ECFP (**Figure 36B**).
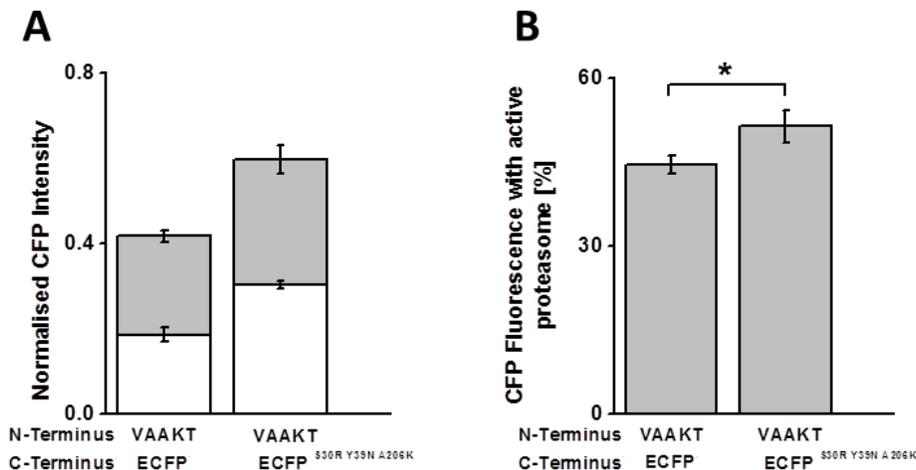
Figure 36: Cell culture characterisation of C-terminal modified components
A) Normalised CFP fluorescence of HEK293T cells transfected with components possessing the N-terminal sequence VAAA and either a C-terminal ECFP or ΔECFP (white). Cells co-incubated with 10 µM MG-132 are shown in grey. **B)** Component CFP fluorescence under non-inhibited conditions as a percentage of maximal CFP fluorescence achieved using MG-132. *$p<0.05$. Error bars ± SD.

4.3.2.4 Enhancing CaM affinity of VAA-ΔSp

The final point of investigation into Integrator modification was to improve the peptide affinity for CaM by the substitution of ΔSp residues for Alanine residues (Montigiani et al., 1996). Several ΔSp peptides were generated with mutations spanning the positions K7, S8A, L11A, F18A and S20A. *In vitro* Ca^{2+} titrations revealed an 82 % and 52 % reduction in complementation for the K7A and S20A peptides respectively. S8A yield no significant difference in complementation and the L11A and F18A exhibited a respective 62 and 85 % increase in complementation (**Figure 37A**). The Ca^{2+} affinities of the peptides found that, of the two peptides, the F18A mutation yield the most significant improvement with an EC_{50} of 420 nM (**Figure 37B**).
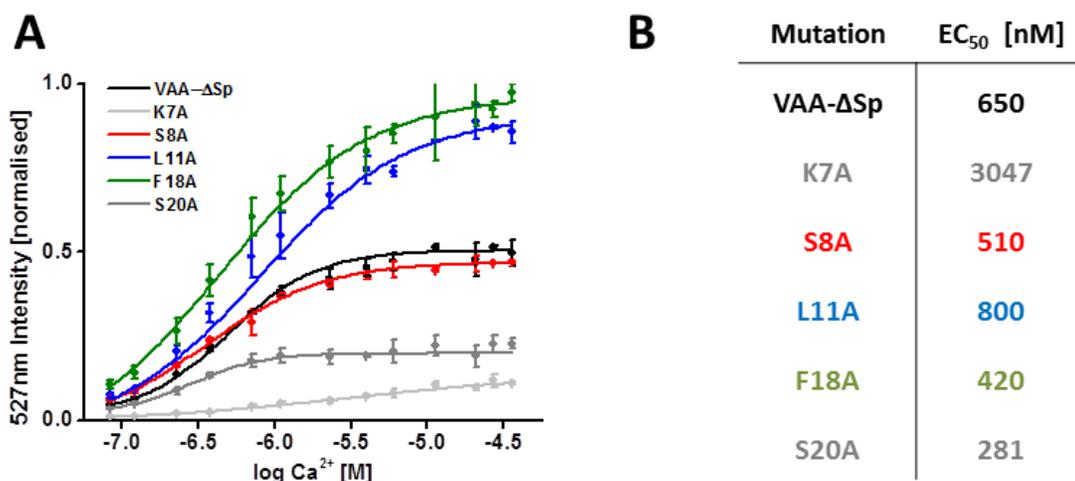
Figure 37: In vitro characterisation of VAAΔSp peptide mutants
A) 4 hour Ca^{2+} titrations of YN-$\Delta CaM^{N60DN97D}$ with; black: "wt" (VAAΔSp-YC- ΔECFP), light grey: K7A, red: S8A, blue: L11A, green: F18A, grey: S20A. **B)** EC_{50} values for all modified peptides.

4.3.2.5   Characterisation of $\Delta CaM^{N60DN97D}$ and VAA-ΔSp^{F18A}

To characterise the fundamental properties of the two Integrator components several points were investigated *in vitro* and in cell culture. The irreversibility of complementation of the YN153-$\Delta CaM^{N60DN97D}$ and VAAΔSp^{F18A}-YC154-ΔECFP components was validated using complementation kinetic studies. *In vitro* studies using 1 mM $CaCl_2$ and application of the Ca^{2+} chelating agent BAPTA (20 mM) after 0.5 or 1 hour resulted in an almost instantaneous cessation in complementation (**Figure 38A**). Furthermore, to complete the *in vitro* characterisation of this peptide a comparison of time-resolved complementation kinetics were undertaken at physiologically relevant Ca^{2+} concentrations of 0, 120, 373, 711 and 1100 nM $CaCl_2$ (1 mM $MgCl_2$) (**Figure 38B**).

In order to determine the interaction properties of the modified CaM and the ΔSp peptide in a cellular environment it was necessary to determine to what extent background was observed in cells in terms of both the degree of background (measured by fluorescence intensity) and the percentage of cell population that displayed background fluorescence. With YN-$\Delta CaM^{N60DN97D}$ and VAA-ΔSp^{F18A}-YC- ΔECFP background fluorescence was observed in 28 % of

HEK293T cells, similar to the ΔCaM/ΔM13 combination, however significantly higher than ΔCaM/ΔSp (**Figure 38C**). Despite the increase in the number of background fluorescence positive cells, a slight increase in the background fluorescence (Citrine/CFP Ratio) of YN-CaM^{N60DN97D} and VAA-ΔSp^{F18A}-YC was noted in comparison to ΔCaM/ΔSp (with CFP transfected separately). Nevertheless, the background fluorescence observed was still significantly lower than that observed using the ΔCaM/ΔM13 original components (**Figure 38D**).
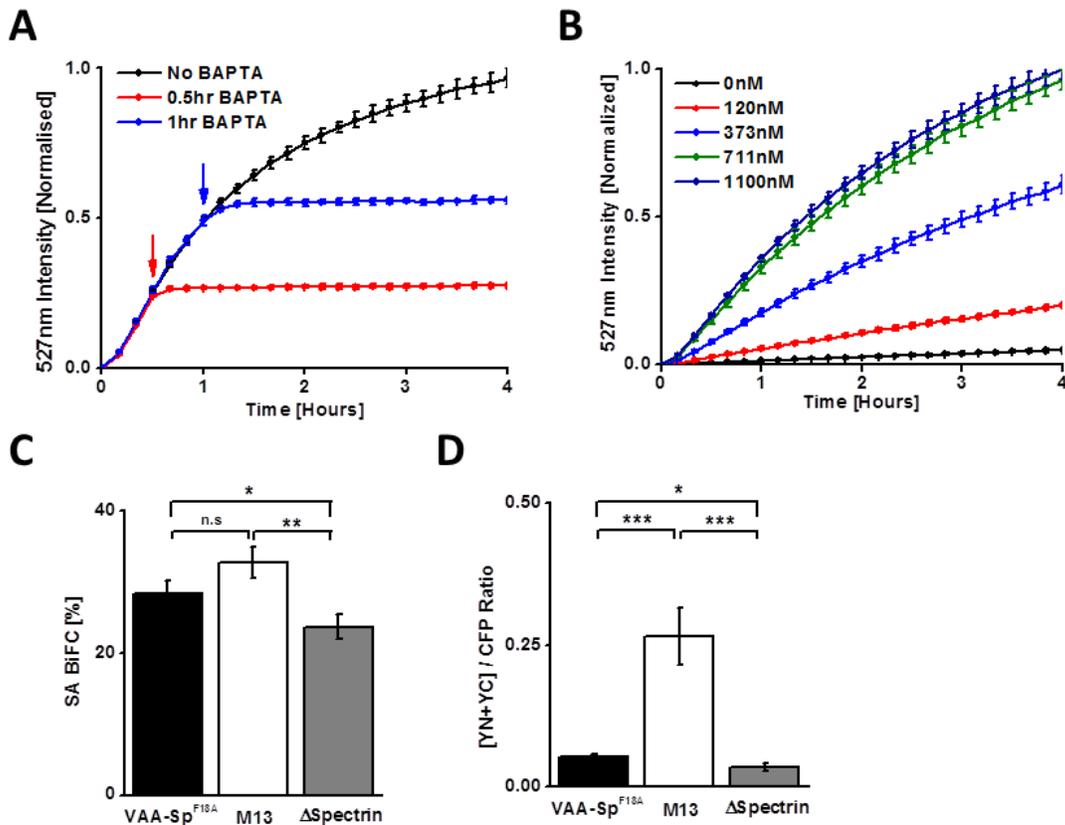
Figure 38: Characterisation of Integrator behaviour *in vitro* and in HEK293T cells
A) Complementation kinetics of YN153-ΔCaM^{N60DN97D} and VAAΔSp^{F18A}-YC154- ΔECFP in a 1mM CaCl$_2$ solution (black). 20 mM BAPTA was added after 0.5 hour (red) or 1 hour (blue). **B)** Complementation kinetics of YN153-ΔCaM^{N60DN97D} and VAAΔSp^{F18A}-YC154- ΔECFP in CaCl$_2$ solutions of 0 (black), 120 nM (red), 373 nM (blue), 711nM (green), or 1100nM (dark blue) with 1 mM MgCl$_2$. **C)** Percentage of HEK293T cells exhibiting background fluorescence. Black: YC-ΔCaM^{N60DN97D}/ VAA-ΔSp^{F18A}-YC- ΔECFP, white: YN-ΔCaM/ΔM13-YC, grey: YN-ΔCaM/ΔSp-YC. **D)** Ratio of complementation observed in background positive cells compared to ECFP. Black: YN-ΔCaM^{N60DN97D}/ VAA-ΔSp^{F18A}-YC, white: YN-ΔCaM/ΔM13-YC, grey: YN-ΔCaM/ΔSp-YC. *p<0.05, **p<0.02, ***p<0.001. A, B error bars ±SEM. C, D error bars ±SD.

4.3.2.6 Cell-based validation of $\Delta CaM^{N60DN97D}$ and $VAA\text{-}\Delta Sp^{F18A}$ interaction specificity

For the evaluation of the interaction between CaM and peptides Bimolecular Fluorescence Complementation cannot be used due to its dependency on two factors, the interaction between the CaM and peptide and whether this interaction is sufficient to yield the irreversible complementation. Therefore the binding efficiency of $CaM^{N60DN97D}$ and $VAA\text{-}\Delta Sp^{F18A}$ was determined by replacing the Citrine fragments YN and YC with ECFP and Citrine (respectively), thus, changing the irreversible output of the Ca^{2+}-dependent interaction into a reversible FRET-based mechanism (**Figure 39A**). Under stimulation-free conditions the Citrine/CFP ratio of $\Delta CaM^{N60DN97D}$/ $VAA\text{-}\Delta Sp^{F18A}$ did not significantly differ from $\Delta CaM/\Delta M13$. However, by replacing $\Delta CaM^{N60DN97D}$ with wtCaM a significant decrease was observed (**Figure 39B**). Using electrical stimulation ECFP-$\Delta CaM^{N60DN97D}$ and $VAA\text{-}\Delta Sp^{F18A}$-Citrine exhibited a 285 % higher $\Delta R/R$ compared to ECFP-ΔCaM and $\Delta M13$-Citrine (**Figure 39C**). Additionally, $VAA\text{-}\Delta Sp^{F18A}$ possessed a 10-fold higher specificity for $\Delta CaM^{N60DN97D}$ compared to wtCaM (**Figure 39D**).

Figure 39: ΔCaM^{N60DN97D} and VAA-ΔSp^{F18A} interaction specificity in cell culture
A) Schematic illustrating the architecture of the CaM/peptide pairs used; ΔCaM/ ΔM13, ΔCaM^{N60DN97D}/ ΔVAA-Sp^{F18A}, and wtCaM/ ΔVAA-Sp^{F18A}. **B)** Citrine/CFP ratios of dissociated hippocampal neurons transiently transfected with ECFP-ΔCaM/ΔM13-Citrine (black), ECFP-ΔCaM^{N60DN97D}/ VAA-ΔSp^{F18A}-Citrine (red), ECFP-wtCaM/ΔVAA-ΔSp^{F18A}-Citrine (blue). **C)** Normalised ΔR/R values for ECFP-ΔCaM/ΔM13-Citrine (black), ECFP-ΔCaM^{N60DN97D}/ VAA-ΔSp^{F18A}-Citrine (red) transfected neurons stimulated with an stimulation pulse (80 Hz PF, 1000 µs PW, 1 sec BD, 30 V FS) applied once every 20 sec for 2 minutes (insert). **D)** Normalised ΔR/R values for ECFP-ΔCaM^{N60DN97D}/ VAA-ΔSp^{F18A}-Citrine (red), ECFP-wtCaM/Δ VAA-ΔSp^{F18A}-Citrine (blue) transfected neurons stimulated with a stimulation pulse (80Hz PF, 1000µs PW, 1sec BD, 30V FS) applied once every 20 sec for 2 min (insert). **p<0.02. Error bars ±SEM.

4.3.2.7 Determination of cellular response of YN-ΔCaM^{N60DN97D}-IRES-VAA-ΔSp^{F18A} -YC- ΔECFP

To unify the two components of this biosensor an Internal Ribosomal Entry Site (IRES) was introduced with the two components flanking either terminus. Under this construction the first component, the YN-ΔCaM^{N60DN97D} was under the vector CMV promoter and the VAA-ΔSp^{F18A} -YC-ΔECFP under the IRES promoter (**Figure 40A**). Transient co-transfection of dissociated hippocampal neurons with the red GECI "R-GECO1" (Zhao et al., 2011) and the Integrator exhibited a stimulation-dependent 223 % increase in Citrine complementation (**Figure 40B, D**). However, no such increase was observed in unstimulated neurons (**Figure 40C, E**). Furthermore, using a 12-well stimulation chamber it was possible to resolve complementation/constitutive FP ratios between unstimulated cells (T=0) and cells stimulated for 1 to 4 hours (**Figure 40F**), whereas substitution of YN-ΔCaM^{N60DN97D} for wtCaM did not yield a significant increase in complementation.
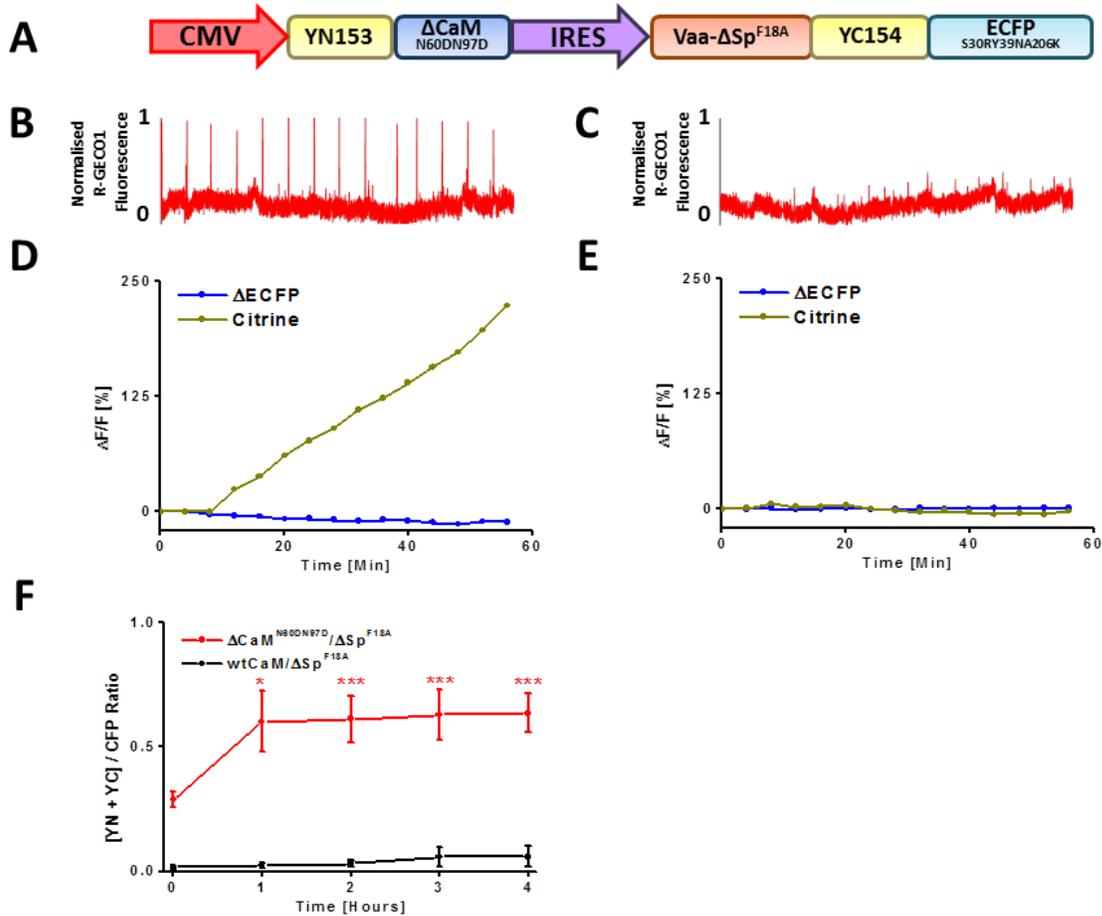
Figure 40: Cell culture evaluation of Integrator coexpressed with R-GECO1
A) Schematic of unified components flanking an IRES site. **B)** Normalised R-GECO1 fluorescence of transiently transfected neuron stimulated with electrical field stimulation (using 80 Hz PF, 1000 µs PW, 1 s BD, 30 V FS, 240 s ITI). **C)** Normalised R-GECO1 fluorescence of transiently transfected unstimulated neuron. **D)** ΔECFP and Citrine ΔF/F values of co-transfected Integrator from the same stimulated neuron displayed in **B**. **E)** ΔECFP and Citrine ΔF/F values of co-transfected Integrator from the same unstimulated neuron displayed in **C**. **F)** Reconstituted Citrine/CFP ratio of dissociated hippocampal neurons stimulated using a 12-well plate stimulation array. Red: YN-ΔCaM^{N60DN97D}-IRES-VAA-ΔSp^{F18A}-YC-ΔECFP, black, YN-wtCaM-IRES-VAA-ΔSp^{F18A}-YC-ΔECFP. *$p<0.05$, ***$p<0.001$. Scale bar: 50 µm. Error bars ± SD.

4.3.3 Semliki Forest Virus delivery of Integrator

Due to the irreversible nature of this Integrator the final criteria remaining was the generation of a virus containing the Integrator in order to acquire temporal control over Integrator expression. The Semliki Forest Virus (SFV) was chosen due to its high protein production rate upon cellular infection.

4.3.3.1 Development of SFV YN-$\Delta CaM^{N60DN97D}$-IRES-VAA-ΔSp^{F18A}-YC- $\Delta ECFP$

Upon transfection of HEK293T cells with the pSCA-Integrator and the pSCA-Helper plasmids the expression of the biosensor was confirmed after 2 days (**Figure 41B**). Transfection of dissociated hippocampal neurons with SFV-Integrator I (SFV-I) for 1 - 6 hours did not yield any constitutive FP ($\Delta ECFP$) fluorescence detected either by western blot (**Figure 41A**) or by fluorescence microscopy (**Figure 41B**). However, it is important to note that apoptotic cells (determined by lack of adhesion or morphology) did exhibit detectable fluorescence.
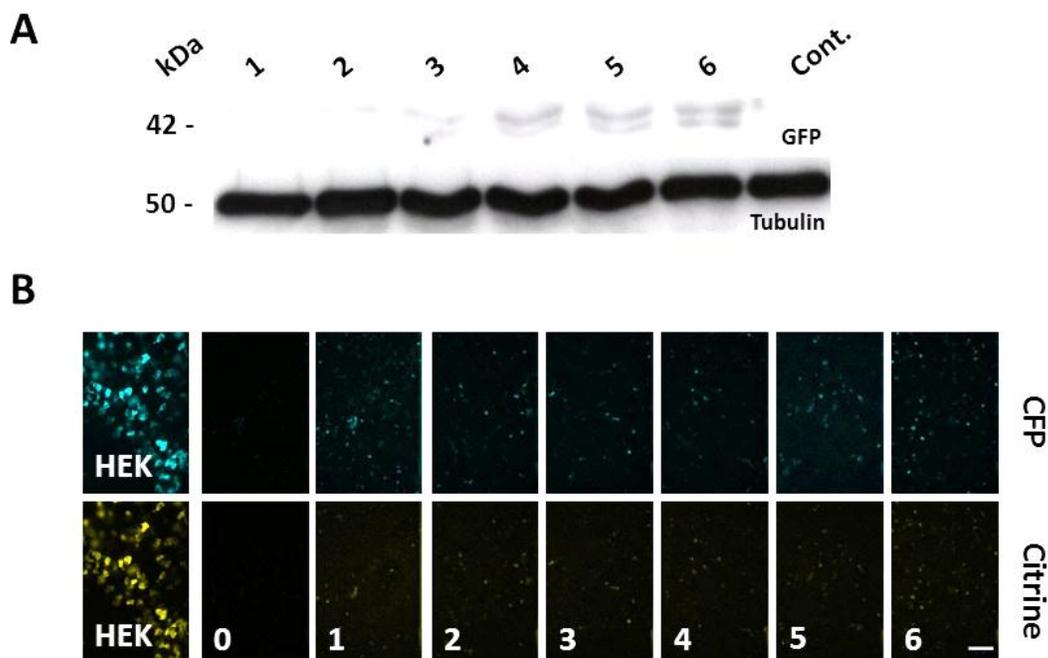
Figure 41: Western blot analysis and expression characterisation of SFV-I
A) Western blot analysis of dissociated hippocampal neurons infected with SFV-I for between 1 and 6 hours using an anti-GFP antibody for the SFV-I and an anti-Tubulin antibody as a control. **B)** Artificially coloured fluorescence images of co-transfected pSCA-Integrator/ pSCA-Helper HEK293T cells and infection time-course of dissociated hippocampal neurons for up to 6 hours. Scale bar: 50 μm.

Upon apoptosis a characteristic high Ca^{2+} influx is observed, and with fluorescence in apoptotic cells observed it was believed that constitutive FP fluorescence may only be achievable once the CaM/CBP forms a Citrine refolded complex. Electrical field stimulation of dissociated hippocampal neurons yield an increase in both Citrine (ΔF/F: 2184 ± 86 %) and constitutive FP (ΔF/F: 653 ± 42 %) fluorescence (**Figure 42B, C**). Additionally, an increase in Citrine fluorescence was also observed upon excitation with CFP (ΔF/F: 1884 ± 78 %) yielding an almost linear FRET increase (ΔR/R: 182 ± 10 %) after 1 hour (**Figure 42D**). Interestingly, no immunoreactivity of the anti-GFP antibody was observed at 42 kDa, corresponding to the VAA-ΔSp^{F18A}-YC-ΔECFP component. However, time-dependent anti-GFP immunoreactivity was observed at 72kDa indicating that constitutive FP fluorescence occurred upon complex formation. It must be noted that it was indistinguishable to what extent Citrine and ΔCFP separately contributed to immunoreactivity (**Figure 42A**).
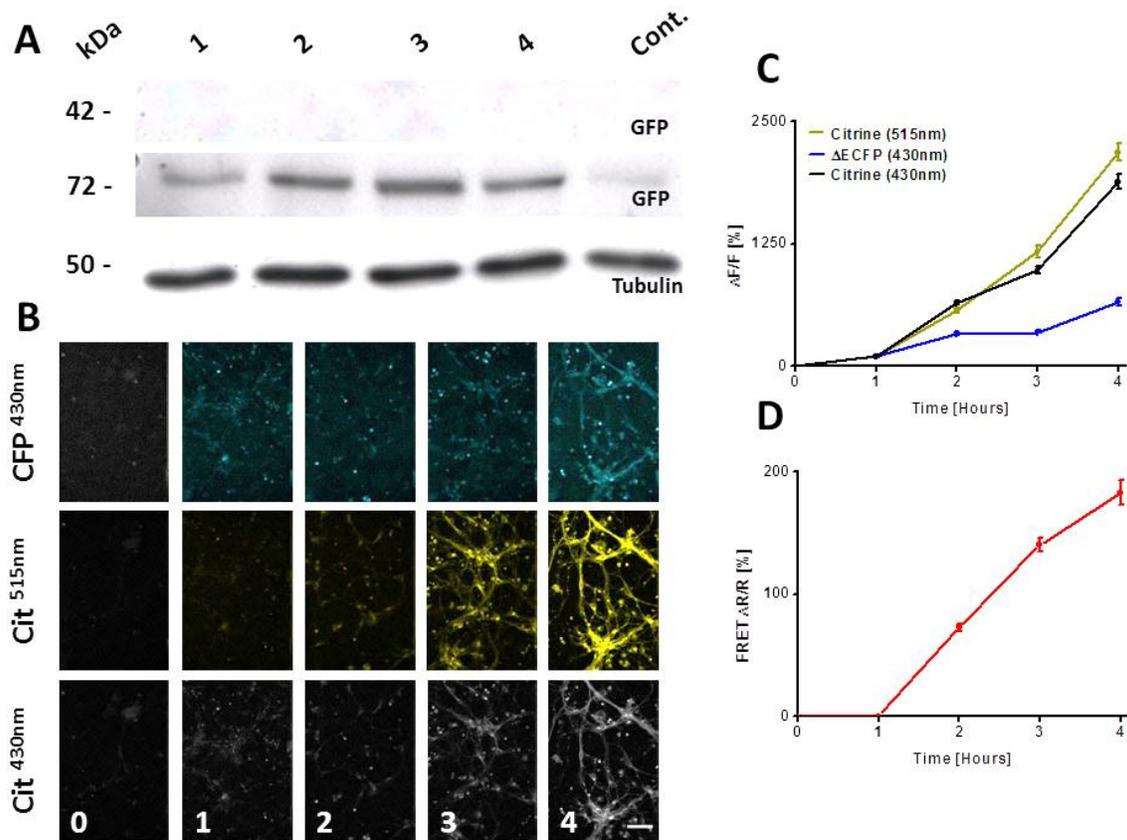
Figure 42: Electrical Field Stimulation characterisation of SFV-I
A) Western blot analysis of dissociated hippocampal neurons infected with SFV-I for a 2 hour preincubation before electrical field stimulation for 1 to 4 hours using 80 Hz PF, 1000 µs PW, 1 s BD, 30 V FS. An anti-GFP antibody was used detection of SFV-I and an anti-Tubulin antibody was used as a control. **B)** Artificially coloured fluorescence microscopy images of CFP (top panels), Citrine (middle panels) and Citrine excited with CFP excitation wavelength of 430 nm (bottom panels). **C)** Quantification of fluorescence of CFP (Blue), Citrine (Yellow) and Citrine excited using 430nm (black). **D)** FRET ΔR/R over 4 hours. Scale bar: 50 µm. Error bars ± SD.

Due to the lack of constitutive FP fluorescence it was determined whether incubation time possessed any effect on SFV-I activity. To achieve this SFV-I responses to field stimulation after either a 2 hour or 16 hour pre-incubation were compared (**Figure 43A**). A significant difference in Citrine fluorescence after 2 and 3 hours was found (**Figure 43B**). Due to the significantly higher complementation observed with a 2 hour compared to 16 hours pre-incubation, the two hour pre-incubation timeframe was used for all subsequent experiments.
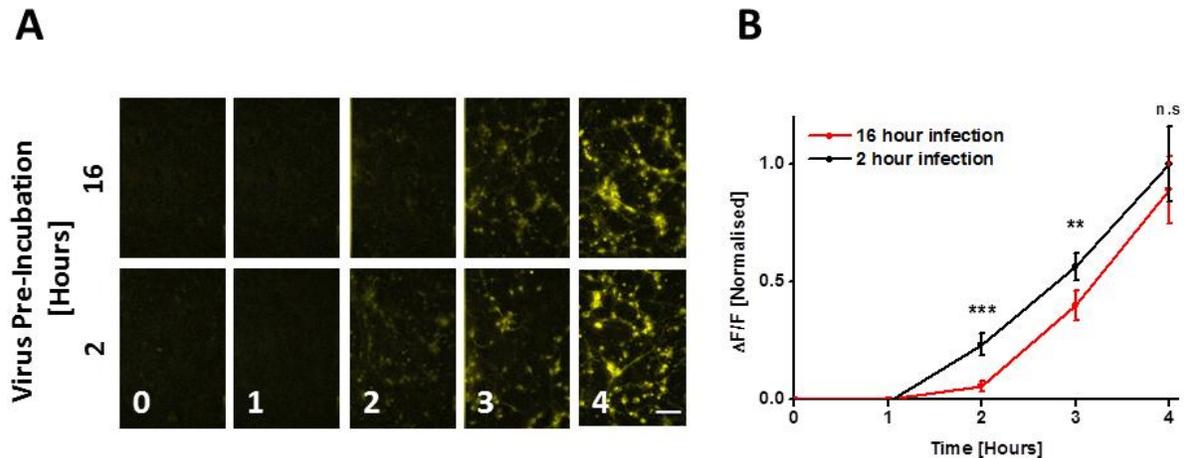
Figure 43: Effect of infection duration of SFV-I activity
A) Artificially coloured fluorescence images of dissociated hippocampal neuron infected with SFV-1 for either 16 or 2 hours before experiment initiation. Upon initiation cells were stimulated with electrical field stimulation using 80 Hz PF, 1000 µs PW, 1 sec BD, 30 V FS parameters. **B)** Quantification of fluorescence of Citrine after 16 hours pre-incubation (red) or 2 hours pre-incubation (black). **p<0.02, ***p<0.001. Scale bar: 50 µm. Error bars ± SD.

4.3.3.2 Generation of alternative SFV variants

To overcome the lack of constitutive FP fluorescence two different approaches were undertaken. The first approach was to replace the ΔCFP with either an improved cyan fluorescent protein mCerulean 3 (Markwardt et al., 2011) or mCherry (Shaner et al., 2004). The second approach was to switch the two components to place the constitutive FP under the CMV promoter and the CaM under the IRES promoter (**Figure 44A**). *In vitro* Ca^{2+} titrations revealed that replacing ΔCFP for either mCerulean 3 or mCherry resulted in a respective 73 % and 64 % reduction of Citrine complementation (**Figure 44B**). Regardless, three virus variants were generated; mCerulean 3 (SFV-II), mCherry (SFV-III) and the reversed component orientation (SFV-IV). Transient transfection of HEK293T cells revealed substantial constitutive FP fluorescence (**Figure 44C** *top panels*); however after 6 hours of viral infection no constitutive FP fluorescence was detectable (**Figure 44C** *bottom panels*).
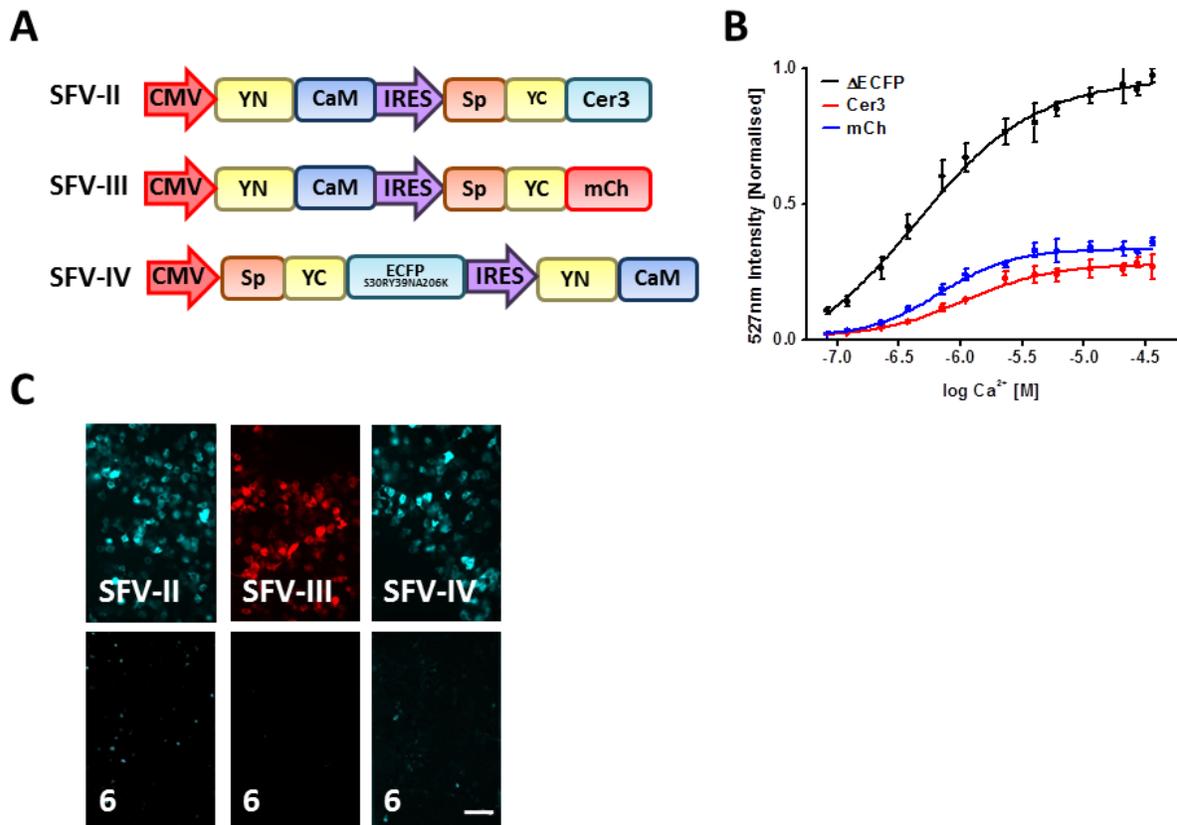
Figure 44: Generation of SFV variants SFV-II, SFV-III and SFV-IV.
A) Schematic of SFV variants. **B)** Ca^{2+} titrations of YN-ΔCaM^{N60DN97D} with; black: VAAΔSp-YC-ΔCFP, blue: VAAΔSp-YC-mCherry, red: VAAΔSp-YC-mCerulean 3. **C)** Top panel: Constitutive FP fluorescence of HEK293T cells transiently transfected for two days with SFV-II, SFV-III and SFV-IV. Bottom Panels: Dissociated hippocampal neurons infected for 6 hours with the respective SFV variant. Scale bar: 50µm. Error bars ± SEM.

Characterisation of the viruses using electrical field stimulation found a significant decrease in Citrine fluorescence of all new variants compared to SFV-I (**Figure 45A**). Interestingly, only the SFV-III displayed any increase in constitutive FP fluorescence that rivaled SFV-I (**Figure 45B**), however, due to the poor performance SFV-I was chosen for continuing characterisation.
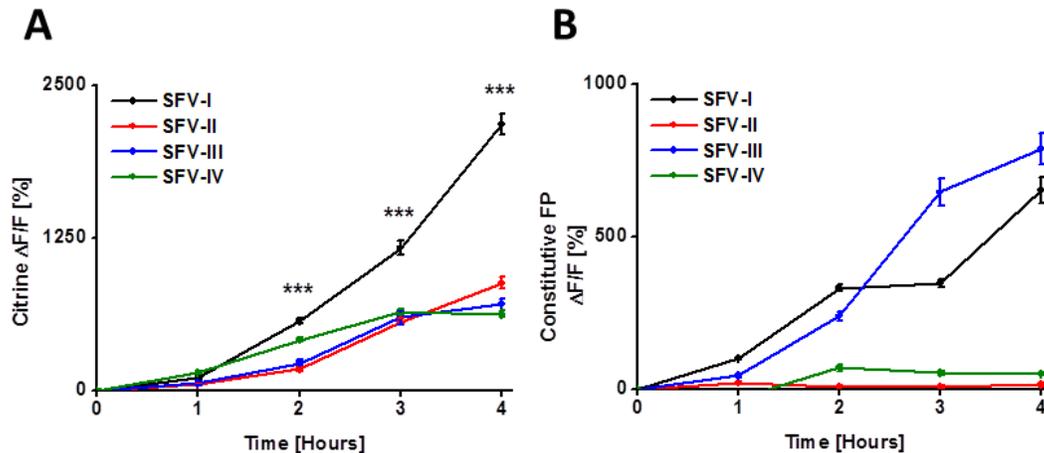
Figure 45: Characterisation of SFV variants SFV-II, SFV-III and SFV-IV
A) Citrine ΔF/F of SFV-I (black), SFV-II (red), SFV-III (blue) and SFV-IV (green) using 80 Hz PF, 1000 μs PW, 1 sec BD, and 30 V FS stimulation parameters. **B)** Constitutive FP ΔF/F for SFV-I (black), SFV-II (red), SFV-III (blue) and SFV-IV (green). *** $p<0.001$

4.3.3.3   Development of physiological Electrical Field Stimulation protocols

To determine whether SFV-I is responsive to physiologically relevant stimuli it was necessary to develop field stimulation protocols that resembled the activity observed in neuron populations. Stimulation protocols were developed to resemble spontaneous activity stimulation (SAS), Hippocampal CA1 neuron Stimulation (HS) (Garaschuk et al., 1997), Primary Afferent neuron Stimulation (PAS) (Enes et al., 2010) and Theta Burst Stimulation (TBS) (Balkowiec and Katz, 2002). These stimulation protocols were selected due to the significant variability in the intertrain intervals (ITI) that varied from a burst every 10 sec (SAS) to every 5 min (PAS) (**Figure 46A-D**). Using the calcium dye Fluo-4 AM a sub-maximal ΔF/F was observed in HS, TBS, and PAS, and no detectible Ca^{2+} transients in SAS (**Figure 46E-H**). Using the LIVE/DEAD cytotoxicity assay we determined no significant effects on cell apoptosis by any stimulation protocol (**Figure 46I-L**).
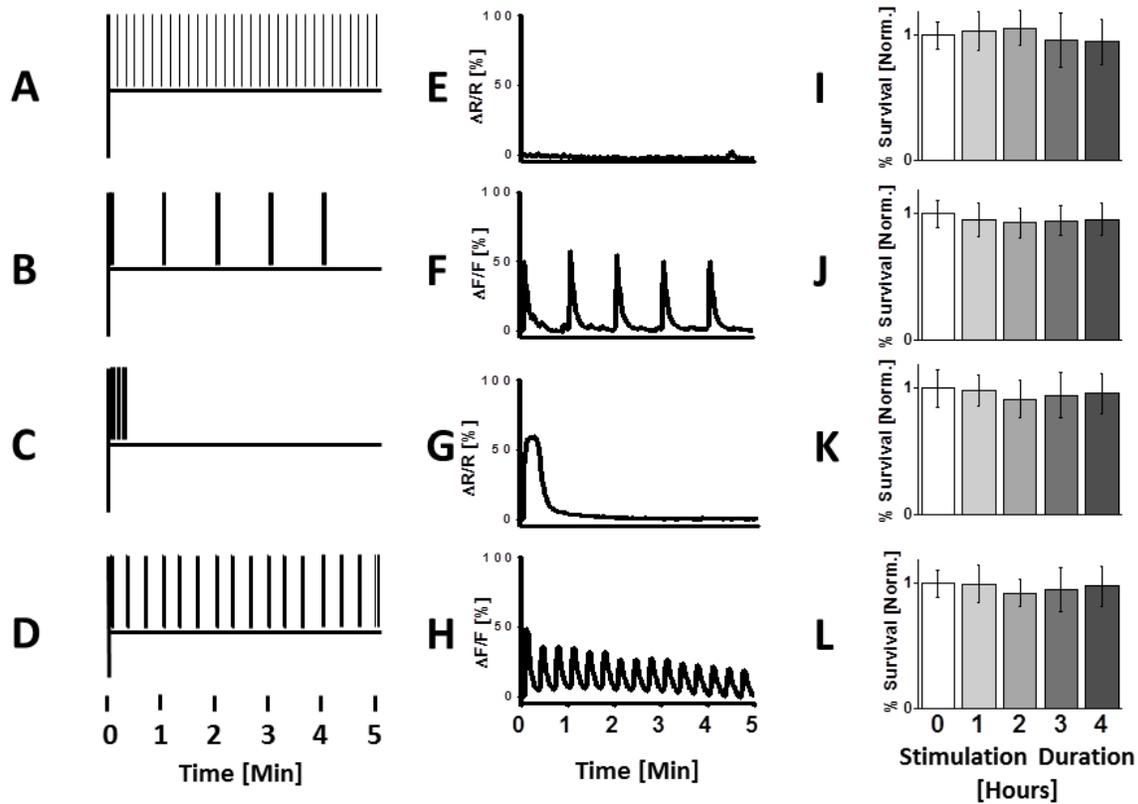
Figure 46: "Physiological" field stimulation protocols
A-D) Illustration of field stimulation protocols; **A:** Spontaneous Activity Stimulation (SAS; 1 Hz PF, 150 μs PW, 1 s BD, 30 V FS, 10 s ITI), **B:** Hippocampal CA1 neuron Stimulation (HS; 50 Hz PF, 150 μs PW, 1 s BD, 30 V FS, 60 s ITI), **C:** Primary Afferent neuron Stimulation (PAS; 20 Hz PF, 150 μs PW, 20 s BD, 30 V FS, 300 s ITI), **D:** Theta Burst Stimulation (TBS; 20 Hz PF, 100 μs PW, 5 s BD, 30 V FS, 20 s ITI). **E-H)** Fluo-4AM ΔF/F using electrical field stimulation protocols outlined in A-D (E: SAS, F: HS, G: PAS, H: TBS). **I-L)** Normalised percentage of cell survival (Live/Dead Cytotoxicity Assay) upon application of electrical field stimulation protocols outlined in A-D (I: SAS, J: HS, K: PAS, L: TBS). Error bars ± SD.

4.3.3.4   Characterisation of SFV-I using physiological stimulation

For evaluation of SFV-I performance under physiological stimulation conditions three parameters were investigated; the $\Delta F/F$ of Citrine, the $\Delta F/F$ of the constitutive FP ($\Delta ECFP$), and the $\Delta R/R$ of the FRET response. Regarding the $\Delta F/F$ of Citrine and the constitutive FP all stimulation protocols (with the exception of SAS) displayed significant increases in fluorescence during four hours. The earliest significant increase was observed using TBS, whereby after two hours fluorescence was recorded in both Citrine and $\Delta ECFP$ (**Figure 47A, B**). HS displayed the largest increase in Citrine $\Delta F/F$ after four hours (1579 ± 43 %); however it displayed no significant increase in constitutive FP fluorescence compared to PAS. Interestingly, TBS yielded a maximal Citrine $\Delta F/F$, after three hours, a 51 % increase compared to the Citrine intensity observed at four hours using HS. In neither case was significant fluorescence observed using SAS. Regarding the FRET response only HS displayed a significant $\Delta R/R$ (108 ± 4 % after 4 hours) indicating that this virus is unsuitable for FRET-based analysis of all neuronal firing patterns (**Figure 47C**). When stimulation of dissociated hippocampal neurons was inhibited, by the application of 1 µM of the voltage-gated sodium channel inhibitor "Tetrodotoxin" (TTX) and the L-type voltage-gated Ca^{2+} channel inhibitor "Nimodipine", all observed $\Delta F/F$ and $\Delta R/R$ responses were abolished (**Figure 47D-F**).
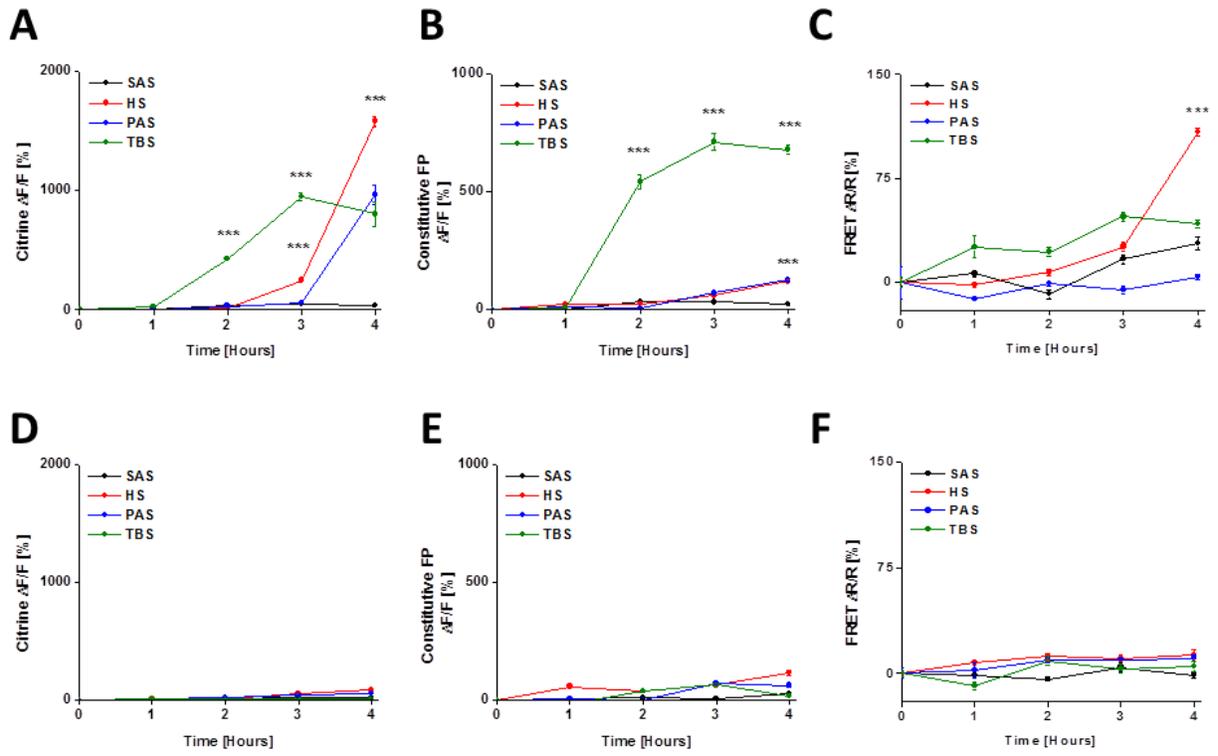
Figure 47: Characterisation of SFV-I using "physiological" field stimulation protocols
A-C) SFV-I responses to SAS (black), HS (red), PAS (blue) and TBS (green) stimulation (**A**: Citrine ΔF/F, **B**: Constitutive FP ΔF/F, **C**: FRET ΔR/R). **D-F)** SFV-I responses to SAS (black), HS (red), PAS (blue) and TBS (green) stimulation in the presence of 1 μM TTX and 1 μM Nimodipine (**D**: Citrine ΔF/F, **E**: Constitutive FP ΔF/F, **F**: FRET ΔR/R). *** p<0.001. Error bars ± SD.

4.3.4 Application of Bimolecular Fluorescence Complementation developed protein-pair for the development of other split-protein based strategies

The lack of an *in vitro* platform for the development of the split-TEV protease Integrator became one of most pertinent issues for the project's dismissal. The subsequent complementation biosensor development has yield the development of a novel CaM/peptide combination that can elicit fluorescence complementation in response to endogenous Ca^{2+} transients. The unique combination developed using Bimolecular Fluorescence Complementation was consequently theorised to be applicable to other split-protein strategies such as the split-TEV. To this end, the Citrine fragments were replaced with the aforementioned TEV fragments. When the transfected components (along with TS-FRET) were subjected to field stimulation a 35 ± 2.7 % decrease in the FRET ratio was observed after 2 hours (**Figure 48**). Thus, not only has the first complementation-based Integrator been engineered to respond to endogenous factors but also the successful application of complementation-engineered proteins to other split-protein based strategies (that cannot be developed *in*) has been demonstrated.
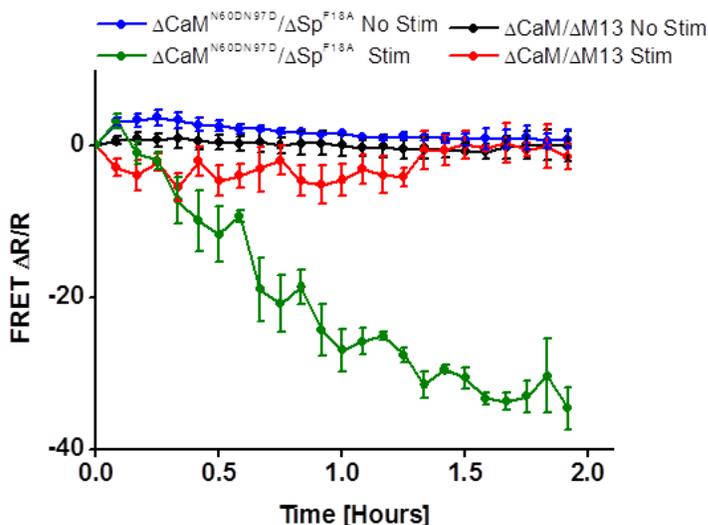
Figure 48: Split-TEV responses to field stimulation using TS-FRET
FRET ΔR/R values for transfected dissociated neurons stimulated for 2 hours with a stimulation burst (80 Hz PF, 1000 µs PW, 1 sec BD, 30 V FS) every 4 minutes. Stimulation of ΔCaM/ΔM13 (red) or unstimulated (black) compared to stimulation of ΔCaM^{N60DN97D}/VAAΔSpF18A (green) or unstimulated (blue). Error bars ±SD.

5 Discussion

5.1 Overview of Integrator development

In order to generate the Integrator biosensor three primary concept designs were undertaken with each being discussed in detail below. In brief the three designs considered were the development of; a Ca^{2+}-dependent protease FRET integrator, an artificial Ca^{2+}-dependent protease with FRET reporter (via either the development of a conformation-dependent TEV Integrator or a split-protein based Integrator), and a complementation Integrator. Of the three models the Bimolecular Fluorescence Complementation design satisfied all *in vitro* criteria and, as a consequence of this, the complementation Integrator was the only design pursued for further development (**Figure 49**). Furthermore, it is important to note that a complementation-based strategy can also be used for the development of other split-protein based strategies.
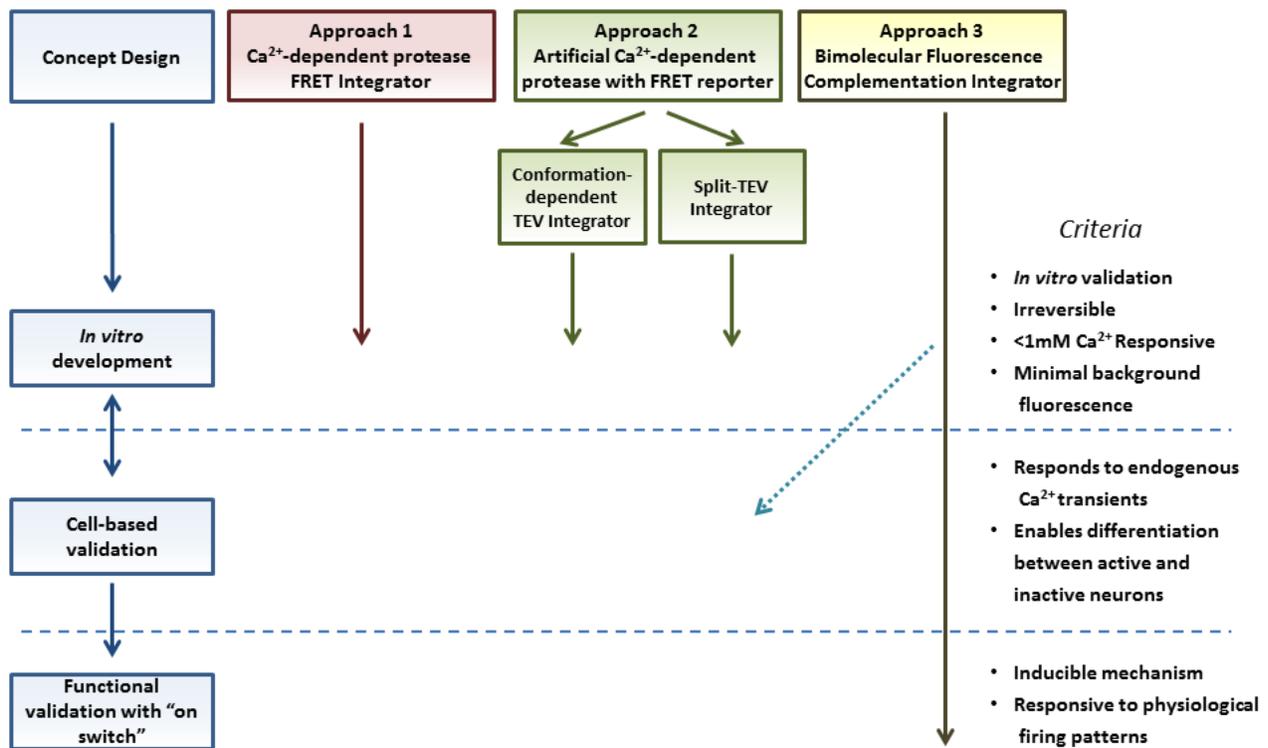
Figure 49: Summary of Integrator design concepts

5.2 Approach 1: Ca²⁺-dependent protease FRET Integrator

Initial approaches in the development of an irreversible Ca^{2+}-dependent Integrator were formulated on the concept of utilising proteases, whether intrinsically Ca^{2+}-dependent or not, to induce the irreversible cleavage of a FRET pair. The first approach took the notion that using the Ca^{2+}-dependent protease μ-Calpain, and the previous research identifying a μ-Calpain responsive FRET-pair, an Integrator could be engineered and tailored for the integration of neuronal Ca^{2+} transients. The proposed approach to this design was to engineer an improved μ-Calpain with an oestrogen receptor ligand binding domain (ER-LBD) that would result in the nuclear translocation of the protease by the administration of the synthetic ligand Tamoxifen. By the addition of a nuclear localisation sequence (NLS) to the FRET-pair the FRET substrate could be restricted to the nucleus.

The first step in any biosensor design is the establishment of an *in vitro* platform from which further design modifications could be verified. Without previous publications providing insight into the development of this platform, purified μ-Calpain was chosen for the characterisation of the FRET-pairs; CSS (Calpain Sensitive Substrate FRET pair) and CIsS (Calpain Insensitive Substrate FRET pair). In the presence of 1 mM Ca^{2+} the CSS displayed the largest reduction in FRET ratio. However, in contrast to previous research the CIsS also displayed a certain degree of Calpain specificity. The residual activity demonstrated by the CIsS can most likely be attributed to the neighbouring C-terminal glycine as μ-Calpain is known to cleave between the Tyr^5 and Gly^6 residues (Harris et al., 1988). Whilst this residual activity was a minor consideration (as the CIsS could easily be re-engineered to remove this activity) it validated the sensitivity of the *in vitro* platform.

With the established *in vitro* platform the development took on a bifurcated approach to determine the physiological Ca^{2+} range of the CSS and the engineering of a μ-Calpain construct from cDNA. Using purified μ-Calpain a minimal threshold of between 10 and 100 μM Ca^{2+} was observed, in agreement with previous literature (Dutt et al., 2002). The discrepancy between *in vitro* and *in vivo* K_d measurements have been reportedly due to the large CAPN1 subunit with various hypotheses postulating Calpain/phospholipid complexes or highly localised

Ca^{2+} concentrations to be the source of this discrepancy. Nevertheless, the attempts at engineering a μ-Calpain construct focused on either combined expression with a constitutive FP (mCherry) or IRES-separated expression of the two subunits. The lack of active μ-Calpain protease isolated from four constructions (μ-C1-4) significantly hindered the development of the Integrator concept that ultimately was discontinued in favour of alternative approaches.

5.3 Approach 2: Artificial Ca^{2+}-dependent protease with FRET reporter

The second approach towards development of an integrator was the generation of an artificially Ca^{2+}-dependent protease that would cleave a FRET reporter in a similar fashion to the μ-Calpain based Integrator. The two strategies considered were either the development of a conformation-dependent protease Integrator or a split-protease Integrator. The protease selected for this approach was the TEV protease (Tobacco Etch Virus) due to the lack of identified mammalian homologs and its well-defined substrate (van den Berg et al., 2006).

For the conformation-dependent protease Integrator it was postulated that, by using a Transposon insertion mechanism, locations within the protease structure could be identified for the insertion of a Ca^{2+} responsive element that would confer protease activity upon Ca^{2+} binding. The high affinity C-lobe (EF-hands III and IV) of Troponin C (TnC) was chosen as the Ca^{2+} responsive element over the architecture favoured by the GCaMP biosensor series due to the small size of the C-lobe that would limit the perturbation of protease function. The initial stages of this design were the modification of the TEV protease to improve kinetics and to identify the positions for TnC insertion. By removal of the auto-inhibitory C-terminal domain and the addition of a mCherry Reporter the K_d improved 760 %. Furthermore, the screening of randomly inserted Transposons yield a bias of insertions between amino acids 170-210 that retained mCherry fluorescence. It can be speculated that insertions outside of this upper- and lower- quartile yield misfolded protease that, in turn, resulted in misfolded mCherry. The random selection of insertion sites did yield both TEV protease variants retaining proteolytic function and variants without function. However, once TnC was inserted into these selected

sites a Ca^{2+}-free and Ca^{2+}-dependent increase in FRET was observed. The exact source of the observed increase in FRET was not been fully identified, however, it was most likely a result of protease/substrate binding in the absence of protease function. At this point this approach was discontinued; nonetheless, several avenues remain open to investigation. Primarily, generation of TEV cp-variants at these locations may provide the initial framework for the development of an Integrator resembling the GCaMP architecture. Furthermore, one could additionally look at the applicability of inserting other EF-hands motifs that possess alternative structural conformations that may enable the gain of function, for example the FrpC Ca^{2+}-binding domain (Osicka, 2004).

The second approach using the TEV protease was based on the research from Moritz Rossner whereby they could recover protease function from split-TEV by inducing FRB/FKBP heterodimerisation via rapamycin addition (Wehr et al., 2006). It was expected that by the substitution of the proteins FRB/FKBP for ΔCaM and ΔM13 a Ca^{2+}-dependent split-protein Integrator could be developed. To this end several orientations of components were investigated *in vitro* with no significant change in the FRET ratio of TS-FRET observed. Once no FRET cleavage was observed using an alternative rapamycin-induced heterodimerisation of FKBP-N-TEV and FRB-C-TEV it was concluded that the *in vitro* platform was not appropriate for studying recombined protease function. To circumvent this, a cell culture stimulation platform was developed for the reliable stimulation of neurons (electrical field stimulation). NT-CaM and M13-CT were tested using high frequency bursts every 4 min and no significant change in TS-FRET ratio was recorded after 2 hours. With the inability to develop this concept *in vitro* and the lack of protease function in cell culture this split-protein approach was discontinued.

5.4 Approach 3: Bimolecular Fluorescence Complementation Integrator

The third approach explored was the application of Bimolecular Fluorescence Complementation that had previously been successfully demonstrated in *vitro* (Hu et al., 2002). Through the application of split-FP architecture several advantages would be conferred over split-protease based approaches. Primarily the reduction of the overall size of the Integrator as this would obviate the requirement of a FRET reporter. Secondly, due to the single wavelength signal the $\Delta F/F$ can be engineered to yield a significantly greater signal than the $\Delta R/R$ FRET changes elicited by FRET-pair cleavage.

5.4.1 In vitro *optimisation of split-FP Integrator*

The first step in generating the complementation Integrator was the development of a suitable biosensor architecture from which further optimisation could be pursued. Two locations were chosen to split the FP, at amino acid positions 155 or 173 (Hu and Kerppola, 2003). Upon fusion to ΔCaM and ΔM13 it was observed that the 154/155 split yield the highest signal (Ca^{2+}-dependent complementation). As both locations exhibited similar background fluorescence, it was necessary to identify whether the responsible interaction was due to the ΔCaM/ΔM13 interaction or due to the split-FP interaction as it has been demonstrated that split FPs can display high levels of self-assembly (Cabantous et al., 2005). Purification of the FP fragments alone led to the identification of the ΔCaM/ΔM13 interaction as being responsible for the background fluorescence observed. By exchanging the mutant form of CaM and M13 for wild-type variants, a significant reduction in the overall signal level was noted. Furthermore, signal was abolished when the mutant and wild-type variants were used in combination. Thus it was demonstrated that the specificity of the ΔM13 for ΔCaM was of an intrinsic value that would determine the success of the Integrator and, by architectural optimisation, one could reduce the spontaneous association between the two components.

The first optimisation strategy aimed to determine the optimal orientation of the Integrator components that would yield the largest signal with the lowest background.

Orientation screening determined the optimal orientation to be the original YN-ΔCaM/ΔM13-YC, in agreement with structural data. The ensuing step was the replacement of Citrine with alternative FPs in order to minimise background fluorescence whilst maintaining high signal. Of the FPs examined (CFP, mKO, mKO2, mOrange, mCherry, mKate and Tag RFP) the only other combination that demonstrated *in vitro* fluorescence was YN172/ CC155. This combination resulted in a FP hybrid of CFP and Citrine with an additional β-sheet and, even though this phenomenon had previously been observed (Hu and Kerppola, 2003), the surprisingly large increase in signal was unforeseen. However, due to the substantial increase in background fluorescence this combination was dismissed as a suitable alternative for the Integrator.

With the selection of the most suitable orientation and the most suitable FP completed the cellular expression of the Integrator found significant Citrine fluorescence after 16 hours in approximately 35 % of cells. Furthermore, when dissociated hippocampal neurons were subjected to the same stimulation parameters as the split-TEV approach (with a burst every 4 min) no significant increase in Citrine fluorescence was observed.

At this point a screen of all currently identified Ca^{2+}-dependent CaM binding peptides was undertaken in order to identify peptides which were better suited for this Integrator approach. The benefit of such a strategy was that it enabled the screening of a variety of peptide recognition motifs (classified according to the hydrophobic anchor residues). For example, by screening a range of peptides, such as the M13 peptide that exhibits a 1-5-8-14 recognition motif or CaMKKβ that exhibits a 1-16 recognition motif, one could determine whether a particular motif bias is preferential for the Integrator (Yamniuk and Vogel, 2004). When generating the CaM peptide-YC component a PCR error led to the inclusion of a ΔSpectrin peptide lacking a Histidine at position 14. After 4-hour incubation the ΔSpectrin peptide displayed the highest level of complementation with low background fluorescence that outperformed the original ΔM13 peptide. Using more sensitive cuvette based experiments a significant improvement in signal was observed with an additional reduction in background fluorescence. These characteristics were also reflected in cell culture experiments where ΔSpectrin exhibited a significant reduction in population of cells exhibiting background

fluorescence and an overall decrease in the fluorescence intensity. Interestingly, Spectrin and M13 possessed a very similar recognition motif (Spectrin: 1-8-14), and the majority of peptides that displayed signal also belonged to one of these two classes. Even though no conclusive explanation can be offered as to the origin of this specificity observed, the similarity of CaM from structural data of complexes of CaM/M13 and CaM/Spectrin was investigated. A comparison of the N-termini from CaM/M13 (PDB: 3EK4) and CaM/Spectrin (PDB: 2FOT) found little variation in CaM orientation (Root Mean Squared Deviation (RMSD) of 0.743), whereas we found a slightly larger RMSD of 1.168 when comparing the C-termini (**Figure 50**). Whilst the C-termini comparison lacks one EF-hand (due to incomplete sequences) this structural deviation cannot wholly account for the discrepancy in signal observed. Thus, the most likely explanation is that by shortening the Spectrin peptide by one amino acid the bump-and-key remodelled CaM forms complexes with a favoured orientation for complementation.
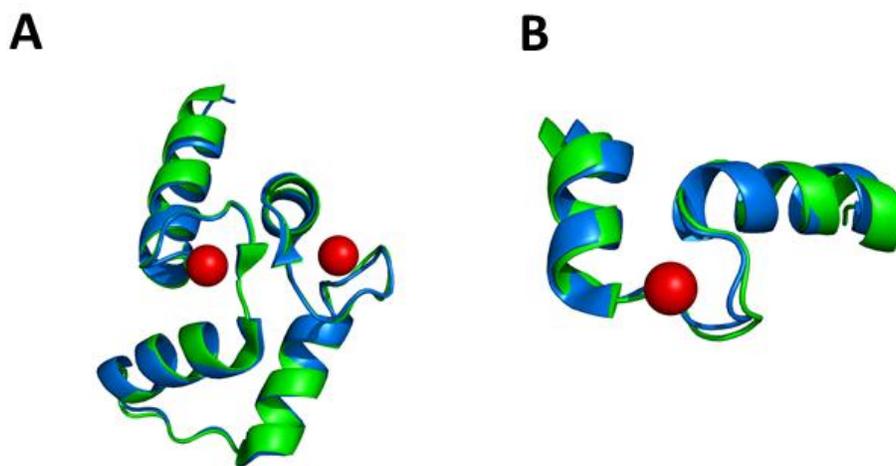
Figure 50: Structural comparison of CaM when bound to M13 or Spectrin
A) N-terminal and **B)** comparison of CaM in complex with M13 (green) or Spectrin (blue). Red spheres denote Ca^{2+} ions. The incomplete structure shown in **B** is due to incomplete PDB data. Green: PDB 3EK4, Blue: PDB 2FOT.

In possession of an improved peptide a further attempt to improve the signal/background ratio was undertaken by the modification of the Citrine fragments. Shifting the fragmentation site or the addition/removal of an extra amino acid led to the hypothesis

that the background fluorescence could be reduced by the induction of sub-optimal complementation. Interestingly a 27 % increase in signal accompanied the expected 22 % reduction in background fluorescence when the fragmentation site was shifted from 154/155 to 153/154; suggesting an improved separation site. Contrastingly, addition or removal of an extra amino acid facilitated the formation of background fluorescence and inhibited signal.

Using the improved separation location the investigation of Integrator function at higher temperatures was performed, as previous research had implicated a temperature-dependent effect on complementation (Robida and Kerppola, 2009). Two approaches were undertaken to try and differentiate between temperature-induced effects on complementation and ΔCaM/ΔSp interaction; i) the incubation of the two components in a Ca^{2+}-saturated solution at different temperatures, to determine the effects of temperature on complementation, and ii) subjection of the two components to more physiologically relevant Ca^{2+} concentrations, in order to determine the effects of temperature on CaM/Ca^{2+} binding. Hereby, it was found that no significant *in vitro* reductions in complementation were observed upon incubation of the two components in Ca^{2+}-saturated solution. In contrast, a progressive reduction in background fluorescence was observed using a series of Ca^{2+} titrations that was concluded to be a reduction in the spontaneous association of ΔCaM/ΔSp. In agreement with the previously observed reduction in background fluorescence a significant decrease in the total complementation was noted when subjected to physiologically relevant Ca^{2+} which suggested that increased temperature either reduces the ΔCaM/ΔSp interaction alone or additionally reduces the CaM/Ca^{2+} binding. Thus, by experimental design one could not distinguish between the affinity of Ca^{2+} for CaM and the ensuing affinity of CaM for the peptide. Despite this reduction in Ca^{2+} affinity it was unclear, at this point, whether functional interactions between ΔCaM/ΔSp could occur in a cellular environment. Exposure of HEK293T cells to a 4 hour Ionomycin and Ca^{2+} treatment resulted in an increase in complementation indicative of functional interaction of ΔCaM/ΔSp. However, subsequent exposure of dissociated hippocampal neurons to intracellular Ca^{2+} transients via field stimulation did not yield any recorded complementation.

5.4.2 Complementation Integrator refinement for response to endogenous Ca^{2+} transients

With the generation of a complementation-based Integrator responsive to exogenous Ca^{2+} application the next step was the further refinement of the Integrator in order to elicit a complementation response to endogenous Ca^{2+} transients. With optimisation of the fundamental architecture already completed the only avenue remaining for architectural modification was the addition of linkers between the components as this had been previously shown to increase biosensor Ca^{2+} affinity (Horikawa et al., 2010). To achieve this, variants of the components were generated to incorporate poly-glycine linkers in order to increase the rotational freedom of ΔCaM or ΔSp with their corresponding Citrine fragment. Although the addition of the majority of linkers to YN-CaM or ΔSp-YC components inhibited complementation, the incorporation of the poly-glycine linker "GGGGS" in-between ΔSp and YC did yield a 31 % improvement in complementation. Nevertheless despite this improvement no linker addition conferred an improvement to Ca^{2+} affinity.

An alternative approach to increase the Ca^{2+} affinity was undertaken based on the "Acid pair hypothesis" that correlates Ca^{2+} affinity with the position of acidic residues in chelating positions of the EF-hand Ca^{2+} binding loop (Tikunova et al., 2001). For this approach, a single or double substitution of the +Z chelating position in CaMs EF-hands II and III (N60D and N97D respectively) was performed to replace the amide amino acid (Asparagine) for an acidic amino acid (Aspartic Acid). On the one hand, the N60D mutation in the low-affinity "structural" N-lobe significantly improved signal but did not confer increased Ca^{2+} affinity. Moreover, the N97D single mutation in the high-affinity "regulatory" C-lobe decreased the overall signal and again conferred no improvement to affinity. However, in contrast to the single substitutions, the combination of the substitutions significantly improved not only the signal but also significantly improved the affinity (with an EC_{50} improvement from 2000 nM to 1460 nM). Despite these substitutions not correlating to improved EF-hand behaviour (as only the adjacent EF-hand in a lobe has any influence in the affinity of the other EF-hand), they suggested a dynamic process whereby improving Ca^{2+} coordination in the structural lobe leads to improved peptide binding

that requires the additional Ca^{2+} affinity improvement in the regulatory lobe for improved complementation.

Due to the CaM mutations requiring modification of the structural lobe it was also necessary to investigate whether the addition of the linker that provided slight signal improvement (ΔSp-GGGGS-YC) would complement these CaM modifications. When combined the improved performance of $CaM^{N60DN97D}$ was abolished and the Ca^{2+} affinity was also reduced. From this observation it was determined that additional flexibility conferred by the integrated linker improved the orientation of the Citrine fragments. However, the additional modification of the CaM/ΔSp interaction surface did not exhibit this improved orientation when combined with the linker. Consequently, as the improved characteristics of $CaM^{N60DN97D}$ outweighed the linker-improved characteristics the linker was dismissed in favour of the CaM mutations.

During the course of improving the Integrator's architecture experimental observations led to the conclusion that the ΔSp-YC component, consisting of a 22 amino acid peptide fused to the 84 amino acid C-terminus of Citrine, was prone to degradation. In order to improve this component's cellular translation efforts to improve the N- and C-terminus were undertaken. The motivation behind C-terminus stabilisation was twofold, the first was the reduction in proteasomal degradation, and the second was that through addition of CFP it would obviate the requirement for additional transfection of CFP. Two CFP variants were selected, the enhanced CFP (ECFP) and ΔECFP, an ECFP variant that contained the improved folding mutations S30R and Y39R, and the monomerisation mutation A206K (Pédelacq et al., 2006). By comparison of the signal behaviour of the two ECFP variants it was anticipated that, not only would this contribute to the fundamental understanding of Bimolecular Fluorescence Complementation, but also determine the applicability of the Integrator as a ratiometric FRET biosensor. The determination of the concentration-corrected excitation and emission fluorescence spectra revealed significant differences in CFP fluorescence with ΔECFP possessing significantly higher proportions of correctly folded FPs compared to ECFP. This observation was also reflected by Ca^{2+} titrations (with YN153-$CaM^{N60DN97D}$), that found increased signal with the inclusion of ΔECFP without improvement of Ca^{2+} affinity. Interestingly, both the ΔECFP and the poorer

performing ECFP elicited similar FRET $\Delta R/R$ changes that, not only confirmed the 1:1 stoichiometry of CaM/CBP interaction, but also confirmed the belief that complementation based architectures retain significantly higher responses as single fluorophore biosensors than as ratiometric biosensors.

In tandem, N-terminal modification of ΔSp were undertaken in accordance to the "N-End Rule" that stipulates that the *in vivo* half-life of a protein is related to the identity of its N-terminal residue (Varshavsky, 2008). Primary destabilisation of ΔSp was reduced via the incorporation of several N-terminal sequence caps that possessed a Valine followed by a varied number of Alanine residues (V, VA, VAA, and VAAA). To validate stabilisation, two parameters were evaluated; the Integrator response and the quantification of component degradation via the ubiquitin pathway. Ca^{2+} titrations yield varied signal responses with no correlation of response to N-cap length. Nevertheless, the VAA-ΔSp (KT) demonstrated the most optimal increase in signal with a significantly improved Ca^{2+} affinity. By comparison of CFP fluorescence under normal and proteasome inhibition conditions all N-terminal modified component demonstrated an almost 100 % reduction in proteasomal degradation. Understandably, the length of the N-terminal cap was not correlated to proteasomal degradation reduction. From the two parameters investigated it was concluded that despite the N-terminal cap conferring significant stability to the component the length of the cap played a significant role in the alteration of Integrator function. Furthermore, ΔECFP replacement with ECFP exhibited a significant increase in proteasomal degradation, thus highlighting the beneficial significance of folding-optimised C-terminal structured elements in the provision of structural stability during translation.

The final step of Integrator development was the introduction of Alanine mutations that had previously been shown to have profound effects on the affinity of the M13 peptide for CaM (Montigiani et al., 1996). Whilst the published research could not be directly extrapolated (due to the modified ΔCaM/ΔSpectrin interface and the multi-factorial readout of complementation) a selection of 5 mutations were selected spanning from residue K7 to S20. *In vitro* analysis

found no direct correlation between complementation and the previously published results; however one mutation, F18A, conferred a significant improvement to signal and Ca^{2+} affinity.

Due to the incorporation of several modifications to the Integrator's design, since the initial proof-of-concept experiment, several points of characterisation were required. Firstly, the most fundamental criteria of the Integrator concept was re-validated, namely the confirmation that this architectural approach confers an irreversible Ca^{2+}-dependent response. Addition of the Ca^{2+} chelating agent BAPTA after either 0.5 or 1 hour proved that the almost instantaneous cessation of complementation was maintained without any observed reduction in fluorescence. Furthermore, the *in vitro* kinetics implied an almost linear increase in complementation between 0 and ~400 nM $CaCl_2$, whereas higher Ca^{2+} concentrations (up to 1.1µM) achieved a more saturated rate of complementation after 4 hours. Secondly, cell characterisation of the modified VAA-ΔSp^{F18A} peptide was undertaken in HEK293T cells to compare the background fluorescence of the VAA-ΔSp^{F18A} peptide with the previously characterised ΔSp and ΔM13 peptides. In comparison to ΔSp the VAA-ΔSp^{F18A} peptide exhibited an increased percentage of cells expressing background fluorescence (that was comparable to ΔM13) whilst maintaining a similar background fluorescence intensity to the ΔSp peptide.

With the substitution of the Citrine fragments for ECFP and Citrine the CaM/CBP modifications were validated on a cell-based platform by the observation of a 285 % increase in FRET ΔR/R of ΔCaM^{N60DN97D}/VAA-ΔSp^{F18A} when compared to the original ΔCaM/ΔM13. As no significant difference was observed in the starting ratio of each pair of interacting proteins, it was concluded that the higher ΔR/R observed upon stimulation of ΔCaM^{N60DN97D}/VAA-ΔSp^{F18A} was due to an improved CaM/CBP interaction. Furthermore, FRET studies of the VAA-ΔSp^{F18A} with wtCaM yielded negligible elevation in ΔR/R suggesting a high degree of specificity of the modified peptide for ΔCaM^{N60DN97D}.

5.4.3 Summary of complementation Integrator development

During the initial planning stages of the complementation integrator a mechanism was proposed demonstrating the process by which this Integrator would function (**Figure 10**). During the course of development, not only has the fundamental architecture been improved, but also the characteristics of each Integrator component. Thus, the initial mechanism was found to represent a simplified idea of what was effectively a very complex process. In order to fully appreciate this complexity a more realistic mechanism has been developed (**Figure 51**) and, when appropriate, some explanation has been offered as to how these modifications have improved the Integrator.
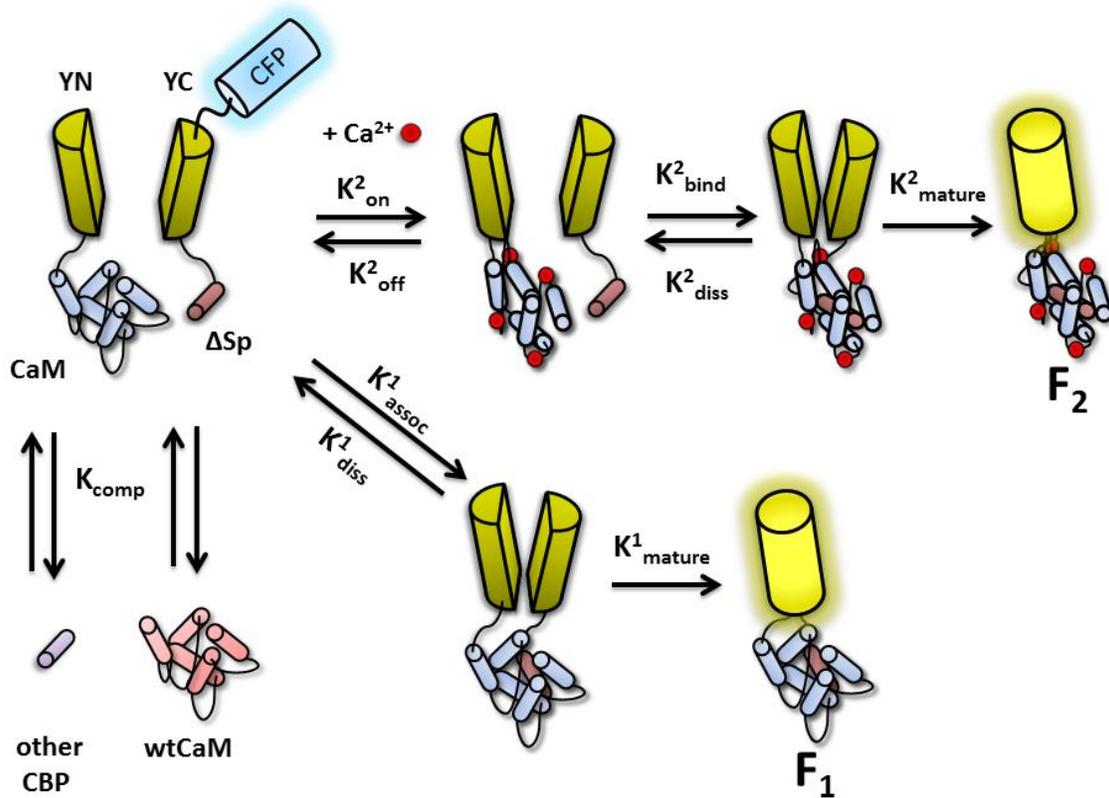
Figure 51: Proposed mechanism of complementation Integrator Activation
Proposed schematic of the interaction of Citrine fragments (YN and YC) fused to CaM and the ΔSp. For clarity the CFP is only shown in the top right. K_{comp}: competition of CaM and the CBP for endogenous CBP's or wtCaM respectively. F_1 pathway: mechanism for spontaneous association; K^1_{assoc}: spontaneous association of apo-CaM and ΔSp, K^1_{diss}: dissociation of apo-CaM and ΔSp. K^1_{mature}: maturation of Citrine. F_2 pathway: mechanism for Ca^{2+} dependent complementation; K^2_{on}: rate of Ca^{2+} binding to CaM, K^2_{off}: rate of CaM-Ca^{2+} dissociation, K^2_{bind}: rate of CaM- ΔSp binding, K^2_{diss}: rate of CaM- ΔSp disassociation, K^2_{mature}: maturation of Citrine.

To summarise the development of the complementation Integrator one can separate improvements into two categories: i) modifications to refine the Integrator architecture and ii) modifications that improve component/Integrator performance. Refinement of this biosensor architecture has been achieved in several ways with the most significant improvement coming from the stabilization of the ΔSp-YC component via the addition of a C-terminal CFP and the removal of the exposed N-Degron. In addition, the optimisation of component orientation and the FP selection also contribute to the refinement of the fundamental Integrator components. Furthermore, significant modifications have been made to directly affect the mechanism of Integrator activation. Through the identification that the high background fluorescence (K^1_{assoc}) was due to the ΔCaM/ΔM13 affinity the peptide screen reduced this (or improved K^1_{diss}) whilst enhancing the Ca^{2+}-dependent CaM/peptide interaction (K^2_{bind}). Shifting the fragmentation site to 153/154 improved Integrator performance by increasing the signal (K^2_{mature}), whilst reducing the background fluorescence (K^1_{mature}). EF-Hand mutations of ΔCaM have led to improved Ca^{2+} coordination (K^2_{on}) and the $ΔSp^{F18A}$ mutation has also improved the CaM-ΔSp interaction (K^2_{bind}). Finally, by developing the Integrator based on mutant forms of CaM a significant reduction of wtCaM interaction with the ΔSp peptide (K_{comp}) has been achieved.

5.4.4   Functional validation and virus characterisation

The two components of the Integrator, YN153- $ΔCaM^{N60DN97D}$ and VAA-$ΔSp^{F18A}$-ΔECFP, were placed under the respective CMV and IRES promoters and using electrical field stimulation a 223 % increase in Citrine fluorescence was detected over the course of 1 hour using live cell imaging. Similarly, when field stimulation was applied to populations of neurons, not under constant observation, it was possible to resolve the ratiometric difference (the ratio of Citrine/CFP excited with a respective 515 nm and 432 nm) after only 1 hour. This provided important validation of one of the most fundamental principles behind the Integrator concept, namely the possibility to differentiate between active and non-active neurons after a certain period of time. Furthermore, by the observation of marginal signal when $ΔCaM^{N60DN97D}$ was substituted for wtCaM it was verified that, not only was wtCaM unsuitable for FRET-based

interactions with VAA-ΔSp^{F18A} (as mentioned above), but also unsuitable for eliciting complementation.

With successful demonstration of Bimolecular Fluorescence Complementation in response to endogenous Ca^{2+} transients the final stage in Integrator development was the introduction of a mechanism for inducing Integrator expression. For this the alphavirus Semliki Forest Virus (SFV) was chosen due to the rapid onset and high expression of the protein of interest. When the virus was expressed for 1 to 6 hours no constitutive FP fluorescence was observed (despite the presence of ΔECFP fluorescence in HEK293T cells used to generate the virus). With the lack of expression additionally confirmed by western blot, a 2 hour pre-incubation time was applied based on the expression of other viruses (incorporating a different class of biosensor) generated in tandem. When field stimulation was applied for 1 to 4 hours, increases in both ΔECFP and Citrine fluorescence as well as Citrine fluorescence when excited with the CFP wavelength (indicating FRET), were observed. Validation of expression by western blot also yield no FP immunoreactivity at 42 kDa (the size of VAA-ΔSp^{F18A}-ΔECFP) but significant immunoreactivity at 72 kDa that corresponded to the complex of YN153- ΔCaM^{N60DN97D} and VAA-ΔSp^{F18A}-ΔECFP.

To overcome the lack of constitutive FP fluorescence two approaches were undertaken; either the replacement of ΔECFP (SFV-I) with mCerulean 3 (SFV-II) or mCherry (SFV-III), or by placing the constitutive FP component under the CMV promoter (SFV-IV). *In vitro* analysis of the replaced constitutive FP did not demonstrate improved Integrator performance and cell-based characterisation of both approaches did not confer any improvement in signal. Interestingly, the mCherry substitution did not show any significant improvements in constitutive FP fluorescence despite the fact that mCherry is not a suitable FRET donor unlike the CFP variants ΔECFP and mCerulean 3. As none of the modified viruses displayed significant improvements SFV-I was chosen to be subjected to stimuli protocols mimicking physiological firing patterns. SFV-I behaviour under different stimulation protocols showed significant constitutive FP fluorescence when using TBS, a fact that was not found using other stimulating patterns. Thus, this suggests that highly repetitive or very active neurons can be differentiated from less

frequently active neurons via the constitutive FP alone. On the other hand, signal was observed in all cases with substantial increases in fluorescence observed from between 2 and 4 hours except for the control spontaneous firing condition (SAS). In the majority of stimulations (SAS, PAS, and TBS) no significant FRET responses was observed. However, a significant FRET response was observed using HS which may provide an indication of regular "medium firing" neurons in an *in vivo* setting. Taken together, these findings implicate a range of possible readout mechanisms to differentiate between diverse firing patterns of neurons. Furthermore, by the abolishment of neuronal response to field stimulation using sodium/ Ca^{2+} channel blockers it was verified that the signal responses, elicited using the various stimulus patters, were indeed due to neuronal Ca^{2+} transients.

At this point a virus-induced Bimolecular Fluorescence Complementation Integrator has been developed to elicit a stimulation-dependent signal response in cell culture. However, the precise origin for the observed lack of constitutive FP fluorescence remains elusive. At present there are several hypotheses as to why no fluorescence was observed and these can be divided into two groups; the first being a lack of fluorescence and the second (and more likely) being a lack of expression. The two possibilities as to why fluorescence is not detectable are either due to the IRES promoter or that there is almost complete FRET from the CFP to the Citrine. The first possibility, the poor promoter-driven expression, is unlikely as not only has previous research incorporated IRES promoters within SFV expression cassettes (Ehrengruber et al., 1999), but also by placing the constitutive FP under the CMV promoter no improvement to constitutive FP fluorescence was observed. The second possibility, that the CFP undergoes complete FRET with Citrine, is also unlikely as replacement of ΔECFP with either an improved cyan variant (mCerulean 3) or a FRET unsuitable FP (mCherry) did not result in an improved performance of the Integrator *in vitro* or in cell culture. The second group of possibilities relies on the lack of FP expression, a concept partially validated via the lack of FP immunoreactivity of virus-infected cells. The first explanation of why this is observed is that, unlike transient transfection of DNA where transcription and translation occur in the transfected cell, viral infection requires the translation of a genomic RNA sequence packed within the virus particle. Thus, it is conceivable that the transcription for viral packaging may be the root of the lack of

constitutive FP expression. The second explanation is that although the SFV packaging limit has been reported to be 3.5 Kb (DiCiommo et al., 2004) the most likely cause for the lack of constitutive FP expression is that the Integrator has exceeded the packaging limit for reliable SFV production.

As a consequence of these observations the next progression from here can be separated into two avenues. Firstly, the performance of SFV-I must be determined *in vivo* to ascertain whether constitutive FP fluorescence is observed when placed in an active neuronal environment. Therefore, evaluation *in vivo* will be the primary goal of the proceeding research. Secondly, generation of alternative viruses, such as the Adenovirus or Lentivirus viral systems, may provide not only suitable alternatives for the induction of Integrator expression but also diversify the possibilities of Integrator application based on production duration or whether integration into the host genome is desired.

6 Conclusion

The research presented here has laid the foundation for the development of a novel type of biosensor for the study of functional neuroanatomy via the cumulative integration of Ca^{2+} transients. Three architectural approaches were considered that have highlighted not only the criteria necessary for generating this novel class of biosensor but also the parameters by which such Integration biosensors should be developed.

Of the three approaches undertaken, the Ca^{2+}-dependent protease FRET integrator and the artificial Ca^{2+}-dependent protease FRET Integrator were unable to be established *in vitro.* However, the split FP-based Bimolecular Fluorescence Complementation Integrator was successfully engineered to possess an EC_{50} of 420 nM. Using a unique CaM/peptide pair developed specifically for split-FP interactions it has been shown that a 285 % higher FRET ΔR/R interaction is achieved in comparison to the initial ΔCaM/ΔM13 pair. Furthermore, the minimal specificity of the modified peptide for wtCaM is indicative of a significantly redesigned CaM/peptide interface that is unperturbed from endogenous protein interference. Using a SFV induction system the complementation Integrator exhibited a 1580 % increase in Citrine intensity after 4 hour stimulation using stimulation parameters resembling physiological firing patterns. Furthermore, the successful application of a virus-induced complementation Integrator has been shown to successfully differentiate between distinct physiological firing patterns with a multitude of readout capabilities. Additionally complementation can be demonstrated to be a suitable method for the *in vitro* development of protein-protein interaction pairs that can be further applied to other split-proteins strategies.

To summarise, the development of this complementation-based Integrator has not only equipped researchers with a novel genetically encoded biosensor but also, with the additional temporal control of SF-I, a ready-to-use method for the study of functional neuroanatomy *in vivo*.

7 Bibliography

Akemann W, Mutoh H, Perron A, Rossier J, Knöpfel T. Imaging brain electric signals with genetically targeted voltage-sensitive fluorescent proteins. *Nat. Methods* 7: 643–649, 2010.

Akerboom J, Rivera JDV, Guilbe MMR, Malavé ECA, Hernandez HH, Tian L, Hires SA, Marvin JS, Looger LL, Schreiter ER. Crystal structures of the GCaMP calcium sensor reveal the mechanism of fluorescence signal change and aid rational design. *J. Biol. Chem.* 284: 6455–6464, 2009.

Audesirk G, Audesirk T, Ferguson C. Culturing Rat Hippocampal Neurons. In: *Current Protocols in Toxicology*, edited by Costa LG, Hodgson E, Lawrence DA, Reed DJ. Hoboken, NJ, USA: John Wiley & Sons, Inc., 2001.

Baird GS, Zacharias DA, Tsien RY. Circular permutation and receptor insertion within green fluorescent proteins. *Proc. Natl. Acad. Sci. U.S.A.* 96: 11241–11246, 1999.

Balkowiec A, Katz DM. Cellular mechanisms regulating activity-dependent release of native brain-derived neurotrophic factor from hippocampal neurons. *J. Neurosci.* 22: 10399–10407, 2002.

Bausenwein B, Fischbach KF. Activity labeling patterns in the medulla of Drosophila melanogaster caused by motion stimuli. *Cell Tissue Res.* 270: 25–35, 1992.

Berg J, Hung YP, Yellen G. A genetically encoded fluorescent reporter of ATP:ADP ratio. *Nat. Methods* 6: 161–166, 2009.

van den Berg S, Löfdahl P-A, Härd T, Berglund H. Improved solubility of TEV protease by directed evolution. *J. Biotechnol.* 121: 291–298, 2006.

Bertini I, Gelis I, Katsaros N, Luchinat C, Provenzani A. Tuning the affinity for lanthanides of calcium binding proteins. *Biochemistry* 42: 8011–8021, 2003.

Borst A, Haag J, Reiff DF. Fly motion vision. *Annu. Rev. Neurosci.* 33: 49–70, 2010.

Cabantous S, Terwilliger TC, Waldo GS. Protein tagging and detection with engineered self-assembling fragments of green fluorescent protein. *Nat. Biotechnol.* 23: 102–107, 2005.

Chalfie M, Tu Y, Euskirchen G, Ward WW, Prasher DC. Green fluorescent protein as a marker for gene expression. *Science* 263: 802–805, 1994.

Chen N, Ye Y, Zou J, Li S, Wang S, Martin A, Wohlhueter R, Yang JJ. Fluorescence complementation via EF-hand interactions. *J. Biotechnol.* 142: 205–213, 2009.

Chiu MI, Katz H, Berlin V. RAPT1, a mammalian homolog of yeast Tor, interacts with the FKBP12/rapamycin complex. *Proc. Natl. Acad. Sci. U.S.A.* 91: 12574–12578, 1994.

Chu J, Zhang Z, Zheng Y, Yang J, Qin L, Lu J, Huang Z-L, Zeng S, Luo Q. A novel far-red bimolecular fluorescence complementation system that allows for efficient visualization of protein interactions under physiological conditions. *Biosens Bioelectron* 25: 234–239, 2009.

Chudakov DM, Matz MV, Lukyanov S, Lukyanov KA. Fluorescent proteins and their applications in imaging living cells and tissues. *Physiol. Rev.* 90: 1103–1163, 2010.

DiCiommo DP, Duckett A, Burcescu I, Bremner R, Gallie BL. Retinoblastoma protein purification and transduction of retina and retinoblastoma cells using improved alphavirus vectors. *Invest. Ophthalmol. Vis. Sci.* 45: 3320–3329, 2004.

Duncan GE, Kaldas RG, Mitra KE, Breese GR, Stumpf WE. High activity neurons in the reticular formation of the medulla oblongata: a high-resolution autoradiographic 2-deoxyglucose study. *Neuroscience* 35: 593–600, 1990.

Durham D, Woolsey TA, Kruger L. Cellular localization of 2-[3H]deoxy-D-glucose from paraffin-embedded brains. *J. Neurosci.* 1: 519–526, 1981.

Dutt P, Spriggs CN, Davies PL, Jia Z, Elce JS. Origins of the difference in Ca2+ requirement for activation of mu- and m-calpain. *Biochem. J.* 367: 263–269, 2002.

Ehrengruber MU, Lundstrom K, Schweitzer C, Heuss C, Schlesinger S, Gähwiler BH. Recombinant Semliki Forest virus and Sindbis virus efficiently infect neurons in hippocampal slice cultures. *Proc. Natl. Acad. Sci. U.S.A.* 96: 7041–7046, 1999.

Enes J, Langwieser N, Ruschel J, Carballosa-Gonzalez MM, Klug A, Traut MH, Ylera B, Tahirovic S, Hofmann F, Stein V, Moosmang S, Hentall ID, Bradke F. Electrical activity suppresses axon growth through Ca(v)1.2 channels in adult primary sensory neurons. *Curr. Biol.* 20: 1154–1164, 2010.

Fan J-Y, Cui Z-Q, Wei H-P, Zhang Z-P, Zhou Y-F, Wang Y-P, Zhang X-E. Split mCherry as a new red bimolecular fluorescence complementation system for visualizing protein-protein interactions in living cells. *Biochem. Biophys. Res. Commun.* 367: 47–53, 2008.

Fischbach K-F, Dittrich APM. The optic lobe of Drosophila melanogaster. I. A Golgi analysis of wild-type structure. *Cell and Tissue Research* 258, 1989.

Forster T. Energiewanderung und Fluoreszenz. *Die Naturwissenschaften* 33: 166–175, 1946.

Friedrich MW, Aramuni G, Mank M, Mackinnon JAG, Griesbeck O. Imaging CREB activation in living cells. *J. Biol. Chem.* 285: 23285–23295, 2010.

Garaschuk O, Yaari Y, Konnerth A. Release and sequestration of calcium by ryanodine-sensitive stores in rat hippocampal neurones. *J. Physiol. (Lond.)* 502 (Pt 1): 13–30, 1997.

Garriga-Canut M, Schoenike B, Qazi R, Bergendahl K, Daley TJ, Pfender RM, Morrison JF, Ockuly J, Stafstrom C, Sutula T, Roopra A. 2-Deoxy-D-glucose reduces epilepsy progression by NRSF-CtBP-dependent metabolic regulation of chromatin structure. *Nat. Neurosci.* 9: 1382–1387, 2006.

Gehl C, Waadt R, Kudla J, Mendel R-R, Hänsch R. New GATEWAY vectors for high throughput analyses of protein-protein interactions by bimolecular fluorescence complementation. *Mol Plant* 2: 1051–1058, 2009.

Ghosh I, Hamilton AD, Regan L. Antiparallel Leucine Zipper-Directed Protein Reassembly: Application to the Green Fluorescent Protein. *Journal of the American Chemical Society* 122: 5658–5659, 2000.

Gifford JL, Walsh MP, Vogel HJ. Structures and metal-ion-binding properties of the Ca2+-binding helix-loop-helix EF-hand motifs. *Biochem. J.* 405: 199–221, 2007.

Gilli R, Lafitte D, Lopez C, Kilhoffer M-C, Makarov A, Briand C, Haiech J. Thermodynamic Analysis of Calcium and Magnesium Binding to Calmodulin †. *Biochemistry* 37: 5450–5456, 1998.

Griesbeck O, Baird GS, Campbell RE, Zacharias DA, Tsien RY. Reducing the environmental sensitivity of yellow fluorescent protein. Mechanism and applications. *J. Biol. Chem.* 276: 29188–29194, 2001.

Guerrero G, Siegel MS, Roska B, Loots E, Isacoff EY. Tuning FlaSh: redesign of the dynamics, voltage range, and color of the genetically encoded optical sensor of membrane potential. *Biophys. J.* 83: 3607–3618, 2002.

Harris AS, Croall DE, Morrow JS. The calmodulin-binding site in alpha-fodrin is near the calcium-dependent protease-I cleavage site. *J. Biol. Chem.* 263: 15754–15761, 1988.

Heim N, Garaschuk O, Friedrich MW, Mank M, Milos RI, Kovalchuk Y, Konnerth A, Griesbeck O. Improved calcium imaging in transgenic mice expressing a troponin C-based biosensor. *Nat. Methods* 4: 127–129, 2007.

Heim N, Griesbeck O. Genetically encoded indicators of cellular calcium dynamics based on troponin C and green fluorescent protein. *J. Biol. Chem.* 279: 14280–14286, 2004.

Hoffman LM, Jendrisak JJ. Transposomes: A system for identifying genes involved in bacterial pathogenesis [Online]. In: *Methods in Enzymology*. Elsevier, p. 128–140.

Horikawa K, Yamada Y, Matsuda T, Kobayashi K, Hashimoto M, Matsu-ura T, Miyawaki A, Michikawa T, Mikoshiba K, Nagai T. Spontaneous network activity visualized by ultrasensitive Ca(2+) indicators, yellow Cameleon-Nano. *Nat. Methods* 7: 729–732, 2010.

Hu C-D, Chinenov Y, Kerppola TK. Visualization of interactions among bZIP and Rel family proteins in living cells using bimolecular fluorescence complementation. *Mol. Cell* 9: 789–798, 2002.

Hu C-D, Kerppola TK. Simultaneous visualization of multiple protein interactions in living cells using multicolor fluorescence complementation analysis. *Nat. Biotechnol.* 21: 539–545, 2003.

Ibraheem A, Campbell RE. Designs and applications of fluorescent protein-based biosensors. *Curr Opin Chem Biol* 14: 30–36, 2010.

Ishida H, Vogel HJ. Protein-peptide interaction studies demonstrate the versatility of calmodulin target protein binding. *Protein Pept. Lett.* 13: 455–465, 2006.

Jach G, Pesch M, Richter K, Frings S, Uhrig JF. An improved mRFP1 adds red to bimolecular fluorescence complementation. *Nat. Methods* 3: 597–600, 2006.

Jayaraman S. Mechanism and Cellular Applications of a Green Fluorescent Protein-based Halide Sensor. *Journal of Biological Chemistry* 275: 6047–6050, 2000.

Johnsson N, Varshavsky A. Split ubiquitin as a sensor of protein interactions in vivo. *Proc. Natl. Acad. Sci. U.S.A.* 91: 10340–10344, 1994.

Jurado LA, Chockalingam PS, Jarrett HW. Apocalmodulin. *Physiol. Rev.* 79: 661–682, 1999.

Kai Kai MA, Pentreath VW. High resolution analysis of [3H]2-deoxyglucose incorporation into neurons and glial cells in invertebrate ganglia: histological processing of nervous tissue for selective marking of glycogen. *J. Neurocytol.* 10: 693–708, 1981.

Kerppola TK. Bimolecular fluorescence complementation (BiFC) analysis as a probe of protein interactions in living cells. *Annu Rev Biophys* 37: 465–487, 2008.

Kim B, Frey KA, Mukhopadhyay S, Ross BD, Meyer CR. Co-registration of MRI and autoradiography of rat brain in three-dimensions following automatic reconstruction of 2D data set [Online]. In: *Computer Vision, Virtual Reality and Robotics in Medicine*, edited by Ayache N. Springer-Verlag, p. 262–266.

Kneen M, Farinas J, Li Y, Verkman AS. Green fluorescent protein as a noninvasive intracellular pH indicator. *Biophys. J.* 74: 1591–1599, 1998.

Kovar JL, Volcheck W, Sevick-Muraca E, Simpson MA, Olive DM. Characterization and performance of a near-infrared 2-deoxyglucose optical imaging agent for mouse cancer models. *Anal. Biochem.* 384: 254–262, 2009.

Kretsinger RH, Nockolds CE. Carp muscle calcium-binding protein. II. Structure determination and general description. *J. Biol. Chem.* 248: 3313–3326, 1973.

Larsen AK, De Veyra T, Jia Z, Wells A, Dutt P, Elce JS. Expression of human, mouse, and rat m-calpains in Escherichia coli and in murine fibroblasts. *Protein Expr. Purif.* 33: 246–255, 2004.

Lee HL, Santé-Lhoutellier V, Vigouroux S, Briand Y, Briand M. Calpain specificity and expression in chicken tissues. *Comp. Biochem. Physiol. B, Biochem. Mol. Biol.* 146: 88–93, 2007.

Livet J, Weissman TA, Kang H, Draft RW, Lu J, Bennis RA, Sanes JR, Lichtman JW. Transgenic strategies for combinatorial expression of fluorescent proteins in the nervous system. *Nature* 450: 56–62, 2007.

Lund-Andersen H. Transport of glucose from blood to brain. *Physiol. Rev.* 59: 305–352, 1979.

Mank M, Griesbeck O. Genetically encoded calcium indicators. *Chem. Rev.* 108: 1550–1564, 2008.

Mank M, Reiff DF, Heim N, Friedrich MW, Borst A, Griesbeck O. A FRET-based calcium biosensor with fast signal kinetics and high fluorescence change. *Biophys. J.* 90: 1790–1796, 2006.

Mank M, Santos AF, Direnberger S, Mrsic-Flogel TD, Hofer SB, Stein V, Hendel T, Reiff DF, Levelt C, Borst A, Bonhoeffer T, Hübener M, Griesbeck O. A genetically encoded calcium indicator for chronic in vivo two-photon imaging. *Nat. Methods* 5: 805–811, 2008.

Markwardt ML, Kremers G-J, Kraft CA, Ray K, Cranfill PJC, Wilson KA, Day RN, Wachter RM, Davidson MW, Rizzo MA. An improved cerulean fluorescent protein with enhanced brightness and reduced reversible photoswitching. *PLoS ONE* 6: e17896, 2011.

Marvin JS, Schreiter ER, Echevarría IM, Looger LL. A genetically encoded, high-signal-to-noise maltose sensor. *Proteins: Structure, Function, and Bioinformatics* 79: 3025–3036, 2011.

McCasland JS. Metabolic activity in antigenically identified neurons: a double labeling method for high-resolution 2-deoxyglucose and immunohistochemistry. *J. Neurosci. Methods* 68: 113–123, 1996.

McClintock B. The origin and behavior of mutable loci in maize. *Proc. Natl. Acad. Sci. U.S.A.* 36: 344–355, 1950.

McCombs JE, Palmer AE. Measuring calcium dynamics in living cells with genetically encodable calcium indicators. *Methods* 46: 152–159, 2008.

McLachlan MJ, Katzenellenbogen JA, Zhao H. A new fluorescence complementation biosensor for detection of estrogenic compounds. *Biotechnol. Bioeng.* 108: 2794–2803, 2011.

Miyawaki A, Llopis J, Heim R, McCaffery JM, Adams JA, Ikura M, Tsien RY. Fluorescent indicators for Ca2+ based on green fluorescent proteins and calmodulin. *Nature* 388: 882–887, 1997.

Montigiani S, Neri G, Neri P, Neri D. Alanine substitutions in calmodulin-binding peptides result in unexpected affinity enhancement. *J. Mol. Biol.* 258: 6–13, 1996.

Nagai T, Ibata K, Park ES, Kubota M, Mikoshiba K, Miyawaki A. A variant of yellow fluorescent protein with fast and efficient maturation for cell-biological applications. *Nature Biotechnology* 20: 87–90, 2002.

Nagai T, Sawano A, Park ES, Miyawaki A. Circularly permuted green fluorescent proteins engineered to sense Ca2+. *Proc. Natl. Acad. Sci. U.S.A.* 98: 3197–3202, 2001.

Nagai T, Yamada S, Tominaga T, Ichikawa M, Miyawaki A. Expanded dynamic range of fluorescent indicators for Ca(2+) by circularly permuted yellow fluorescent proteins. *Proc. Natl. Acad. Sci. U.S.A.* 101: 10554–10559, 2004.

Nakai J, Ohkura M, Imoto K. A high signal-to-noise Ca(2+) probe composed of a single green fluorescent protein. *Nat. Biotechnol.* 19: 137–141, 2001.

Nausch LWM, Ledoux J, Bonev AD, Nelson MT, Dostmann WR. Differential patterning of cGMP in vascular smooth muscle cells revealed by single GFP-linked biosensors. *Proc. Natl. Acad. Sci. U.S.A.* 105: 365–370, 2008.

Niino Y, Hotta K, Oka K. Blue fluorescent cGMP sensor for multiparameter fluorescence imaging. *PLoS ONE* 5: e9164, 2010.

Nunn CM, Jeeves M, Cliff MJ, Urquhart GT, George RR, Chao LH, Tscuchia Y, Djordjevic S. Crystal structure of tobacco etch virus protease shows the protein C terminus bound within the active site. *J. Mol. Biol.* 350: 145–155, 2005.

Ormö M, Cubitt AB, Kallio K, Gross LA, Tsien RY, Remington SJ. Crystal structure of the Aequorea victoria green fluorescent protein. *Science* 273: 1392–1395, 1996.

Osicka R. A Novel "Clip-and-link" Activity of Repeat in Toxin (RTX) Proteins from Gram-negative Pathogens: COVALENT PROTEIN CROSS-LINKING BY AN ASP-LYS ISOPEPTIDE BOND UPON CALCIUM-DEPENDENT PROCESSING AT AN ASP-PRO BOND. *Journal of Biological Chemistry* 279: 24944–24956, 2004.

Ouyang M, Huang H, Shaner NC, Remacle AG, Shiryaev SA, Strongin AY, Tsien RY, Wang Y. Simultaneous visualization of protumorigenic Src and MT1-MMP activities with fluorescence resonance energy transfer. *Cancer Res.* 70: 2204–2212, 2010.

Ouyang M, Lu S, Li X-Y, Xu J, Seong J, Giepmans BNG, Shyy JY-J, Weiss SJ, Wang Y. Visualization of polarized membrane type 1 matrix metalloproteinase activity in live cells by fluorescence resonance energy transfer imaging. *J. Biol. Chem.* 283: 17740–17748, 2008.

Palmer AE, Giacomello M, Kortemme T, Hires SA, Lev-Ram V, Baker D, Tsien RY. Ca2+ indicators based on computationally redesigned calmodulin-peptide pairs. *Chem. Biol.* 13: 521–530, 2006.

Parmacek MS, Bengur AR, Vora AJ, Leiden JM. The structure and regulation of expression of the murine fast skeletal troponin C gene. Identification of a developmentally regulated, muscle-specific transcriptional enhancer. *J. Biol. Chem.* 265: 15970–15976, 1990.

Patel LR, Curran T, Kerppola TK. Energy transfer analysis of Fos-Jun dimerization and DNA binding. *Proc. Natl. Acad. Sci. U.S.A.* 91: 7360–7364, 1994.

Paulmurugan R, Gambhir SS. Monitoring protein-protein interactions using split synthetic renilla luciferase protein-fragment-assisted complementation. *Anal. Chem.* 75: 1584–1589, 2003.

Paulmurugan R, Umezawa Y, Gambhir SS. Noninvasive imaging of protein-protein interactions in living subjects by using reporter protein complementation and reconstitution strategies. *Proc. Natl. Acad. Sci. U.S.A.* 99: 15608–15613, 2002.

Pédelacq J-D, Cabantous S, Tran T, Terwilliger TC, Waldo GS. Engineering and characterization of a superfolder green fluorescent protein. *Nat. Biotechnol.* 24: 79–88, 2006.

Pelletier JN, Campbell-Valois FX, Michnick SW. Oligomerization domain-directed reassembly of active dihydrofolate reductase from rationally designed fragments. *Proc. Natl. Acad. Sci. U.S.A.* 95: 12141–12146, 1998.

Piston DW, Kremers G-J. Fluorescent protein FRET: the good, the bad and the ugly. *Trends Biochem. Sci.* 32: 407–414, 2007.

Prasher DC, Eckenrode VK, Ward WW, Prendergast FG, Cormier MJ. Primary structure of the Aequorea victoria green-fluorescent protein. *Gene* 111: 229–233, 1992.

Qin L, Chu J, Zheng Y, Luo Q, Zeng S, Zhang Z. A new red bimolecular fluorescence complementation based on TagRFP. SPIE, p. 71910G–71910G–6.

Richards FM. On the Enzymic Activity of Subtilisin-Modified Ribonuclease. *Proc. Natl. Acad. Sci. U.S.A.* 44: 162–166, 1958.

Robida AM, Kerppola TK. Bimolecular fluorescence complementation analysis of inducible protein interactions: effects of factors affecting protein folding on fluorescent protein fragment association. *J. Mol. Biol.* 394: 391–409, 2009.

Rose RH, Briddon SJ, Holliday ND. Bimolecular fluorescence complementation: lighting up seven transmembrane domain receptor signalling networks. *Br. J. Pharmacol.* 159: 738–750, 2010.

Des Rosiers MH, Descarries L. [Adaptation of the deoxyglucose method to the cellular level: histologic preparation of the central nervous system for high resolution radioautography]. *C.R. Hebd. Seances Acad. Sci., Ser. D, Sci. Nat.* 287: 153–156, 1978.

Rossi F, Charlton CA, Blau HM. Monitoring protein-protein interactions in intact eukaryotic cells by beta-galactosidase complementation. *Proc. Natl. Acad. Sci. U.S.A.* 94: 8405–8410, 1997.

Roy R, Hohng S, Ha T. A practical guide to single-molecule FRET. *Nat. Methods* 5: 507–516, 2008.

Saez ME, Ramirez-Lorca R, Moron FJ, Ruiz A. The therapeutic potential of the calpain family: new aspects. *Drug Discov. Today* 11: 917–923, 2006.

Sakaguchi R, Endoh T, Yamamoto S, Tainaka K, Sugimoto K, Fujieda N, Kiyonaka S, Mori Y, Morii T. A single circularly permuted GFP sensor for inositol-1,3,4,5-tetrakisphosphate based on a split PH domain. *Bioorg. Med. Chem.* 17: 7381–7386, 2009.

Shaner NC, Campbell RE, Steinbach PA, Giepmans BNG, Palmer AE, Tsien RY. Improved monomeric red, orange and yellow fluorescent proteins derived from Discosoma sp. red fluorescent protein. *Nat. Biotechnol.* 22: 1567–1572, 2004.

Shimomura O, Johnson FH, Saiga Y. Extraction, purification and properties of aequorin, a bioluminescent protein from the luminous hydromedusan, Aequorea. *J Cell Comp Physiol* 59: 223–239, 1962.

da Silva EF, Oliveira VH, Sorenson MM, Barrabin H, Scofano HM. Converting troponin C into calmodulin: effects of mutations in the central helix and of changes in temperature. *Int. J. Biochem. Cell Biol.* 34: 657–667, 2002.

Sokoloff L, Reivich M, Kennedy C, Rosiers MHD, Patlak CS, Pettigrew KD, Sakurada O, Shinohara M. THE [14C]DEOXYGLUCOSE METHOD FOR THE MEASUREMENT OF LOCAL CEREBRAL GLUCOSE UTILIZATION: THEORY, PROCEDURE, AND NORMAL VALUES IN THE CONSCIOUS AND ANESTHETIZED ALBINO RAT. *Journal of Neurochemistry* 28: 897–916, 1977.

Song Y-H, Wilmanns M. Bimolecular fluorescence complementation in structural biology. *Methods* 45: 219–222, 2008.

Takatsuka K, Ishii TM, Ohmori H. A novel Ca2+ indicator protein using FRET and calpain-sensitive linker. *Biochem. Biophys. Res. Commun.* 336: 316–323, 2005.

Tallini YN. Imaging cellular signals in the heart in vivo: Cardiac expression of the high-signal Ca2+ indicator GCaMP2. *Proceedings of the National Academy of Sciences* 103: 4753–4758, 2006.

Tian L, Hires SA, Mao T, Huber D, Chiappe ME, Chalasani SH, Petreanu L, Akerboom J, McKinney SA, Schreiter ER, Bargmann CI, Jayaraman V, Svoboda K, Looger LL. Imaging neural activity in worms, flies and mice with improved GCaMP calcium indicators. *Nat. Methods* 6: 875–881, 2009.

Tikunova SB, Black DJ, Johnson JD, Davis JP. Modifying Mg2+ binding and exchange with the N-terminal of calmodulin. *Biochemistry* 40: 3348–3353, 2001.

Tripet B, De Crescenzo G, Grothe S, O'Connor-McCourt M, Hodges RS. Kinetic analysis of the interactions between troponin C (TnC) and troponin I (TnI) binding peptides: evidence for separate binding sites for the "structural" N-terminus and the "regulatory" C-terminus of TnI on TnC. *J. Mol. Recognit.* 16: 37–53, 2003.

Tsien R, Pozzan T. Measurement of cytosolic free Ca2+ with quin2. *Meth. Enzymol.* 172: 230–262, 1989.

Tsien RY. A non-disruptive technique for loading calcium buffers and indicators into cells. *Nature* 290: 527–528, 1981.

Tsytsarev V, Maslov KI, Yao J, Parameswar AR, Demchenko AV, Wang LV. In vivo imaging of epileptic activity using 2-NBDG, a fluorescent deoxyglucose analog. *J. Neurosci. Methods* 203: 136–140, 2012.

Vanderklish PW, Krushel LA, Holst BH, Gally JA, Crossin KL, Edelman GM. Marking synaptic activity in dendritic spines with a calpain substrate exhibiting fluorescence resonance energy transfer. *Proc. Natl. Acad. Sci. U.S.A.* 97: 2253–2258, 2000.

Varshavsky A. The N-end rule at atomic resolution. *Nat. Struct. Mol. Biol.* 15: 1238–1240, 2008.

Wallace DJ, Meyer zum Alten Borgloh S, Astori S, Yang Y, Bausen M, Kügler S, Palmer AE, Tsien RY, Sprengel R, Kerr JND, Denk W, Hasan MT. Single-spike detection in vitro and in vivo with a genetic Ca2+ sensor. *Nat. Methods* 5: 797–804, 2008.

Wang Q, Shui B, Kotlikoff MI, Sondermann H. Structural basis for calcium sensing by GCaMP2. *Structure* 16: 1817–1827, 2008.

Wehr MC, Laage R, Bolz U, Fischer TM, Grünewald S, Scheek S, Bach A, Nave K-A, Rossner MJ. Monitoring regulated protein-protein interactions using split TEV. *Nat. Methods* 3: 985–993, 2006.

Wickersham IR, Finke S, Conzelmann K-K, Callaway EM. Retrograde neuronal tracing with a deletion-mutant rabies virus. *Nat. Methods* 4: 47–49, 2007.

Wiegand TW, Reznikoff WS. Characterization of two hypertransposing Tn5 mutants. *J. Bacteriol.* 174: 1229–1239, 1992.

Wu X, Simone J, Hewgill D, Siegel R, Lipsky PE, He L. Measurement of two caspase activities simultaneously in living cells by a novel dual FRET fluorescent indicator probe. *Cytometry A* 69: 477–486, 2006.

Xu X, Gerard AL, Huang BC, Anderson DC, Payan DG, Luo Y. Detection of programmed cell death using fluorescence energy transfer. *Nucleic Acids Res.* 26: 2034–2035, 1998.

Yamniuk AP, Vogel HJ. Calmodulin's flexibility allows for promiscuity in its interactions with target proteins and peptides. *Mol. Biotechnol.* 27: 33–57, 2004.

Yang F, Moss LG, Phillips GN Jr. The molecular structure of green fluorescent protein. *Nat. Biotechnol.* 14: 1246–1251, 1996.

Zhao Y, Araki S, Wu J, Teramoto T, Chang Y-F, Nakano M, Abdelfattah AS, Fujiwara M, Ishihara T, Nagai T, Campbell RE. An expanded palette of genetically encoded Ca^{2+} indicators. *Science* 333: 1888–1891, 2011.

Zhdanov AS, Phan J, Evdokimov AG, Tropea JE, Kapust RB, Li M, Wlodawer A, Waugh DS. [Tobacco etch virus proteinase: crystal structure of the active enzyme and its inactive mutant]. *Bioorg. Khim.* 29: 457–460, 2003.

Acknowledgements

First and foremost I would like to thank my "Doktorvater", Oliver Griesbeck, for giving me the opportunity to undertake my PhD in his lab. His driving force and guidance towards my project has been both insightful and inspirational. I further want to express my gratitude to Axel Borst for always being supportive and helpful towards the students of the MPIN.

It goes without saying that I would not be in this position without the amazing and unhindered support from "se Griesenbecks". I cannot fully express my appreciation to: my "IPP partner" Martina Schifferer, my "street buddy" Danish (who is *not* a spy), "Mr. Conversation" Oselm Geiger, my "clown-schooled" Munich encyclopaedia Steph-man-Joe Direnberger, the crazy Armenian "նապաստակ" Gayane Aramuni, the "ever so lovely and nice" Julia Litzlbauer, the "Oracle" Marco Mank, and the "bio-cybernetic" Johannes Plett; without these guys I would have no idea what I am doing. I also wish to thank the "ever so hungry" Anja Moritz and "Lasers!!" David Ng for their entertainment and help, especially with developing the stimulation setup! I would also like to thank the Borst group and Herr Lehmacher for a very entertaining department and for always keeping my eye on the goal! There are many more people that I should thank from the MPIN for making my introduction and existence in Munich a hilarious venture, if you're reading this you know who you are!

Two people who should win an Oscar for being the best technicians a lab can ever have go to Birgit Kunkel and Louise Gaitanos. Birgit has helped me through every hurdle of the PhD life, and without her dedication half of this thesis would not have been possible. Louise has always helped a Griesbeck-in-need and the occasional turning a blind eye has saved many of us. Thank you to you both!

I would also like to thank my family for their unwavering support and visits throughout my time here; I could not have lasted without them! Most importantly, I would like to express my deepest thanks and love to my "cariño" Nerea Gallastegui de la Rosa for always lovingly supporting me; we've shared a lot over the last years and I cannot find the words to adequately explain how much she means to me.

Versicherung

Eidesstattliche Versicherung

Ich versichere hiermit an Eides statt, dass die vorgelegte Dissertation von mir selbständig und ohne unerlaubte Hilfe angefertigt ist.

München, 26.04.12

…………………………………………

Jonathan A.G. Mackinnon

Erklärung

Hiermit erkläre ich, dass die Dissertation nicht ganz oder in wesentlichen Teilen einer anderen Prüfungskommission vorgelegt worden ist und dass ich mich anderweitig einer Doktorprüfung ohne Erfolg nicht unterzogen habe.

München, 26.04.12

…………………………………………

Jonathan A.G. Mackinnon